

Dissertation zur Erlangung des Doktorgrades  
der Fakultät für Chemie und Pharmazie  
der Ludwig-Maximilians-Universität München

**Translational quality control mechanisms  
that mitigate stop codon readthrough and  
ensure protein homeostasis**

Martin Bernhard Dietrich Müller

aus

Wiesbaden, Deutschland

2023

### Erklärung

Diese Dissertation wurde im Sinne von § 7 der Promotionsordnung vom 28. November 2011 von Herrn Prof. Dr. F.-Ulrich Hartl betreut.

### Eidesstattliche Versicherung

Diese Dissertation wurde eigenständig und ohne unerlaubte Hilfe erarbeitet

München, 08.08.2023

Martin Müller

Dissertation eingereicht am: 11.08.2023

1. Gutachter: Prof. Dr. F.-Ulrich Hartl

2. Gutachter: Prof. Dr. Roland Beckmann

Mündliche Prüfung am: 28.09.2023

## Table of contents

<b>INTRODUCTION</b> .....	<b>5</b>
DNA REPLICATION AND TRANSCRIPTION .....	5
TRANSLATION .....	6
FUNCTION OF 3'UTRs .....	10
PROTEIN FOLDING AND AGGREGATION PREVENTION.....	11
CHAPERONINS .....	14
SMALL HEAT SHOCK PROTEINS (sHSPs) .....	16
CLEARANCE OF MISFOLDED PROTEINS.....	18
TRANSLATIONAL KINETICS AND PROTEIN FOLDING .....	22
TRANSMEMBRANE PROTEIN BIOGENESIS AND QUALITY CONTROL.....	23
TRANSLATION AND AGEING .....	26
SENSING, CLEARING, AND PREVENTING RIBOSOMAL COLLISIONS .....	29
TRANSLATION READTHROUGH MITIGATION .....	33
<b>SUMMARY</b> .....	<b>34</b>
<b>MATERIALS AND METHODS</b> .....	<b>35</b>
C. ELEGANS STRAINS AND MAINTENANCE .....	42
Cas9 EXPRESSION AND PURIFICATION .....	42
CRISPR/Cas9-MEDIATED HOMOLOGOUS RECOMBINATION.....	42
IMMUNOBLOTTING.....	43
LC-MS/MS ANALYSIS .....	43
MS DATA ANALYSIS .....	44
MRNA PULLDOWN.....	44
HUMAN CELL CULTURE AND TRANSFECTION.....	45
CRISPR KNOCKOUT CELL LINES .....	45
SIRNA TREATMENT .....	45
FLOW CYTOMETRY.....	45
AGGREGATE FRACTIONATION .....	46
PROTEIN PULLDOWN.....	46
PREPARATION OF TOTAL PROTEIN EXTRACTS FOR IMMUNOBLOT ANALYSIS.....	47
TOTAL RNA ISOLATION .....	47
QUANTITATIVE REAL-TIME PCR .....	48
MRNA SEQUENCING.....	48
PREPARATION OF TOTAL RIBOSOME FRACTION FOR RIBO-SEQ .....	48
PREPARATION OF RIBOSOME FRACTIONS FOR GCN-1-IPED RIBO-SEQ.....	49
SLAM-SEQ .....	50
POLYSOME GRADIENT ANALYSIS .....	50
SDS-PAGE .....	51

MICROSCOPY .....	51
IMAGE ANALYSIS .....	51
ANALYSIS OF RIBO-SEQ AND MRNA-SEQ DATA .....	51
STATISTICS .....	52
<b>RESULTS .....</b>	<b>54</b>
THE BAG6 COMPLEX DEGRADES HYDROPHOBIC READTHROUGH PRODUCTS.....	54
STOP CODON READTHROUGH LEADS TO mRNA DECAY VIA GCN-1-CCR4/NOT COMPLEX RECRUITMENT .....	67
MECHANISM OF READTHROUGH MITIGATION IS EVOLUTIONARILY CONSERVED .....	74
GCN-1 IS A GENERAL COTRANSLATIONAL SURVEILLANCE FACTOR FOR TRANSLATIONAL READTHROUGH AND TRANSMEMBRANE PROTEINS.....	83
COLLAGENS ARE ENDOGENOUS SUBSTRATES OF GCN-1 .....	89
GCN-1 SENSES SLOW TRANSLATING RIBOSOMES.....	95
THE FUNCTION OF GCN-1 IS CONSERVED IN MAMMALIAN CELLS AND IS REQUIRED FOR STRESS SIGNALING.....	98
<i>GCN1 is a global modulator of mRNA stability</i> .....	101
<b>DISCUSSION .....</b>	<b>111</b>
INTERPLAY OF BAG6/RNF-126 AND SHSPs IN QUALITY CONTROL OF READTHROUGH PROTEINS.....	111
GCN-1 MEDIATED MRNA DECAY .....	114
GCN1 SURVEILS TRANSLATION .....	115
IMPLICATIONS OF GCN-1 FUNCTION IN AGEING.....	118
<b>ACKNOWLEDGEMENTS .....</b>	<b>121</b>
<b>REFERENCES.....</b>	<b>122</b>

## Introduction

### DNA replication and transcription

Genetically encoded information is maintained and converted into final gene products by three processes: replication, transcription, and translation. Replication is the process by which cells duplicate their genomes during cell division. This process requires a high degree of accuracy to prevent mutations that potentially lead to non-functional gene products impairing cell fitness. During maturation of an oocyte to the final adult organism, the genetic material is replicated as many as  $4 \times 10^{13}$  times (Fragkos et al., 2015). An increased accumulation of DNA replication errors is observed in stem cells of aged organisms (Flach et al., 2014). In eukaryotes, DNA replication takes place at DNA replication forks that begin unwinding the DNA at specific locations called origins of replication. The DNA is then replicated by a DNA polymerase holoenzyme, consistent of two subunits (DNA Pol $\epsilon$  and Pol $\delta$ ) each replicating one single stranded DNA template (Garcia-Muse and Aguilera, 2016). In contrast, the RNA polymerase holoenzyme consists of one subunit that engages the double stranded DNA, unwinding it to enable transcription in a so-called 'transcription bubble' (Figure 1). The RNA is then synthesized in the active pocket of the RNA polymerase by forming RNA-DNA hybrids of 9-11 nucleotides in length and is aided by transcription factors (Garcia-Muse and Aguilera, 2016). The RNA is co-transcriptionally processed, e.g. by exon splicing or 5' capping, maturing it into messenger RNA (mRNA) (Merkhofer et al., 2014).

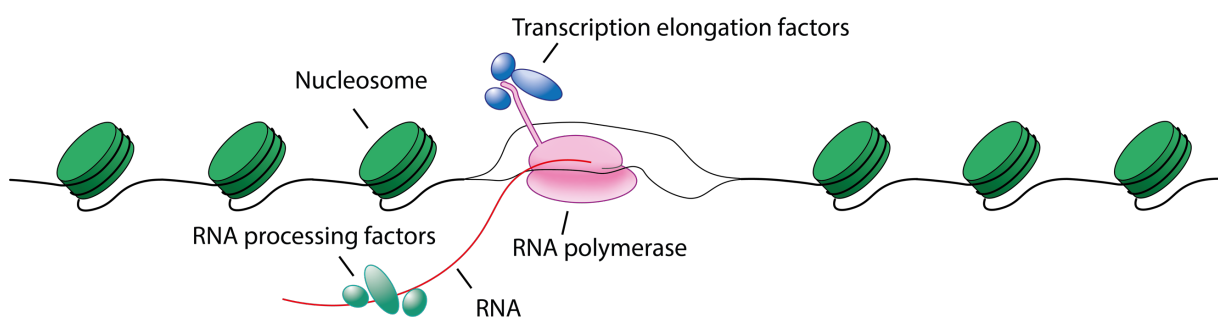


*Figure 1: Schematic representation of DNA transcription to produce mRNA molecules. The double-stranded DNA is partially unwound by the RNA polymerase to allow local transcription in the so-called transcription bubble. This unwinding results in a positive (upstream of the polymerase) and negative (downstream of the polymerase) supercoiling, which is resolved by topoisomerases. For the transcription to proceed, the RNA polymerase requires transcription*

elongation factors, and downstream RNA processing of the nascent strand is carried out co-transcriptionally. Adapted from Garcia-Muse and Aguilera, 2016.

## Translation

Proteins are synthesized by macromolecular machines, called ribosomes, that translate encoded information of mRNAs into polypeptide sequences. The ribosome translates one codon at a time, each consisting of 3 nucleotides. Individual codons are recognized by tRNAs charged with specific amino acids, forming codon:anticodon pairs and amino acids are joined by peptide bond formation. The ribosome then continues to elongate the nascent polypeptide with the corresponding amino acid (Schuller and Green, 2018). The process of translation can be divided into 5 phases, consisting of scanning, initiation, elongation, termination and recycling, whose general principles are conserved across all domains of life (Figure 2).

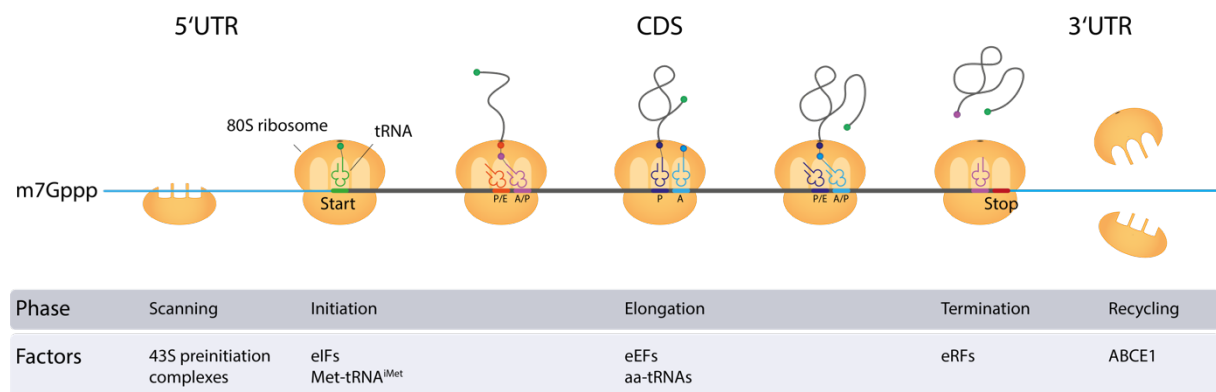


Figure 2: The 43S preinitiation complex scans the mRNA for the AUG start codon and represents the first step of translation. Once the start codon is recognized by the methionyl-tRNA, 60S subunit and 48S initiation complex are joined to form 80S ribosomes to initiate translation. This process is aided by eukaryotic translation initiation factors (eIFs). The polypeptide is then further elongated by the ribosome via an interplay of aminoacylated tRNAs and eukaryotic elongation factors (eEFs). Finally, termination occurs either by encountering a stop codon (UAA, UAG, UGA) or when there are translational errors. In the last step the ribosomal subunits are recycled by ABCE1 to enter a subsequent round of translation. Adapted from Schuller and Green, 2018.

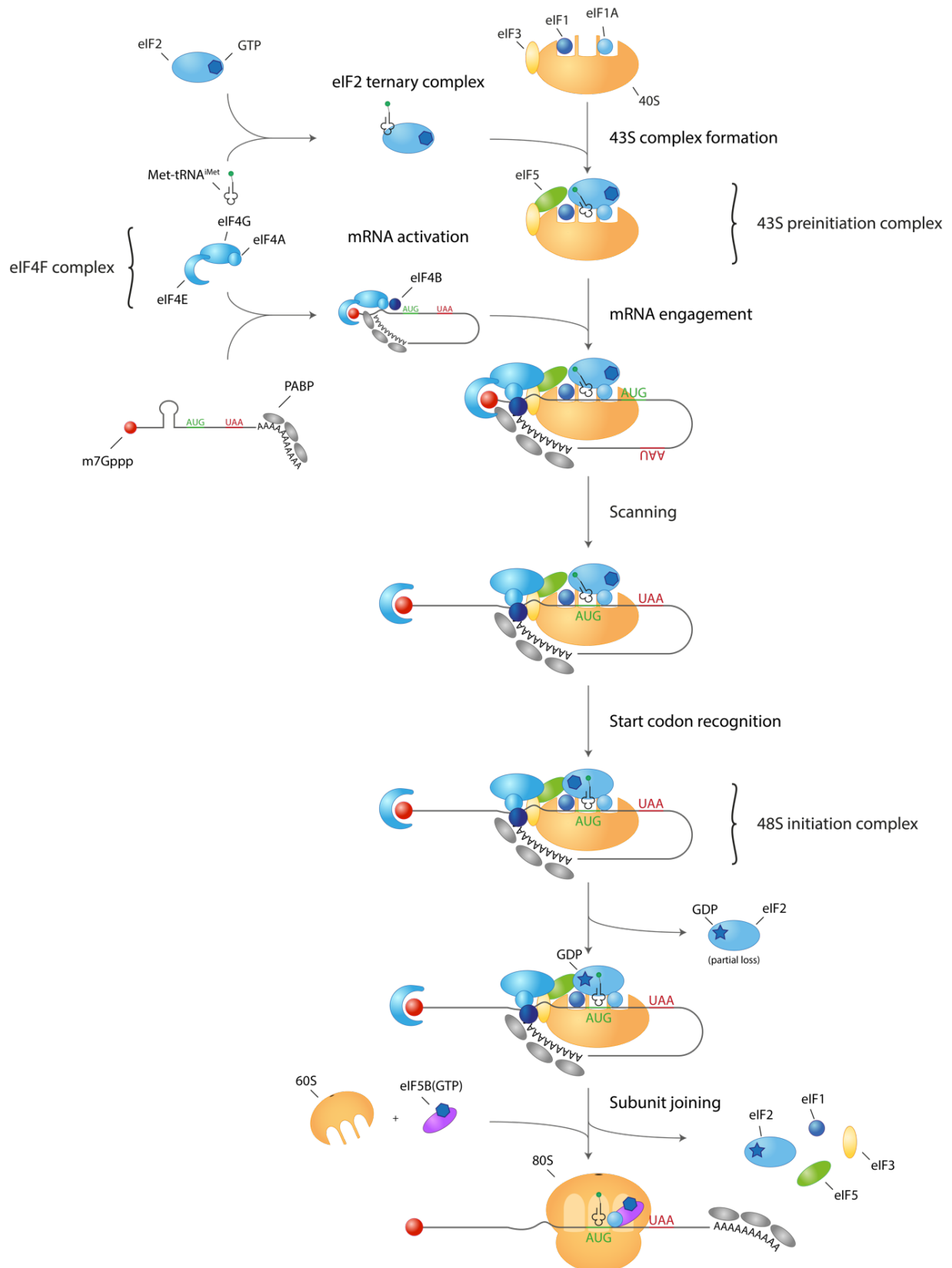


Figure 3: eIF2 complex and 40S ribosome form 43S preinitiation complex. The eIF4F complex activates mRNA and allows engagement of 43S preinitiation complex to form the 48S initiation complex. The 60S ribosomal subunit and eIF5B displace the bound eIFs to form the 80S ribosomal subunit and translation commences. Adapted from Jackson et al., 2010.

Translation initiation starts with the formation of the 43S complex, consisting of the 40S ribosomal subunit, eIF1, eIF1A, eIF2 and initiator methionyl-tRNA. The 43S complex binds to capped mRNAs at the 5' proximal region (Figure 3). This is followed by mRNA activation by eIF4A, eIF4B and eIF4F which function to unwind the 5' terminal secondary structure and allowing the engagement by the 43S pre-initiation complex (Jackson et al., 2010). While in the initial model AUG start codon scanning by the 43S pre-initiation complex was thought to be unidirectional (5' to 3' direction), recent observations suggest a bidirectional scanning mechanism (Gu et al., 2021). Once the AUG codon is recognized, the 48S initiation complex is formed. Next, eIF5 and eIF5B promote the hydrolyses of GTP bound to eIF2 and subsequently the displacement of eIFs, allowing the 40S and 60S subunits to join (Jackson et al., 2010).

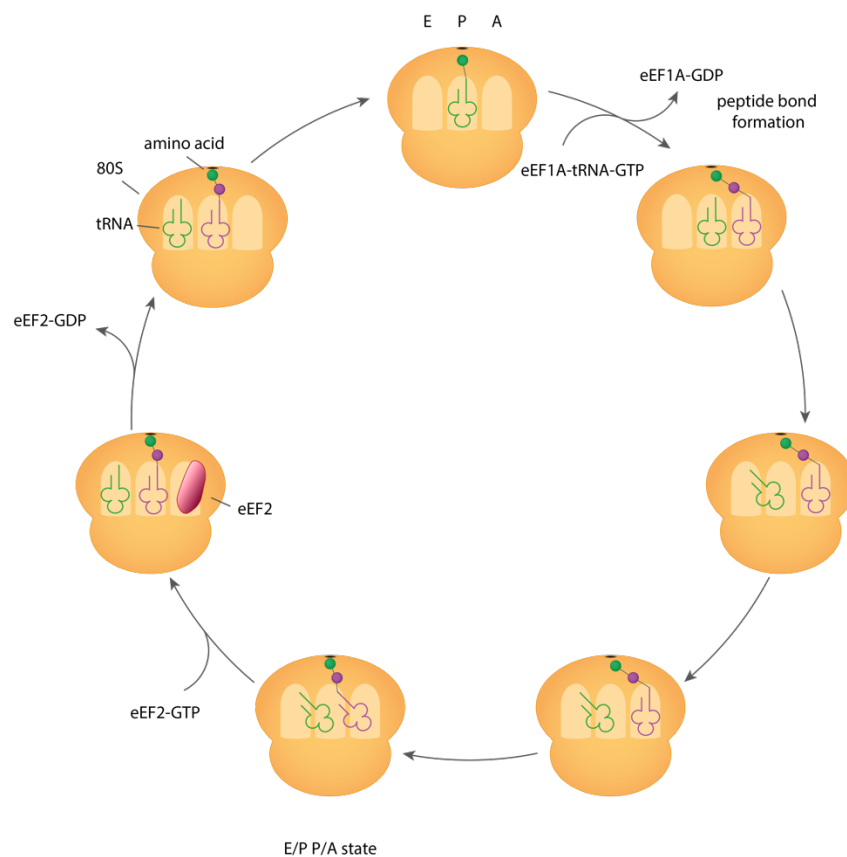


Figure 4: Schematic overview of the translation elongation cycle. Adapted from Ranjan et al., 2021 and Lareau et al., 2014. At the beginning, an eEF1A-tRNA-GTP ternary complex binds to the A-site of ribosomes, with the anticodon-loop of the tRNA contacting the mRNA. This is followed by the hydrolysis of GTP and the release of eEF1A-GDP, which accommodates the aminoacylated tRNA at the A-site. During the formation of the peptide bond, the P- and A-site bound tRNAs change in their positioning to form a hybrid state, occupying E/P- and P/A-sites,

respectively. In the next step, eEF2-GTP is recruited to the A-site, aiding in the translocation of the tRNAs into the E- and P-site. After the release of the tRNA situated at the E-site of the ribosomes, the next elongation cycle is initiated.

During translation elongation, the nascent peptide is synthesized at a rate of  $\sim 6$  amino acids per second (Bukau et al., 2000; Ingolia et al., 2011). The ribosome undergoes substantial structural rearrangements during each cycle due to orchestrated rotations of the two ribosomal subunits (Zhang et al., 2009) (Figure 4). Each cycle starts with the delivery of aminoacylated tRNAs in a preformed complex with eEF1A to the empty A-site of the 80S ribosome. Once the corresponding tRNA establishes a stable interaction with the A-site codon, a peptide bond is formed between the amino acid and the nascent polypeptide. During the process of elongation, the tRNA passes vectorially through the three sites (A-, P- and E-site) at the ribosome and is released after reaching the E-site, which concludes each cycle (Lareau et al., 2014).

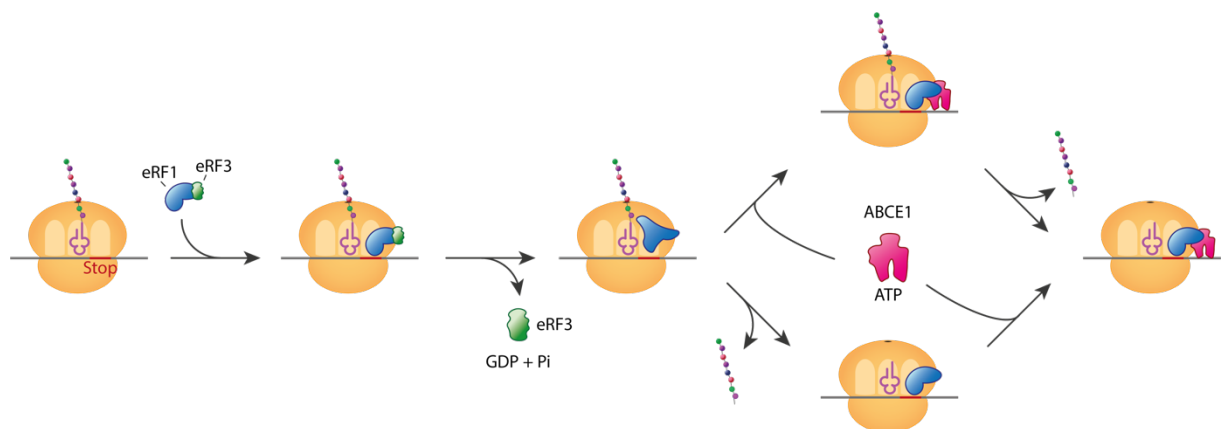


Figure 5: Schematic overview of translation termination. Adapted from Preis et al., 2014. Translation termination is initiated by the recognition of a stop codon at the A-site of translating ribosomes by the eRF1-eRF3-GTP ternary complex. Upon the hydrolysis of GTP, eRF3 dissociates from the complex and is released from the ribosome. Hereon, there are two possible scenarios: 1) The active conformation of eRF1 is stabilized by the binding of ABCE1, stimulating nascent peptide release, or 2) eRF1 alone enables chain release. In the last step, ABCE1 and eRF1 function to dissociate small and large ribosomal subunits.

Translation termination concludes the elongation of nascent polypeptides as ribosomes reach stop codons in the A-site. In eukaryotes, all three stop codons (UAA, UAG and UGA) are

recognized by eRF1, which is delivered to the vacant A-site (Figure 5). eRF1 is structurally similar to tRNAs, thus enabling it to bind to the ribosomal A-site (Schuller and Green, 2018). Two distinct structural motifs play important roles in stop codon recognition and nascent chain release: The NIKS motif consisting of Asn–Ile–Lys–Ser facilitates the recognition of stop codons, whereas the GGQ motif (Gly–Gly–Gln) aids in the nascent chain release (Brown et al., 2015; Frolova et al., 1994; Frolova et al., 1999; Matheisl et al., 2015; Song et al., 2000). Like tRNAs, eRF1 requires a GTPase, eRF3, to carry out its function. Together with ABCE1, eRF1 facilitates the release of the nascent chain and subsequent subunit dissociation (Preis et al., 2014).

### Function of 3'UTRs

The sequence space of 3'UTRs in higher eukaryotes has largely expanded and correlates with increasing complexity which is defined by the number of different cell types observed (Chen et al., 2012; Derti et al., 2012; Jan et al., 2011; Mayr, 2017). While the median 3'UTR length in nematodes is ~140 nt, it is up to ~1200 nt in humans. Although 3'UTRs are less conserved than coding regions, they still show a high degree of conservation, particularly for known binding sites of miRNAs and RNA binding proteins (RBPs) (Friedman et al., 2009; Xie et al., 2005).

The best-known functions of 3'UTRs are in regulating mRNA stability, translation rates and mRNA localization, which are partly mediated by RBPs, which in turn may recruit deadenylases (Zaessinger et al., 2006) or decapping enzymes (Chen et al., 2014). AU-rich elements within 3'UTRs are associated with rapid mRNA decay and are found in genes that require tight regulation, such as cytokines (Barreau et al., 2005; Chen and Shyu, 1995). Likewise, 3'UTRs can act as binding sites for miRNAs that modulate mRNA turnover, as exemplified by proto-oncogenes (Chen and Shyu, 1995).

Beyond their modulating role in translation and decay, 3'UTRs mediate protein-protein interactions that ultimately define the fate of the nascent chain. For example, CD47 (or MER6), a known plasma receptor, is found in two different mRNA isoforms with varying 3'UTR lengths, but identical coding sequences. Only the long 3'UTR isoform promotes the localization to plasma membranes of CD47, whereas the short form is expressed in the cytosol. This localization to the plasma membrane depends on the ability of the long 3'UTR of CD47 to interact with ELAVL1 and SET (Berkovits and Mayr, 2015). Another example for 3'UTR-mediated protein-protein interactions is the recruitment of the signal recognition particle (SRP) to translating ribosomes before the signal peptide has emerged from the ribosomal exit

tunnel, challenging the original model that SRP is directly recruited to the signal sequence of secretory proteins (Chartron et al., 2016). Moreover, the cotranslational assembly of peripherin, which forms filamentous structures in neurons, was described to be dependent on its 3'UTR (Chang et al., 2006). RBPs mediating the clustering of peripherin mRNAs is one possible mechanism on how cotranslational assembly might be mediated by 3'UTRs. Intriguingly, cotranslational assembly has also been described for other filamentous structures, such as myosin (Isaacs and Fulton, 1987) and vimentin (Isaacs et al., 1989), raising the possibility that such a 3'UTR-mediated cotranslational assembly is more widespread for cytoskeleton structures in cells.

### Protein folding and aggregation prevention

Since the first observations that small proteins can fold spontaneously without the aid of additional factors, subsequent studies provided deep mechanistic insights (Anfinsen, 1973; Balchin et al., 2020). Despite major recent advances in predicting protein structures, the protein-folding problem remains unsolved, and a unifying folding mechanism is yet to be determined (Dill and MacCallum, 2012; Moore et al., 2022). In the cell, chaperones assist nascent proteins to traverse through a rugged energy landscape, guiding them to their native confirmations (Figure 6).

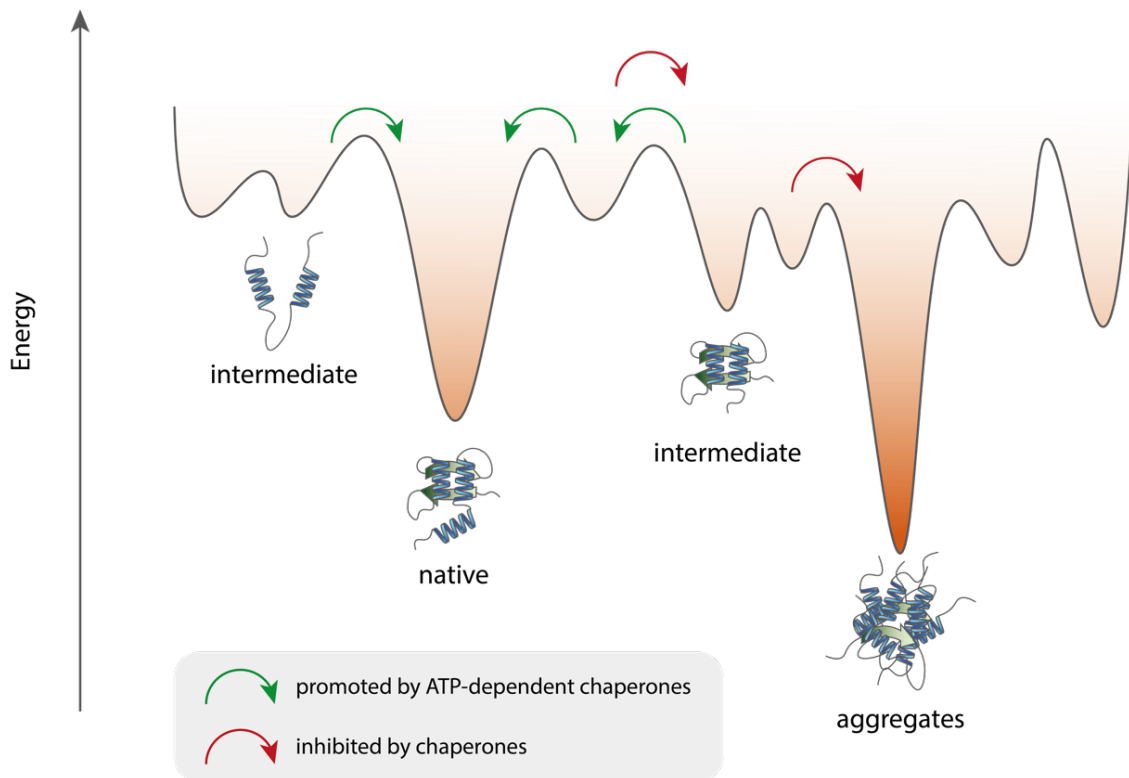


*Figure 6: The energy landscape of protein folding is shaped by molecular chaperones. Nascent proteins pass through different intermediate conformational states to arrive at their final native conformation, which is usually the energetically most stable. En route proteins can be trapped in kinetically stable, yet non-native states, which are prone to form aggregated species. Molecular chaperones guide chaperones to their native conformations by preventing aggregation and promoting the interconversion of folding intermediates. Adapted from Balchin et al., 2020.*

Proteins that meander off-path are at risk of forming kinetically trapped intermediates (Dinner et al., 2000). By exposing hydrophobic regions, these intermediates are at further risk to aggregate. This is particularly problematic under the conditions of macromolecular crowding in cells (~200 to 300 g protein/l), where aggregation is strongly enhanced (Ellis and Minton, 2006). Chaperones have evolved to counteract this problem: They engage nascent chains co-translationally, thereby minimizing the chance of aberrant protein interactions (Liutkute et al., 2020). Reversible binding to hydrophobic, aggregation-prone sequences is a common feature of chaperones, allowing them to shape the folding path of nascent polypeptides (Balchin et al., 2020).

Members of the HSP70 chaperone class are among the most studied molecular chaperones. They are involved in a broad spectrum of cellular processes, including protein folding, translocation, trafficking, disaggregation, and degradation. The binding motif of HSP70 is defined by 5-7 amino acids which are enriched in hydrophobic residues, often flanked by positively charged amino acids (Rudiger et al., 1997). HSP70-mediated folding of proteins is assisted by HSP40s, which coordinate the ATP-hydrolysis driven conformational cycle of HSP70 (Szabo et al., 1994).

Several chaperones bind directly to the ribosome to receive the nascent chain as it emerges. A prominent example is Ssb in *S. cerevisiae*, a member of the HSP70 family. Ssb interacts with the ribosome via the ribosome-associated complex (RAC), consisting of the HSP70 Ssz and the J-domain protein Zuo1 (Gautschi et al., 2002; Kramer et al., 2019; Pechmann et al., 2013; Preissler and Deuerling, 2012; Zhang et al., 2017). Ssb has a central role in co-translational folding and its deletion leads to widespread protein misfolding and aggregation of newly synthesized polypeptides, including ribosomal subunits (Albanese et al., 2010; Doring et al., 2017; Koplín et al., 2010; Willmund et al., 2013). Another major ribosome-binding chaperone is the nascent-polypeptide-associated complex (NAC), which forms a heterodimer via its NAC-domains. The  $\alpha$ NAC subunit contains a ubiquitin-associated (UBA) domain at its C-terminus, whereas the  $\beta$ NAC subunit contains a positively charged sequence close to the N-terminus which anchors NAC to ribosomes (Jomaa et al., 2022). NAC is expressed at equimolar concentrations relative to ribosomes. Further, the complex has a low nanomolar affinity for ribosomes (Jomaa et al., 2022). Its positioning close to the exit tunnel of ribosomes and abundance would indicate a central role in de novo protein biogenesis. This is underlined by its essentiality across different species, including worms, flies, and mice (Bloss et al., 2003; Deng and Behringer, 1995; Markesich et al., 2000). NAC binds directly to nascent chains as they emerge and deletion of NAC leads to an increased ubiquitylation of nascent proteins (Duttler et al., 2013; Wang et al., 2013; Wiedmann et al., 1994). This data would indicate a protective role of NAC in preventing the premature degradation of nascent polypeptides. Accordingly, NAC is required during conditions of increased misfolding, which supports a model in which NAC acts as a molecular chaperone (Duttler et al., 2013). A similar role has been established for the chaperone trigger factor (TF) in prokaryotes, which binds to ribosomes and is involved in the co-translational folding of newly synthesized polypeptides (Deuerling et al., 1999; Teter et al., 1999). Like NAC, TF binds near the ribosomal exit tunnel,

exposing its hydrophobic surface towards the emerging nascent polypeptide (Ferbitz et al., 2004). The presence of TF prevents incorrect folding of nascent proteins, by stabilizing partially folded intermediates (Agashe et al., 2004; Kaiser et al., 2006; Singhal et al., 2015; Wruck et al., 2018). However, it remains unclear whether NAC operates similar to TF in the context of co-translational folding.

## Chaperonins

Chaperonins are composed of two stacked rings with 7-9 subunits per ring (Kim et al., 2013). Unlike other chaperones, they encapsulate their substrates within their central cavity to allow folding in the absence of aggregation (Bukau and Horwich, 1998; Hartl, 1996; Hartl et al., 2011). Within the protein family of chaperonins there are two major classes: Group I (GroEL/HSP60) and group II (archaeal thermosome and eukaryotic TRiC/CCT) which have distinct structural features.

The group I chaperonins are found in bacterial cells (GroEL), plant chloroplasts (Cpn60) and mitochondria (Hsp60). Each ring within the chaperonin is made up of 7 identical subunits to form a homo-oligomer. They are further characterized by their lid-shaped co-chaperone (GroES/Hsp10/Cpn10&Cpn20), which acts in closing the folding chamber to isolate the substrate from the crowded surrounding. The ATPase domain of each GroEL subunit is located equatorially, whereas the apical domains shape the gateway to the folding cavity (Horwich et al., 2007; Mayer, 2010). Further, they contain hydrophobic residues which are exposed, mediating substrate capture and typically involving multiple apical domains (Horwich et al., 2007). The GroEL cavity provides space for proteins up to ~60 kDa, which remain encapsulated in the cage for up to 10s at a time, regulated by the time needed for hydrolysis of 7 ATP in the GroEL ring (Tang et al., 2008). After dissociation of GroES, induced by ATP binding to the opposite ring, folded protein is released from the GroEL cavity. However, the exact coordination of the folding cycle remains under debate. Encapsulating the protein within the central cavity provides a favorable folding environment by constraining substrates sterically and therefore smoothing the folding energy landscape (Baumketner et al., 2003; Hayer-Hartl and Minton, 2006; Sirur and Best, 2013).

While the overall cylindrical structures of group I and group II chaperonins are similar, there are substantial differences. In contrast to group I chaperonins, where a separate protein complex (GroES) forms a lid, class II chaperonins use helical extensions from the apical

domains to close and open the cavity. Also, the arrangement of the subunits differs between group I and group II chaperonins: while in group II chaperonins the subunits are stacked directly between rings, in group I chaperonins the rings are slightly rotated relative to each other so that each subunit of one ring is located between two subunits of the opposite ring (Horwich et al., 2007). Another difference is that the rings of group II chaperonins typically contain 8 (and sometimes 9) subunits. In case of TRiC/CCT the rings are composed of eight different, paralogous subunits. Like GroEL/ES, group II chaperonins cycle between open (substrate-binding/release) and closed states (folding) and substrate encapsulation is required for efficient folding. The transition from the open to the closed state is characterized by the pairwise association of helical extensions mediated by ATP hydrolysis, closing the cavity and releasing the substrate into the central chamber (Cong et al., 2012). The folding cycle of TRiC is believed to be substantially slower than that of GroEL, leaving the substrate encapsulated for a significantly longer time (Reissmann et al., 2007). Additionally, the iris-like closing mechanism allows the encapsulation of subdomains of proteins which otherwise would be too large to be encapsulated in their entirety (Russmann et al., 2012).

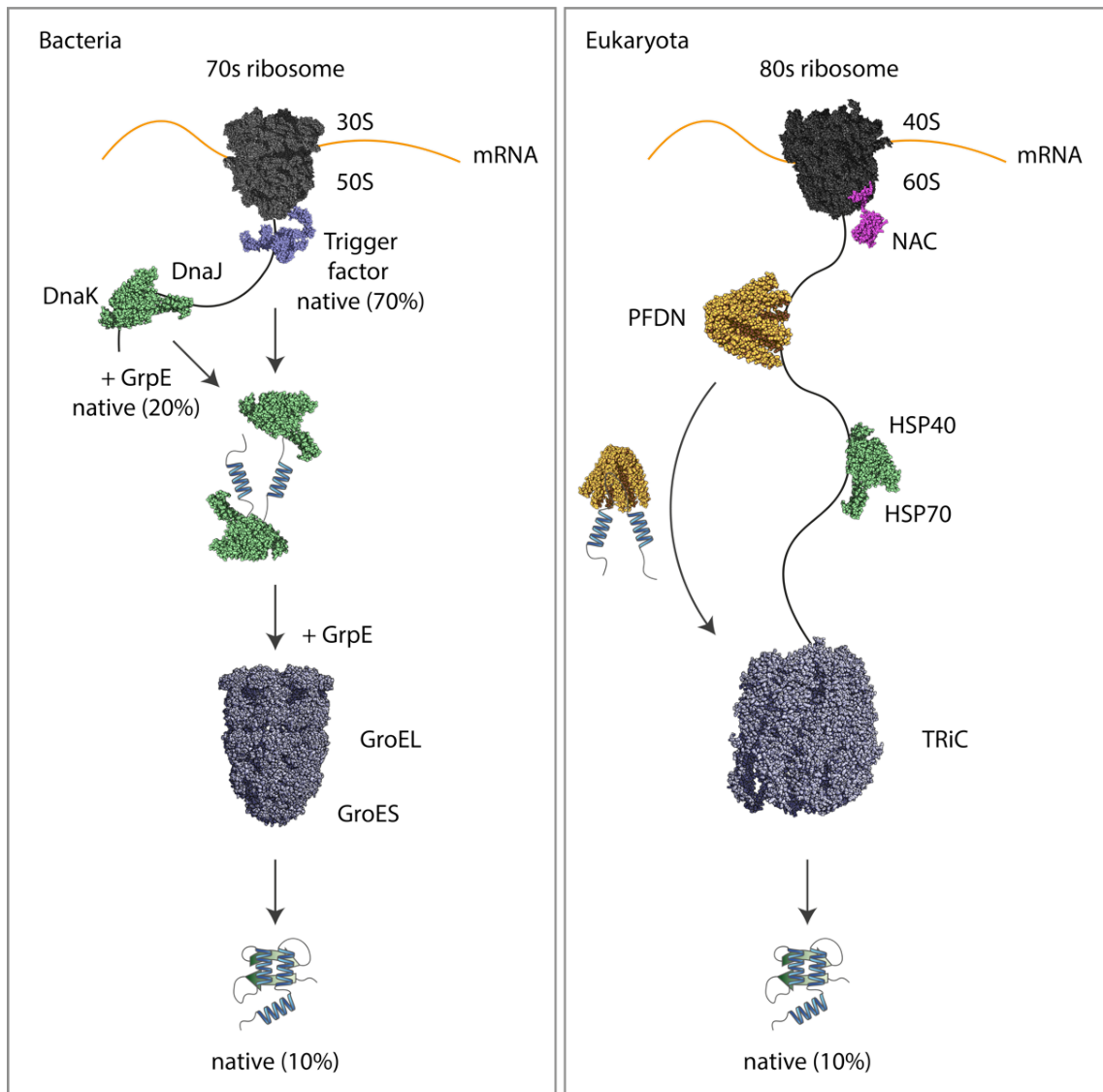
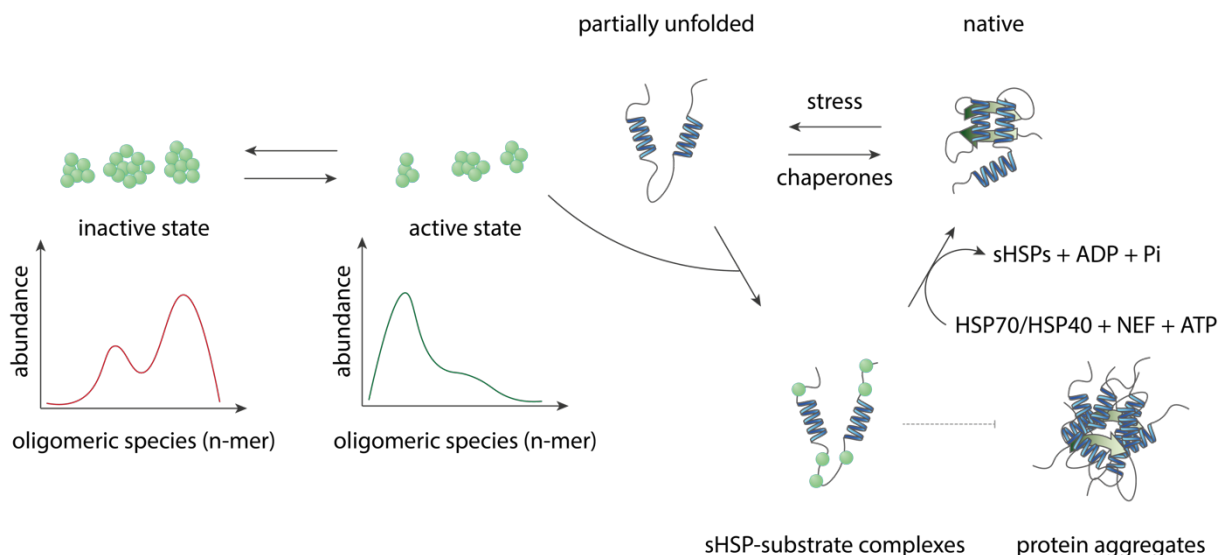


Figure 7: ~70% of newly synthesized proteins are estimated to interact with the ribosome-binding chaperones trigger factor (TF; bacteria) or nascent chain-associated complex (NAC; eukaryota). Downstream, several chaperone members facilitate the folding of nascent polypeptides, with the HSP70/HSP40 system at the center, facilitating ~20% of folding reactions. The remaining 10% of the proteome are thought to be passed on to chaperonins for folding. This step is aided in eukaryotes by prefoldin (PFDN). Adapted from Balchin et al., 2016.

### Small heat shock proteins (sHSPs)

If protein folding fails, the cells have developed different systems to either shield and rescue misfolded proteins or clear aberrant species. Small heat shock proteins (sHSPs) are an ancient class of ATP-independent molecular chaperones, which bind to misfolded proteins and prevent them from forming irreversible protein aggregates (Horwitz and Ricanati, 1992; Jakob

et al., 1993; McHaourab et al., 2002). Since they lack the ability of utilizing ATP, they usually exhibit no refolding properties themselves, but stabilize kinetically trapped aggregation-prone folding intermediates and thereby prevent aggregation (Haslbeck et al., 1999; Ungelenk et al., 2016). These partially unfolded protein species either arise from failed *de novo* folding reactions, or during several proteotoxic stresses, such as heat shock. Due to their function in aggregation prevention, yet lacking the ability to refold proteins themselves, they are often referred to as ‘holdases’. While the majority of sHSPs are almost exclusively expressed during acute stress conditions, some sHSPs are present at physiological growth conditions. The ratio of substrate to sHSPs, as well as temperature, shapes the conformation and size of substrate/sHSPs complexes. When sHSPs are present in excess over substrate, they adopt a polydisperse, yet soluble conformation. However, when substrate is in excess, sHSPs are incorporated into large dynamic and seemingly amorphous aggregates (Basha et al., 2004; Friedrich et al., 2004; Haslbeck et al., 1999; Lee et al., 1997). This type of behavior is seen *in vivo* in a multitude of stresses, such as protein overexpression, heat stress, or ageing (Allen et al., 1992; Arrigo et al., 1988; Haslbeck et al., 2019; Kampinga et al., 1994; Stege et al., 1994; Walther et al., 2015). As sHSPs are not able to refold protein themselves, inclusion reversal is often performed by the ATP-driven HSP70/HSP40 system. The sequestration of aggregation-prone, misfolded proteins *in vivo* is linked to enhancing cellular fitness and increased cell survival during stress (Escusa-Toret et al., 2013; Specht et al., 2011; Ungelenk et al., 2016).



*Figure 8: Schematic overview for molecular function of sHSPs. At basal conditions, sHSPs are in an inactive state. As substrate concentration increases, e.g. during proteotoxic stress, the oligomeric state of sHSPs change, leading to their activated state. The active confirmation of sHSPs engages substrate, shields it from forming aggregates and aids in the refolding, which*

*is facilitated by HSP70/HSP40 in orchestration with a nucleotide exchange factor (NEF) and hydrolyzing ATP. Adapted from Haslbeck et al., 2019.*

### Clearance of misfolded proteins

Misfolded proteins that fail to be refolded are prone to aggregation. In some cases, toxicity arises from the protein not being able to fulfill its function, as in the case of CFTR misfolding and loss of function in cystic fibrosis. However, in most scenarios, the toxicity of aggregates can be attributed to interference with crucial cellular processes in a gain of function manner (Chiti and Dobson, 2017; Valastyan and Lindquist, 2014). Several neurodegenerative diseases are associated with toxic protein aggregation, with ageing being a key risk factor for the development of aggregates and disease progression. Parkinson's disease and Alzheimer's disease are among the best-known examples, with the formation of protein plaques in the brain as a major hallmark (Sweeney et al., 2017). Cells have developed defense strategies, to mitigate the toxicity of protein aggregates and ensure protein homeostasis (Hipp et al., 2019; Sontag et al., 2017). Stresses that increase the load of misfolded proteins induce the production of protein quality control components (PQC), while shutting down general translation to reduce pressure on the proteostasis network (Costa-Mattioli and Walter, 2020). At the same time, protein clearance is initiated, and misfolded proteins are either degraded by the ubiquitin proteasome system or through autophagy.

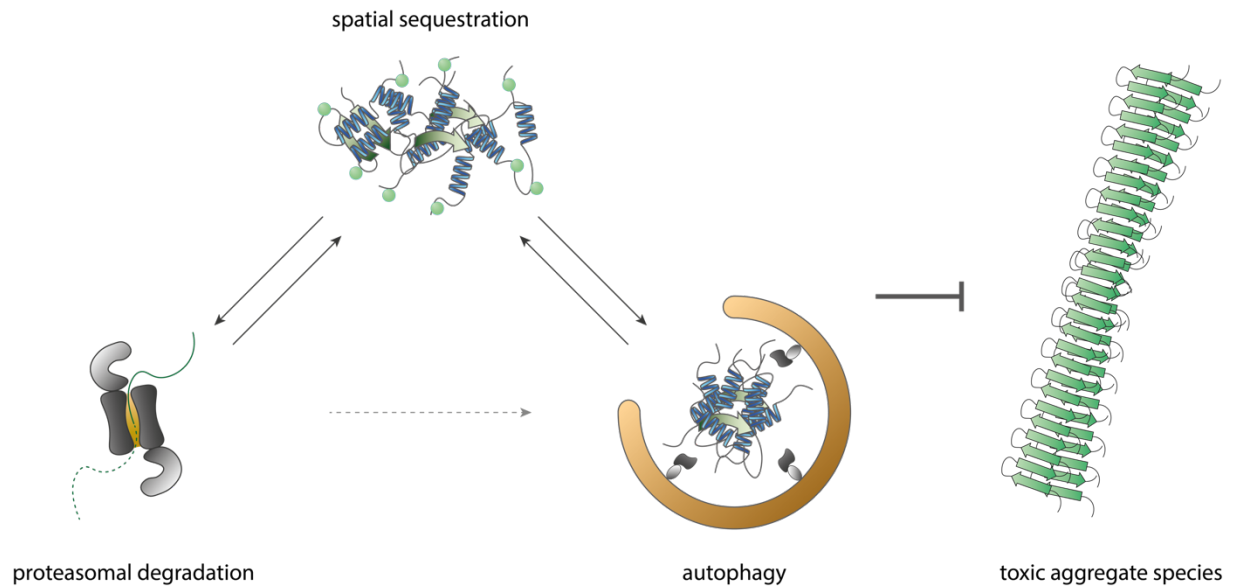


*Figure 9: Overview of protein clearance systems that prevent the formation of toxic aggregate species, such as amyloids. Spatial sequestration facilitated by factors, such as chaperones, aid in keeping the proteins in a soluble state. This makes proteins accessible for proteasomal degradation. Locally concentrating proteins that are to be cleared allows the formation of autophagosomes, which engulf the protein cargo and ultimately degrades it by fusing to the lysosome. This in turn prevents the formation of toxic (amyloid) aggregate species.*

Chaperones form the first line of defense against proteotoxic stress, recognizing misfolded proteins based on the exposure of hydrophobic amino acid residues (Johnston and Samant, 2021). By binding to the misfolded proteins, these hydrophobic regions are shielded and are no longer available to form aberrant interactions with other proteins.

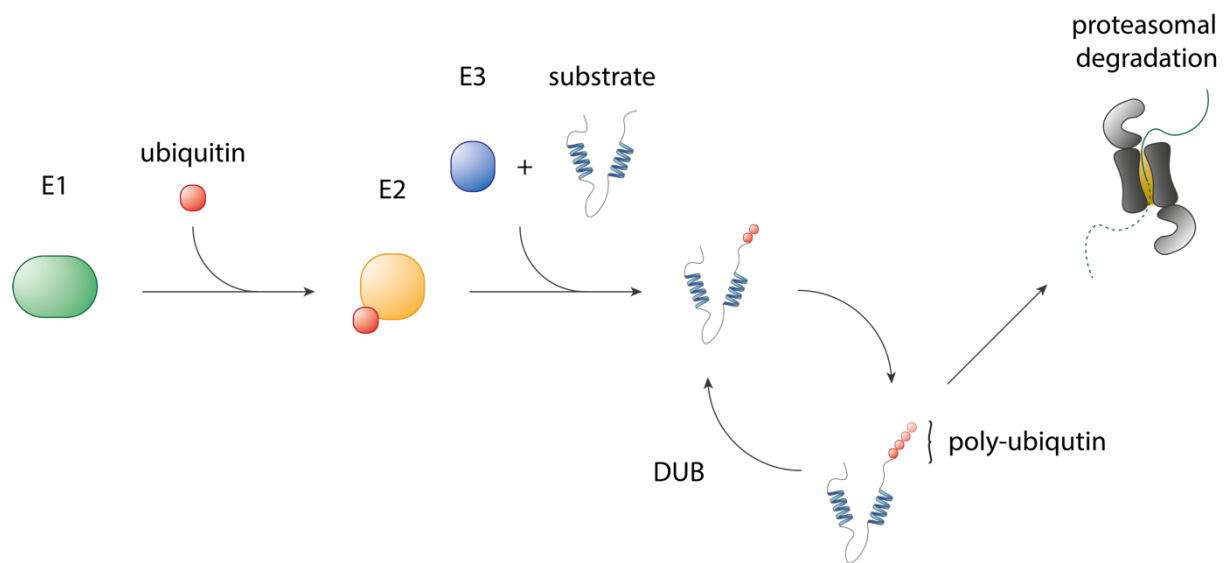
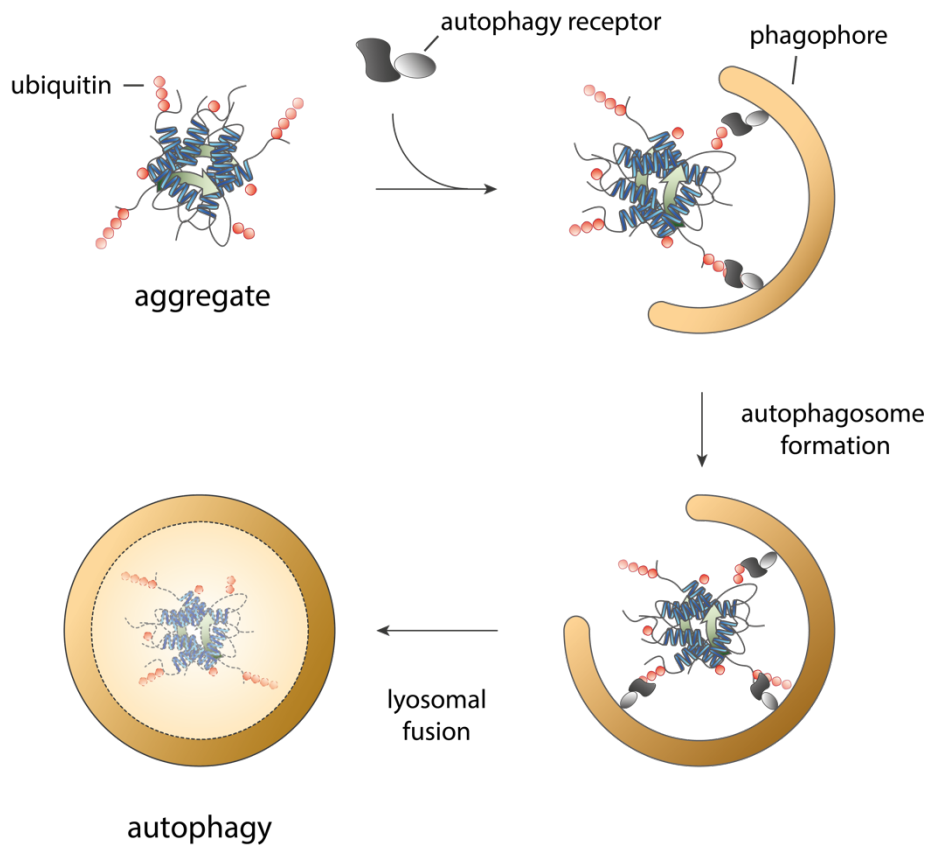


Figure 10: Schematic overview of the ubiquitin proteasome system (UPS), involving an E1 ubiquitin activating enzyme, that transfers the ubiquitin molecule to E2 ubiquitin-conjugating enzymes. Next, the ubiquitin molecule is attached to the substrate mediated by an E3 ubiquitin ligase. K48 polyubiquitinated substrates are then recognized and degraded by the 26S proteasome.

If refolding fails, typically E3 ubiquitin ligases are recruited (Quintana-Gallardo et al., 2019) to attach ubiquitin molecules to either lysine residues or the N-terminal methionine of misfolded proteins (Figure 10). The attached ubiquitin itself can be modified with additional ubiquitin molecules, forming long poly-ubiquitin chains, typically by either K48 or K11 linkages (Figure 9) (Amm et al., 2014). Poly-ubiquitinated proteins are transported to the proteasome, which consists of 20S core and 19S regulatory particles, facilitating their degradation. The 19S particle recognizes ubiquitin, allowing the docking of substrates. Once the substrate is bound, it is threaded through the catalytic core of the proteasome by a set of choreographed structural rearrangements (Bard et al., 2018; Dong et al., 2019). The catalytic core cleaves the substrate into small peptides, which are further digested by non-proteasomal endopeptidases, releasing individual amino acids that can be repurposed for synthesizing new proteins (Saric et al., 2004).



*Figure 11: Exposed ubiquitin chains of large inclusions formed by misfolded proteins are recognized by autophagic receptors, delivering them to growing phagophores. The substrate is engulfed and matures into an autophagosome, which fuses with the lysosome and degrades its cargo.*

Autophagy represents the second main branch by which cells clear misfolded protein species. While initially both UPS and autophagy were seen as bulk recycling machineries, in recent years it became clear that they act with a high degree of specificity and selectivity (Pohl and Dikic, 2019). The choice of which pathway is being utilized is mainly made based on the size of the substrate. While single misfolded proteins or smaller oligomeric assemblies are cleared by the UPS, larger inclusions are preferably targeted by autophagy (Dikic, 2017). Autophagy relies on members of the ATG8 protein family, which are conjugated to phosphatidylethanolamine or phosphatidylserine and thereby anchoring them to membranes and forming the phagophore (Pohl and Dikic, 2019). Substrates are selectively delivered to the growing phagophores by autophagic receptors, such as p62. Those receptors are often equipped with ubiquitin binding domains (UBDs) that link ubiquitinated proteins marked for degradation to phagophores, mediating their engulfment and ultimately their degradation

(Rogov et al., 2014). Current estimates assume that more than half of substrates for selective autophagy rely on ubiquitin as a degradation signal (Khaminets et al., 2016).

### Translational kinetics and protein folding

Besides chaperones, the elongation rate of translation modulates folding efficiency. The speed of translation is influenced by factors including tRNA availability, wobble-base interactions, mRNA secondary structures and protein sequences (Chaney and Clark, 2015; Choi et al., 2018; Rodnina, 2016). The nascent polypeptide can likewise negatively influence translational speed, e.g. decoding prolines is a challenging task and results in ribosome slowdown, as this amino acid creates an unfavorable positioning for the peptidyl transferase reaction (Choi et al., 2018; Wohlgemuth et al., 2008). Generally, slowdown of translation elongation is thought to provide nascent polypeptides more time to reach their native confirmation, but it also bears the risk of frameshifting and amino acid misincorporations, which can result in misfolding (Pechmann and Frydman, 2013; Rodnina, 2016; Wolf and Grayhack, 2015).

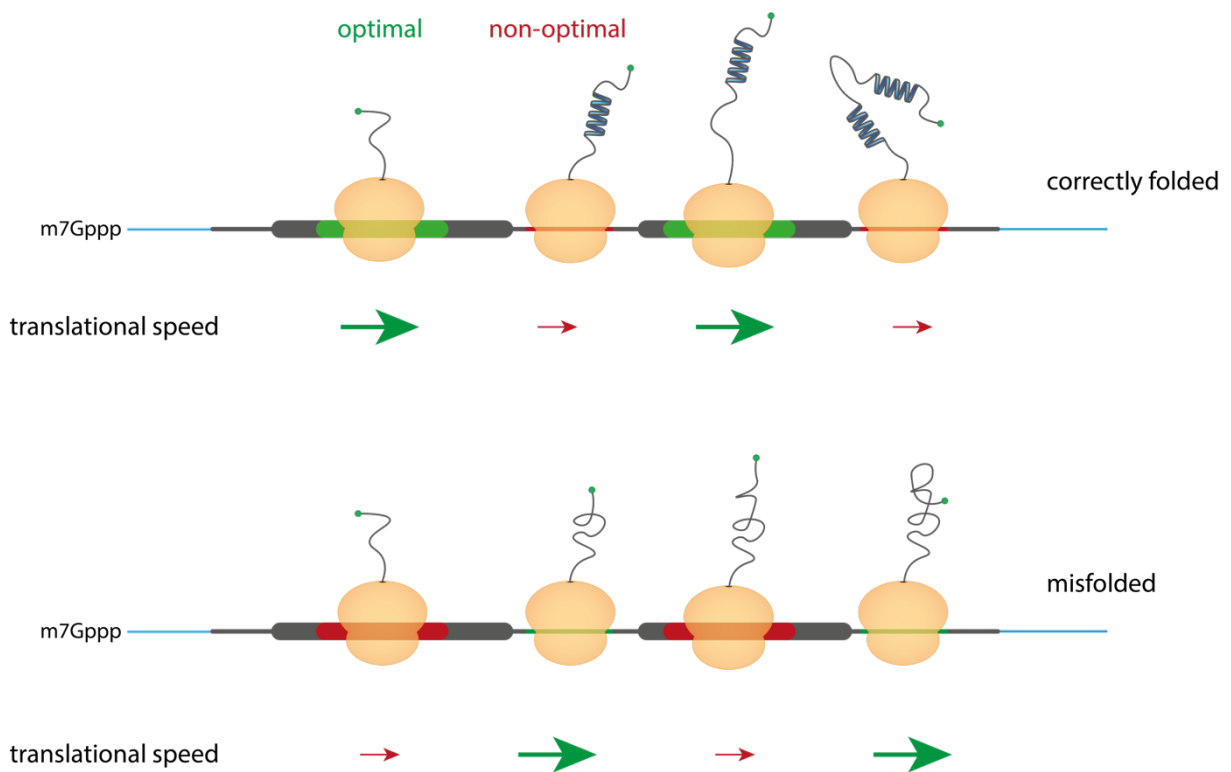


*Figure 12: Translational speed influences co-translational protein folding. Stretches of non-optimal codons following structural elements increase time for folding, while optimal codons within structural elements increase translational fidelity. Adapted from Hanson and Collier, 2018.*

The idea that translational slowdown is crucial for protein folding is a long-standing concept in the field (Purvis et al., 1987) (Figure 12). Subsequent studies showed that the codon context around structural elements is important to reach the correct fold (Thanaraj and Argos, 1996). Additionally, it was discovered that increased codon optimality in *E. coli* results in higher protein yields, however, the alterations can also lead to misfolding and non-functional protein species (Komar et al., 1999; Zhang et al., 2009). Altering tRNA abundances and thereby increase their availability led to misfolding, elucidating how tRNA levels influence translational speed, which in turn affects protein folding (Zhang et al., 2009). Similar results have been obtained in a cell-free translation system using luciferase as a model substrate. While changing non-optimal codons to optimal codons led to higher protein yields, the overall level of functional protein was reduced (Yu et al., 2015).

### Transmembrane protein biogenesis and quality control

Roughly one-third of all newly synthesized proteins are delivered to the endoplasmic reticulum (ER) in eukaryotic cells (Hsieh and Shan, 2021). This class of proteins is particularly prone to misfolding in the cytosol as their transmembrane domains (TMD) form large hydrophobic surfaces increasing the risk of undesirable interactions. Mislocalized membrane proteins are thus rapidly degraded (Hegde and Keenan, 2022). While there are also  $\beta$ -barrel structures inserted into membranes (Seshadri et al., 1998), most transmembrane domain segments consist of an  $\alpha$ -helix, shielding the hydrophilic amide backbone from the surrounding lipids (White and von Heijne, 2005). The topologies of transmembrane domains are quite variable and therefore necessitate multiple routes of membrane insertion. Currently, there are three established routes of insertion, which are chosen dependent on hydrophobicity and position of targeting sequences and/or the signal sequence.

To prevent promiscuous interactions from forming and ensure correct protein targeting, a cotranslational targeting system has evolved, mediated by the signal recognition particle (SRP) - the main mechanism of ER-targeting (Shao and Hegde, 2011). During the targeting process, the hydrophobic signal sequence, typically 7-9 amino acids in length and located towards the N-terminus of TMD proteins, is recognized by SRP and delivered to the SRP receptor anchored to the ER membrane (Hegde and Keenan, 2022). The nascent chain emerging from the ribosomal exit tunnel is initially shielded by the nascent polypeptide-associated complex (NAC), which under normal conditions prevents SRP from binding to the

ribosome, acting as a gatekeeper to prevent potential mistargeting of non-ER proteins (Figure 13). As the hydrophobic signal sequence emerges, NAC is displaced from the exit tunnel and enables SRP to engage the ribosome. The UBA domain of NAC tethers SRP to the ribosome and by a complex rearrangement of NAC. This allows SRP to directly engage the signal sequence. Throughout the process of SRP-mediated targeting, NAC stays always bound to the ribosome (Jomaa et al., 2022).

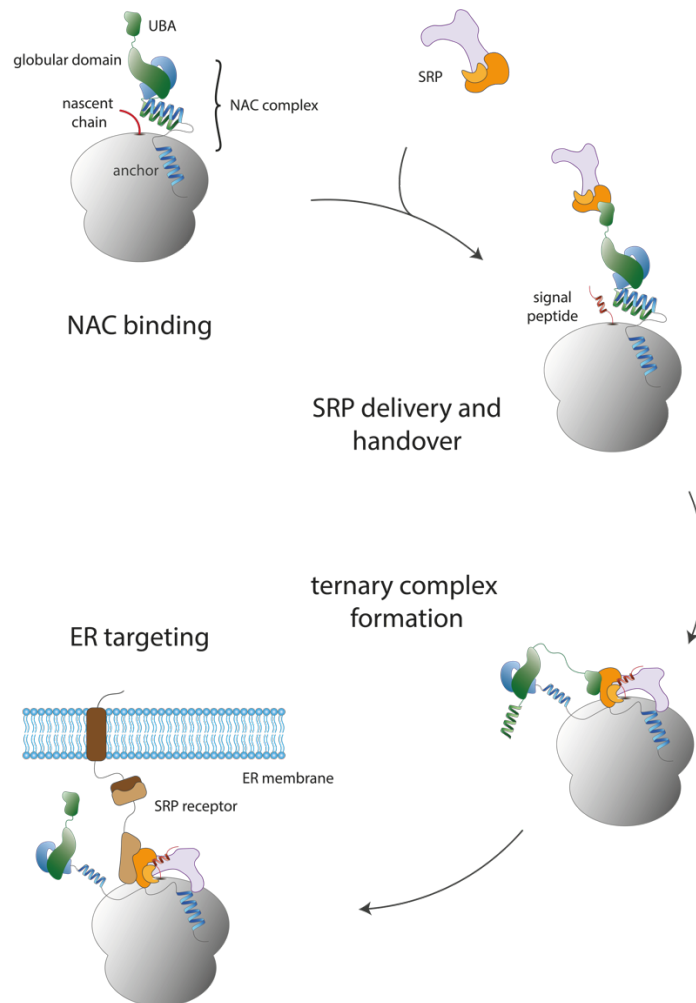


*Figure 13: NAC-mediated handover of ER signal-peptide to SRP to facilitate cotranslational insertion of proteins into the ER. Adapted from Jomaa et al., 2022. The N-terminal hydrophobic signal peptide pushes the NAC complex to the side as it emerges from the exit tunnel. At the same time, SRP is tethered to the ribosome by the NAC complex, forming an SRP-NAC ternary complex. Lastly, SRP binds to the SRP receptor, anchoring ribosomes to ER membranes, initiating the insertion of nascent chains into the translocon.*

Certain TMD containing proteins are targeted by a mechanism independent of SRP, with tail-anchored proteins (TA) being such a class, carrying a single transmembrane domain close to their carboxyl end. SRPs tight association with the ribosome ensures its priority over the GET pathway for TMD substrates. However, in the scenario for TA proteins, as their TMD remains buried in the exit tunnel till translation is concluded, SRP is unable to bind to the hydrophobic transmembrane segment (Schuldiner et al., 2008; Yamamoto and Sakisaka, 2012). As for SRP, the process of TA targeting, at least in part, occurs cotranslationally. The chaperones BAG6 and SGTA bind ribosomes close to the exit tunnel with the latter capturing the TMD as it emerges from the exit tunnel after translation is concluded (Mariappan et al., 2010; Zhang et al., 2021). The SGTA-bound TA is then handed over to ASNA1 while bound to the BAG6 complex, which facilitates the insertion of TA proteins into the membrane via GET1/WRB and GET2/CAML acting as a receptor (Schuldiner et al., 2008; Yamamoto and Sakisaka, 2012).

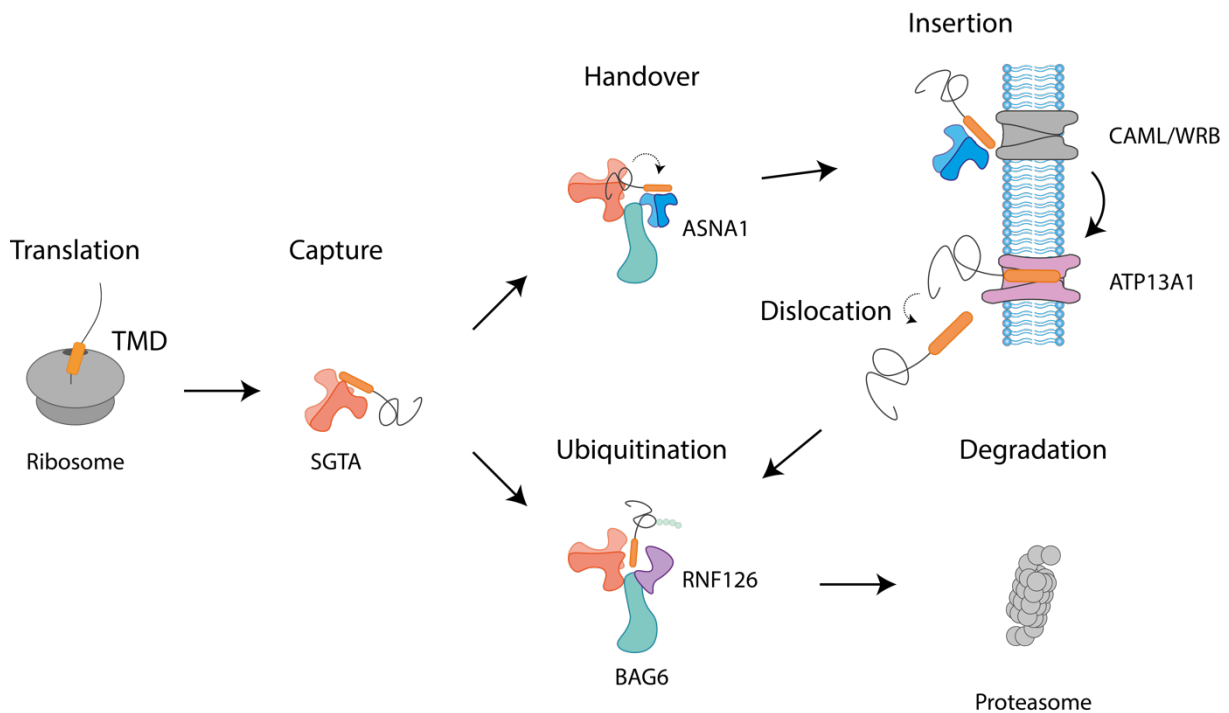


*Figure 14: Tail-anchored protein biogenesis and quality control. SGTA captures the TMD segment of the TA-protein co- or posttranslationally and recruits it to BAG6, where it either is handed over to ASNA1 for membrane insertion via CAML/WRB, or ubiquitinated by RNF126 and degraded by the proteasome. Mistargeted TA-proteins at the ER are retrotranslocated by ATP13A1 to be captured by the BAG6 complex, which either leads to another attempt at insertion or their degradation.*

Failure of TA protein targeting poses the risk of orphaned TMD proteins in the cytosol. In that case, SGTA binds to mislocalized TA and delivers the bound substrate to BAG6. The N-terminus of BAG6 in turn is recruiting the E3 ubiquitin ligase RNF126, and ubiquitinates the bound substrate. Ubiquitylation of orphaned TA proteins prevents the rebinding of SGTA and targets them to the proteasome for degradation (Hessa et al., 2011; Rodrigo-Brenni et al., 2014). Likewise, transmembrane proteins can end up being inserted into the wrong cellular compartment. Cells have developed defense strategies to clear such incorrectly inserted membrane proteins and retro-translocate them to the cytosol. In ER membranes, the P5A-ATPase ATP13A1 has been identified to recognize mistargeted membrane proteins and ATAD1 as the mitochondrial counterpart (McKenna et al., 2020; Wohlever et al., 2017).

### Translation and ageing

Ageing is characterized by a progressive decline in proteostasis capacity resulting in an increasing susceptibility to develop proteome imbalance (Walther et al., 2015). It is the main risk factor for a multitude of neurodegenerative diseases, such as Alzheimer's disease and Parkinson's disease (Chiti and Dobson, 2017). Proteins need to be folded into their correct structures to be functional. In *E. coli*, it is estimated that roughly one-third of the proteome is folded cotranslationally (Ciryam et al., 2013). Cotranslational protein folding depends on optimal translation rates and translational fidelity. However, as the organism ages, translational fidelity is increasingly impaired. As a result, proteins accumulate in non-functional aggregates in the cytosol, posing the risk of sequestering other factors by promiscuous interactions, thereby driving the proteostatic collapse (Chiti and Dobson, 2017).

Translation elongation rates and translation initiation generally decline with age, reducing overall protein production (Gerashchenko et al., 2021). Many lifespan extending pathways have been linked to altered translation rates, such as the insulin-like growth factor (IGF-1) pathway, target of rapamycin (TOR) pathway, p38 mitogen-activated protein kinase (MAPK) pathway or integrated stress response (ISR) (Gonskikh and Polacek, 2017).

Experimental evidence suggests that down-regulation of translation has a beneficial effect on lifespan in a large variety of organisms. Therefore, the question arises whether the observed reduced protein biosynthesis in aged organisms causes ageing or is a response to physiological changes during ageing. In yeast, gene deletion of several ribosomal proteins, which in turn reduce protein biosynthesis, were found to have lifespan-extending effects

(Chiocchetti et al., 2007; Kaeberlein et al., 2005). Likewise, siRNA-mediated depletion of several ribosomal subunits reduced translation which led to an extended lifespan in *C. elegans* (Hansen et al., 2007). In contrast, reducing translation fidelity of ribosomes leads to accelerated ageing phenotypes and reduced lifespan (Shcherbakov et al., 2022). In line with the idea that reduced translation is beneficial for ageing, down-regulation of translation initiation factors was shown to increase lifespan significantly (Curran and Ruvkun, 2007).

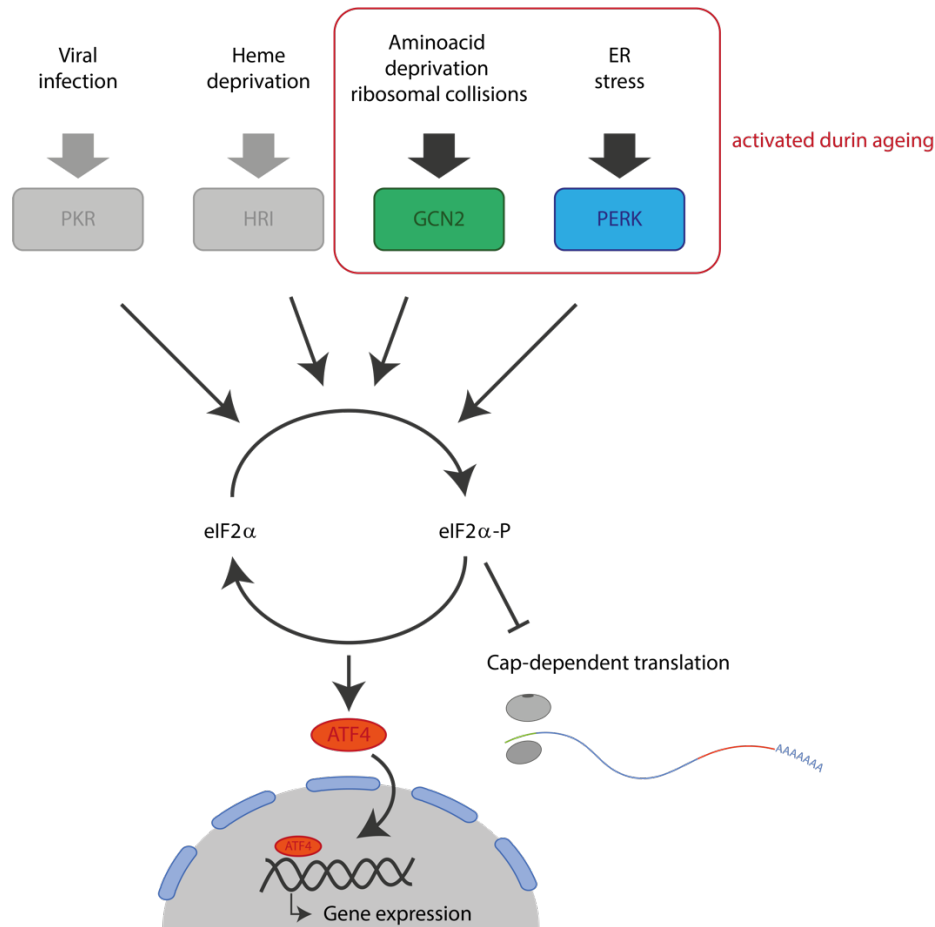


Figure 15: Schematic overview of integrated stress response signaling. There are four known phosphokinases that phosphorylate eIF2 $\alpha$ , which are activated by different stresses, such as viral infection (PKR), heme deprivation (HRI), ER stress (PERK) and amino acid depletion and/or ribosomal collision (GCN2). Moreover, GCN2 and PERK are activated during ageing leading to increased phosphorylation of eIF2 $\alpha$ , which leads to the activation of increased transcription of stress-related genes via ATF4 and inhibits cap-dependent translation.

The ISR acts as a translation control pathway by modulating translation initiation. Stress signaling is mediated by several kinases, which phosphorylate eIF2 $\alpha$ . That in turn stabilizes the interaction of eIF2 $\alpha$  with its GTP exchange factor eIF2B, thereby reducing global

translation rates. So far there are four kinases known to initiate the ISR, with each kinase responding to a distinct form of stress. Two kinases, eukaryotic translation initiation factor 2- $\alpha$  kinase (EIF2AK4), also known as GCN2, and PKR-like endoplasmic reticulum kinase (PERK), which are both activated by amino-acid starvation or ER-stress, respectively, have also previously been described to be activated during ageing. Besides acting as a global repressor of mRNA translation, ISR activates the translation of specific genes involved in the response to stress. Activating transcription factor 4 (ATF4) is a well-studied target that is regulated via an upstream open reading frame (uORF), and under normal conditions repressed. However, upon phosphorylation of eIF2 $\alpha$ , ribosomes translate past the uORF, driving the expression of ATF4 coding sequence (CDS). ATF4 acts as a transcription factor, inducing the expression of the C/EBP homologous protein (CHOP), which in turn increases apoptotic signaling.

The unfolded protein response activates the ISR via PERK in a situation of accumulating misfolded protein in the ER (Chadwick and Lajoie, 2019). Several chaperones are required to maintain the folding capacity within the ER lumen and ensure proper formation and secretion of newly synthesized proteins (Woodward and Shirokikh, 2021). If the folding capacity is impaired, the UPR is activated, which in turn triggers the ISR via PERK, shutting down global protein biosynthesis (Estebanez et al., 2018). In aged organisms, the abundance of ER chaperones is decreased, which results in an imbalance in protein folding capacity and therefore in the accumulation of misfolded proteins, activating PERK (Chadwick et al., 2020). GCN2 is the second known kinase that can trigger the ISR and is activated as the organism ages. In yeast, lowering eIF2 $\alpha$ -P reduced lifespan, while its induction had a positive influence on autophagy, resulting in a prolonged lifespan (Hu et al., 2018). However, there are conflicting reports in *C. elegans*. While one study demonstrated that loss of eIF2 $\alpha$  phosphorylation had a positive effect on lifespan (Derisbourg et al., 2021), another report showed that in the long-lived *daf-2* mutant animals, eIF2 $\alpha$  phosphorylation contributes to the lifespan extension (Li et al., 2021). This would indicate that based on the situation, the ISR is operating in an optimal activation window (Costa-Mattioli and Walter, 2020).

The ISR has been implicated in several neurological processes. A low-level activation of the ISR is beneficial for memory formation (Bellato and Hajj, 2016; Delaidelli et al., 2019), while a prolonged hyperactivated ISR in the brain is implicated in several neurodegenerative diseases including Alzheimer's disease, and Parkinson's disease. Inhibition of the ISR by an ISR

inhibitor (ISRIB) was shown to improve the disease phenotype and prevent memory deficits in aged mice (Jan et al., 2018; Krukowski et al., 2020; Longo et al., 2021).

While ISR activation seems to be overall protective in aged single cell organisms, hyperactive ISR can have the opposite effect in multicellular animals (Moon et al., 2018). The extent to which ISR is beneficial for different cell types in higher eukaryotes remains unclear, and further research is required.

There are several reasons that could explain the underlying mechanism for prolonged lifespan caused by reduced translation rates. Translation is energetically a very expensive process. By reducing the translation rates, energy can be redistributed to other processes, such as DNA quality control (Gonskikh and Polacek, 2017). High translation rates also result in the accumulation of faulty protein products, caused by either inefficient co-translational folding or translational errors (Anisimova et al., 2020). This either leads to the loss of function of proteins or gain of toxicity by forming potentially toxic aggregates cells. Reducing overall protein synthesis rates might aid in reducing the burden on the proteostasis network by allowing efficient detection and refolding of faulty products, or their degradation.

### Sensing, clearing, and preventing ribosomal collisions

The decline in translational fidelity with increasing age of the organism has been observed across different species including yeast, mice, and humans (Gerashchenko et al., 2021; Hu et al., 2018; van Heesch et al., 2019). The loss of fidelity and slowdown of translation is accompanied by increased ribosomal stalling at certain motifs, including polybasic stretches (Stein et al., 2022). Ribosomal stalling eventually can lead to ribosome collisions if the trailing ribosome catches up to the stalled lead ribosome. Ribosomal stalling may result in production of incomplete proteins, which are unable to fold and may cause toxic effects. To deal with such aberrant and incomplete polypeptides, cells have evolved a ribosome associated quality control (RQC) pathway (Sitron and Brandman, 2020).

Ribosomal collisions, the main triggers for RQC, are sensed by the E3 ubiquitin RING ligase ZNF598 (Hel2 in yeast) (Juszkiewicz et al., 2018), which facilitates the clearance of the nascent polypeptide. ZNF598 binds to the 40S-40S interface of the two collided ribosomes and ubiquitinates proteins of the small ribosomal subunit, such as RPS3, RPS10 and RPS20. The flagged ribosomes are subsequently recognized by the RQC trigger (RQT) complex, which

facilitates ribosomal splitting. The nascent chain that stays attached to the 60S subunit of the ribosome is engaged by NEMF (RQC2). NEMF non-canonically elongates the nascent chain with alanine and threonine residues (commonly referred to as CAT tails) (Shen et al., 2015), which have been shown to act as a potent degron (Sitron and Brandman, 2019; Udagawa et al., 2021). Additionally, the E3 ubiquitin ligase listerin 1 (LTN1) is recruited by NEMF to the 60S ribosome, ubiquitinating the nascent chain (Choe et al., 2016). The subsequent nascent chain release is orchestrated by ANKZF1, a peptidyl tRNA hydrolase, and VCP, extracting the polypeptide from the 60S ribosomal exit tunnel (Sitron and Brandman, 2020). The ubiquitinated nascent chain is then degraded by the proteasome. The process of protein clearance is tightly coupled to degradation of such potentially aberrant mRNAs, which is facilitated by the exosome with SKIV2L acting as an adapter protein or by XRN1 (Park et al., 2021).

Recently a second line of defense against ribosomal collisions has been identified. Several stresses, such as ribotoxins or UV radiation led to a global increase of ribosomal collisions. Ribosome-associated factors initiate cellular stress responses such as the ISR or ribotoxic stress response (RSR), attenuating general translation and dependent on the extent and duration of collision persistence, decide the cellular fate of either stress resolution or activation of cell death (Wu et al., 2020). Ribosome collisions lead to the phosphorylation of eIF2 $\alpha$  via GCN2, activating the ISR. GCN2 was originally shown to play a central role in sensing amino acid deprivation. It exhibits sequence similarities to the histidyl-tRNA synthase, likely allowing the interaction with uncharged tRNAs and thereby surveilling cellular tRNA charging status (Dong et al., 2000). Further, GCN2 binds directly to ribosomes via the P-stalk, mediating the GCN2-dependent activation of ISR (Harding et al., 2019; Inglis et al., 2019). Treatment of cells with intermediate doses of the translation inhibitor anisomycin induces the ISR in a GCN2-dependent manner mediated by ZAK $\alpha$  (a MAPKKK kinase) and GCN1 (a GCN2 cofactor). In contrast, a saturating dose of anisomycin is unable to induce the ISR, indicative of ribosomal collisions as a pre-requisite for induction (Wu et al., 2020). In an acute situation of ribosomal collisions, activation of ISR is believed to increase cellular survival by reducing the translational load (Wu et al., 2020). ZAK $\alpha$  is known to associate with the ribosome itself, signaling the RSR when ribosomes frequently collide, and collisions persist. ZAK $\alpha$  is autophosphorylated upon prolonged collisions and activates the RSR via the MAPK cascade, with downstream

phosphorylation of p38 and JNK, implicated in apoptosis and inflammation responses (Canovas and Nebreda, 2021; Coffey, 2014; Wu et al., 2020).

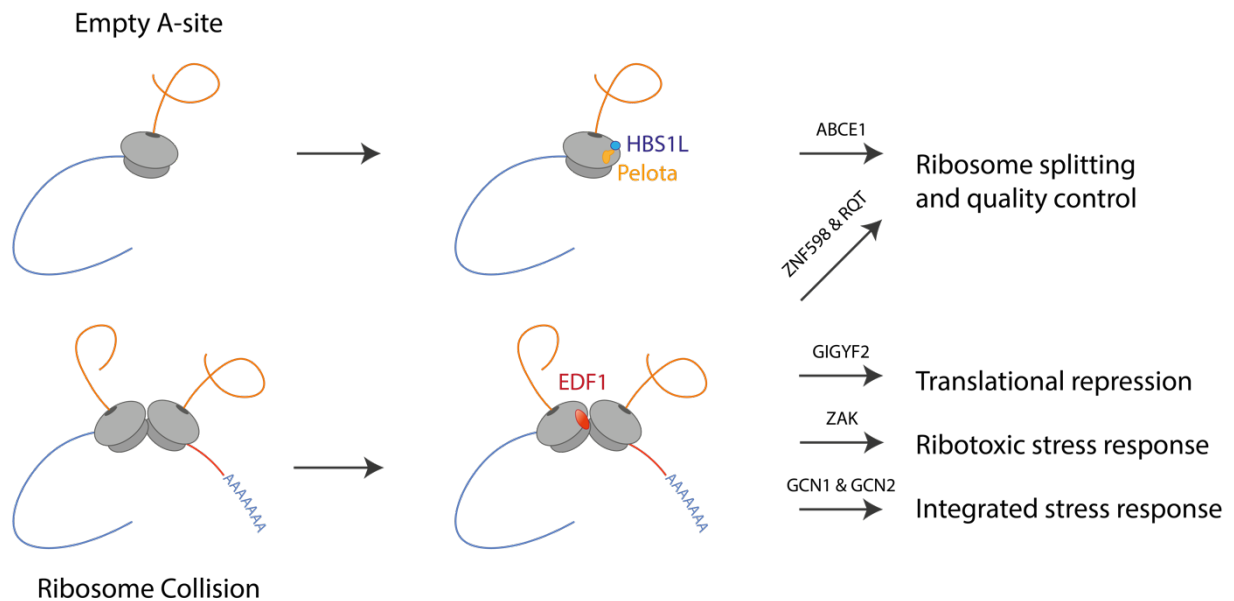


*Figure 16: Mechanisms of sensing and rescuing stalled ribosomes. Ribosomes that reach the end of a cleaved transcript fail to terminate translation and are trapped on the mRNA. In such a situation, ribosomal splitting and recycling is aided by HBS1L and Pelota together with ABCE1. The nascent chain is then removed by the RQC machinery. Ribosomes can also be stalled and eventually collide for extended periods when translating either poly-basic stretches, sequences rich in nonoptimal codons or polyproline regions. Such collided ribosomes are identified by EDF1 orchestrating downstream responses, such as translational repression via GIGYF2. If collisions remain unresolved, induction of the ribotoxic stress response occurs via ZAK, or the integrated stress response involving GCN1 and GCN2. This lowers the general translational output of cells to prevent further ribosomal collisions.*

On the other hand, EDF1 is believed to be the first protein to engage collided ribosomes before invoking the RQC (Juszkiewicz et al., 2020; Sinha et al., 2020). Only if collisions persist, are the stalling sensor ZNF598 and GIGYF2-4EHP recruited. The latter acts as a translation repressor and trigger for mRNA decay, whereas ZNF598 ubiquitinates RPS subunits initiating the RQC cascade (Hickey et al., 2020; Juszkiewicz et al., 2020; Weber et al., 2020). Interestingly, EDF1 has been found to be associated with GCN1 during the process of sensing collided ribosomes.

Here, the role of EDF1 is likely to suppress frameshifting, that may arise as a consequence of ribosomal collisions (Pochopien et al., 2021; Simms et al., 2019).

While the three known ribosome-associated surveillance pathways have their unique initiation sensors, like ZNF598 for the RQC pathway, GCN1/2 for ISR, and ZAK $\alpha$  for RSR, they share collided ribosomes as their trigger. This invites the question why three pathways have evolved independently to deal with the same problem. Most likely, there is crosstalk between the three described pathways, potentially acting as failsafe options for one another. This idea is supported by the fact that although RQC activation is not dependent on RSR (Vind et al., 2020), the RSR is aggravated in the absence of ZNF598 (Wu et al., 2020).

Disome-profiling experiments have revealed that ribosomal collisions are frequent events on endogenous mRNAs at basal conditions (up to ~10% of total ribosomes) (Arpat et al., 2020; Han et al., 2020; Meydan and Guydosh, 2020; Zhao et al., 2021). As discussed before, ribosomal collisions can be induced by several factors such as unfavorable codon-pairs, proline/lysine/arginine stretches and during translation termination. However, not all ribosome collisions will elicit protective responses. Some stalling and collision events are essential for co-translational regulation, e.g. targeting of proteins to certain organelles (e.g. XBP1) or efficient folding of certain domains (Zhao et al., 2021). Thus, a question arises – How do cells differentiate between productive stalling/collision events and collisions that results from erroneous processes? While the exact mechanisms remain unclear, it is currently believed that when pathological collisions occur only on a few selected mRNAs, RQC is the prioritized response. However, if collisions happen at a global scale, and eventually overwhelm the RQC machinery, the fail-safe mechanisms such as ISR and RSR are activated. This model is challenged, however, by the recent finding that GCN1 is found to be bound to ~50% of collided ribosomes at basal conditions (Fedry et al., 2023). Nevertheless, the GCN1/2-dependent activation of ISR would reduce global translation, thereby reducing the chances for further ribosomal clashes and promoting the expression of stress-related genes via ATF4. If that does not lead to a mitigation of collisions, RSR is activated via ZAK $\alpha$ , ultimately signaling for apoptosis of the affected cell, while ensuring the overall survival of a multicellular organism.

## Translation readthrough mitigation

A potentially significant source of aberrant translation products is the failure of translation termination at the stop codon, resulting in read-through of ribosomes into the 3' untranslated region, thereby generating C-terminally extended polypeptides (CTE). Translation through the 3'UTR into the polyA tail generates ribosome-stalled nascent chains that trigger the activation of the ribosome quality control (RQC) pathway (Sitron and Brandman, 2020). However, the 3'UTR sequences preceding the polyA sequence can be rather long, in some cases exceed a few kilobases, and for most transcripts an additional termination codon occurs before the ribosome reaches the polyA tail. The resulting nascent polypeptides are therefore not substrates of the RQC pathway. Depending on the mRNA, readthrough can add up to hundreds of amino acids to the nascent chain. Several pathologies are caused by late frameshifts or stop codon mutations resulting in proteins with 3'UTR-encoded CTEs with some of them resulting in a loss of function and some leading to the production of aberrant proteins that may form gain of function toxic aggregates. Moreover, ageing has been associated with increased stop codon readthrough in *Drosophila*, with neurons being particularly susceptible to translation termination errors (Chen et al., 2020). Although the fidelity of protein translation termination is crucial, readthrough is much more pervasive than initially thought, with readthrough efficiencies estimated to vary from <1% to 10% or more (Dunn et al., 2013), posing a sizable problem.

Nematodes limit the toxic effects of readthrough proteins by efficiently clearing them, especially when their 3'UTRs encode for amino acid sequences hydrophobic in nature (Arribere et al., 2016). There are different proposed models as to how that mitigation is facilitated. While ubiquitin-dependent proteasomal degradation has been implicated in this process of readthrough mitigation (Dhamija et al., 2020; Shibata et al., 2015), other studies suggested ribosome queuing and translation inhibition as a means of limiting CTE protein production (Hashimoto et al., 2019; Yordanova et al., 2018). More recently, elimination of readthrough proteins was reported to occur via lysosomal degradation independent of the ubiquitin proteasome system (Kramarski and Arbely, 2020). Thus the underlying clearance mechanism and the machineries involved in translation readthrough mitigation remain to be characterized.

## Summary

Cells invest tremendously to maintain the fidelity for transcription and translation to ensure accurate transmission of the genetic code into proteins. Yet, errors may occur at each stage. During transcription, errors arise at a rate of  $\sim 10^{-5}$ - $10^{-4}$  per base, whereas the error rate during translation is around a magnitude higher with  $\sim 10^{-4}$ - $10^{-3}$  amino acid misincorporations per codon. Such errors become increasingly frequent with ageing, posing a sizable risk for the organism. In some instances, this leads to missing or misread stop codons, allowing translation to continue into the 3'UTRs of transcripts. Such C-terminal extensions may interfere with the folding of proteins, or worse, promote promiscuous interactions with other proteins, which in turn may disturb cellular processes and reduce overall fitness. Translation into the polyA-tail of transcripts leads to the activation of the ribosome quality control (RQC) complex, which clears both aberrant protein and mRNA.

However, in most cases, translation would be terminated at stop codons within the 3'UTR before the ribosome reaches the polyA-tail. Such readthrough events would therefore not be recognized by the RQC. While previous studies suggested that such readthrough products are recognized and efficiently cleared by cells, the underlying mechanism remained unclear. Given the decline in translational fidelity during ageing, this clearance pathway is expected to become increasingly important to release the burden on the proteostasis network. Using the nematode *C. elegans* as a model for ageing, we aimed to identify the quality control mechanisms mitigating translational readthrough and investigated the consequences of their failure during ageing.

Using this approach, we identified in *C. elegans* and human cells that readthrough proteins are cleared through a coupled, two-level quality control pathway involving the BAG6 chaperone complex and the ribosome collision-sensing protein GCN1. Readthrough proteins with hydrophobic C-terminal extensions are recognized by SGTA-BAG6 and ubiquitylated by RNF126 for proteasomal degradation. Additionally, cotranslational mRNA decay mediated by GCN1 and CCR4/NOT limits the accumulation of readthrough proteins. Selective ribosome profiling uncovered a general role of GCN1 in regulating translation dynamics when ribosomes encounter non-optimal codons, a feature of 3'UTR sequences. Dysfunction of GCN1 results in mRNA and proteome imbalance, increasingly affecting transmembrane proteins and collagens during ageing. These results define GCN1 as a key factor acting during translation in maintaining protein homeostasis.

## Materials and methods

Reagent or Resource	Source	Identifier
<b>Antibodies</b>		
M2 Flag antibody	Sigma	F1804
GFP antibody	Roche	11814460001
$\alpha$ -tubulin	Merck	T6199
Phospho-eIF2 $\alpha$	Abcam	ab32157
Phospho-p38 MAPK	Cell Signaling	9211S
eRF3	Abcam	ab126090
eRF1	Santa Cruz	sc-365686
<b>Recombinant DNA</b>		
unc-54p::YFP-STOP	This study	pPK86
unc-54p::YFP-UTR	This study	pPK89
unc-54p::mScarlet-T2A-YFP(NotI)myo-3p::CFP	This study	pMM23
unc-54p::mScarlet-T2A-YFP-slc-17.5(3UTR) myo-3p::CFP	This study	pMM24
unc-54p::mScarlet-T2A-YFP-F40D4.17(3UTR) myo-3p::CFP	This study	pMM25
unc-54p::mScarlet-T2A-YFP-R160.3(3UTR) myo-3p::CFP	This study	pMM26
unc-54p::mScarlet-T2A-YFP-T21C12.3(3UTR) myo-3p::CFP	This study	pMM27
unc-54p::mScarlet-T2A-YFP-sec-61.b myo-3p::CFP	This study	pMM28
unc-54p::mScarlet-T2A-YFP-sec-61.b(TA) myo-3p::CFP	This study	pMM29
unc-54p::mScarlet-T2A-YFP-STOP-slc-17.5(3UTR) myo-3p::CFP	This study	pMM30

unc-54p::mScarlet-T2A-YFP-STOP-F40D4.17(3UTR) myo-3p::CFP	This study	pMM31
unc-54p::mScarlet-T2A-YFP-STOP-R160.3(3UTR) myo-3p::CFP	This study	pMM32
unc-54p::mScarlet-T2A-YFP-STOP-T21C12.3(3UTR) myo-3p::CFP	This study	pMM33
unc-54p::mScarlet-T2A-YFP-STOP-sec-61.b myo-3p::CFP	This study	pMM34
unc-54p::mScarlet-T2A-YFP-STOP-sec-61.b(TA) myo-3p::CFP	This study	pMM35
unc-54p::mScarlet-T2A-T2A-YFP	This study	pMM36
unc-54p::mScarlet-T2A-F40D4.17(3UTR)-T2A-YFP	This study	pMM37
unc-54p::mScarlet-T2A-F40D4.17(3UTR)-T2A-YFP codon optimized 1	This study	pMM38
unc-54p::mScarlet-T2A-F40D4.17(3UTR)-T2A-YFP codon optimized 2	This study	pMM39
unc-54p::mScarlet-T2A-SLC-17.5(3UTR)-T2A-YFP	This study	pMM40
unc-54p::mScarlet-T2A-SLC-17.5(3UTR)-T2A-YFP codon optimized 1	This study	pMM41
unc-54p::mScarlet-T2A-SLC-17.5(3UTR)-T2A-YFP codon optimized 2	This study	pMM42
unc-54p::mScarlet-T2A-K <sub>20</sub> (AAA)T2A-YFP	This study	pMM43
pCMV-mScarlet-P2A-P2A-EYFP(XbaI) pCMV-mTurq2	This study	pMM44
pCMV-mScarlet-P2A-P2A-EYFP-TCEAL1(3UTR) pCMV-mTurq2	This study	pMM45

pCMV-mScarlet-P2A-P2A-EYFP-(3UTR) pCMV-mTurq2	This study	pMM46
pCMV-mScarlet-P2A-P2A-EYFP- CNIH3(3UTR) pCMV-mTurq2	This study	pMM47
pCMV-mScarlet-P2A-P2A-EYFP- OR8D4(3UTR) pCMV-mTurq2	This study	pMM48
pCMV-mScarlet-P2A-P2A-EYFP- CCK(3UTR) pCMV-mTurq2	This study	pMM49
pCMV-mScarlet-P2A-P2A-EYFP-SEC- 61.B pCMV-mTurq2	This study	pMM50
pCMV-mScarlet-P2A-P2A-EYFP-SEC- 61.B(TA) pCMV-mTurq2	This study	pMM51
pCMV-EYFP	This study	pMM52
pCMV-EYFP-TCEAL(3UTR)	This study	pMM53
pCMV-EYFP pCMV-mTurquoise2	This study	pMM54
pCMV-mScarlet pCMV-mTurquoise2	This study	pMM55
<b>Oligonucleotides</b>		
qPCR tba-1 fw: ACCAACAAGCCGATGGAGAA	This study	N/A
qPCR tba-1 rev: ACCACGAGCGTAGTTGTTGG	This study	N/A
qPCR pmp-3 fw: CACTTTCACCGCCCAATGAC	This study	N/A
qPCR pmp-3 rev: TCGACGCCAATGACAATCCA	This study	N/A
qPCR EYFP fw: TGAACCTCAAGATCCGCCACA	This study	N/A
qPCR EYFP rev: TTCTCGTTGGGGTCTTTGCT	This study	N/A
qPCR hsp-16.1 fw: AGATATGGCTCAGATGGAACGTC	This study	N/A
qPCR hsp-16.1 rev: GCTTGAAGTGCAGACATTGAG	This study	N/A

qPCR hsp-16.2 fw: TCCATCTGAGTCTTCTGAGATTGTT	This study	N/A
qPCR hsp-16.2 rev: TGATAGCGTACGACCATCCAAA	This study	N/A
qPCR hsp-16.48 fw: GCTCATGCTCCGTTCTCCAT	This study	N/A
qPCR hsp-16.48 rev: TGAGAAACATCGAGTTGAACAGAGA	This study	N/A
qPCR hsp-70 fw: CCGTTGAAAAGGCACTTCG	This study	N/A
qPCR hsp-70 rev: GAGCAGTTGAGGTCCTCCC	This study	N/A
YFP Probe #1 TGAAGTTGTGGCCGTTTACG	This study	N/A
YFP Probe #2 TGGTGCAGATGAACTTCAGG	This study	N/A
YFP Probe #3 TAGCCGAAGGTGGTCACGAG	This study	N/A
YFP Probe #4 AAGAAGTCGTGCTGCTTCAT	This study	N/A
YFP Probe #5 CTTGAAGAAGATGGTGCCT	This study	N/A
YFP Probe #6 TTGAAGTCGATGCCCTTCAG	This study	N/A
YFP Probe #7 TAGACGTTGTGGCTGTTGTA	This study	N/A
YFP Probe #8 CTTGAAGTTCACCTTGATGC	This study	N/A
YFP Probe #9 TAGCTCAGGTAGTGGTTGTC	This study	N/A
YFP Probe #10 TCGTCCATGCCGAGAGTGAT	This study	N/A

<b><i>C.elegans</i> strains</b>		
<i>unc-54p::YFP-STOP</i>	This study	FUH277
<i>unc-54p::YFP-UTR</i>	This study	FUH279
<i>unc-54p::YFP-UTR; rpn-10 (ok1865)</i>	This study	FUH492
<i>unc-54p::YFP-UTR; hsp-16s (mar01)</i>	This study	FUH370
<i>unc-54p::YFP-STOP; hsp-16s (mar01)</i>	This study	FUH369
<i>unc-54p::YFP-UTR; rnf-126 (gk504603)</i>	This study	FUH432
<i>unc-54p::YFP-UTR; gcn-1 (nc40)</i>	This study	FUH491
<i>unc-54p::YFP-UTR; skih-2 (cc2854)</i>	This study	FUH483
<i>3xFLAG-gcn-1(mar02)</i>	This study	FUH503
<i>skih-2(cc2854) 2x BC</i>	Andrew Fire lab	PD2860
<i>gcn-1(nc40)</i>	CGC	ST60
<i>rnf-126(gk504603) 6x BC</i>	CGC	FUH431
<b>Cell lines</b>		
HEK293T	ATCC	-
<b>Enzymes and Chemicals</b>		
Cycloheximide	Sigma Aldrich	01810
riboPOOL Ribo-Seq 12 reaction Kit	Biozym	27DP-K012-000067
SUPERase•In RNase Inhibitor	Thermo	AM2694
5' DNA Adenylation kit	NEB	E2610L
cOmplete EDTA-free Protease Inhibitor Cocktail	Roche	11873580001
microRNA marker	NEB	N2102S
Direct-zol RNA Miniprep	Zymo	R2050
Novex TBE-Urea Gels	Thermo	EC68852BOX
Ultra-Low Range DNA Ladder	Thermo	10597012
T4 Polynucleotide Kinase	NEB	M0201S
T4 RNA Ligase 2, truncated K227Q	NEB	M0351S
Deadenylase	NEB	M0331S

ProtoScript® II Reverse Transcriptase	NEB	M0368L
Quantit Ribogreen RNA reagent	Invitrogen	R11490
RNAseI 10u/ul	Biozym	173010
Circ ligase I	Biozym	131401
Novex TBE Gels 8% 15-well	Thermo	EC62155BOX
Lipofectamine 3000	Thermo	L3000008
TRIzol Reagent	Thermo	15596026
QuantiTect Rev. Transcription Kit	Qiagen	205311
NEBuilder HiFi DNA Assembly Master Mix	NEB	E2621L
GFP-Trap Magnetic Agarose	Chromotek	gtma
Anti-FLAG® M2 Magnetic Beads	Sigma Aldrich	M8823
iST Kit 96x	preomics	P.O.00027
Phusion	NEB	M0530L
CC-885	MedChemExpress	HY-101488
Geneticin Selective Antibiotic (G418 Sulfate)	Thermo	10131027
<b>Software and Algorithms</b>		
DESeq2	<a href="https://github.com/mikelove/DESeq2">https://github.com/mikelove/DESeq2</a>	N/A
STAR	<a href="https://github.com/alexdobin/STAR">https://github.com/alexdobin/STAR</a>	N/A
Bowtie2	<a href="https://github.com/BenLangmead/bowtie2">https://github.com/BenLangmead/bowtie2</a>	N/A
umi_tools	<a href="https://github.com/CGATOxford/UMI-tools">https://github.com/CGATOxford/UMI-tools</a>	N/A
RiboWaltz	<a href="https://github.com/LabTranslationalArchitectomics/riboWaltz">https://github.com/LabTranslationalArchitectomics/riboWaltz</a>	N/A
RiboMiner	<a href="https://github.com/xryanglab/RiboMiner">https://github.com/xryanglab/RiboMiner</a>	N/A
codonDT	<a href="https://github.com/cgob/codonDT_snake">https://github.com/cgob/codonDT_snake</a> make	N/A
Fiji		N/A
Graphpad Prism		N/A
biopython	<a href="https://github.com/biopython/biopython">https://github.com/biopython/biopython</a>	N/A
kplogo	<a href="http://kplogo.wi.mit.edu/">http://kplogo.wi.mit.edu/</a>	N/A
GeneOntology	<a href="http://geneontology.org/">http://geneontology.org/</a>	N/A
Perseus		N/A

MaxQuant		N/A

### C. elegans strains and maintenance

The Bristol strain N2 was used as wild-type. Strains used in this study are listed in the Key Resource Table. Worms were grown on nematode growth medium (NGM) seeded with OP50 bacteria and maintained at 20°C unless otherwise indicated. For liquid culture, worm eggs were collected by bleaching and synchronized populations of L1 larvae were obtained by overnight growth in M9 medium. The L1 larvae were grown in S Basal in presence of OP50 bacteria.

### Cas9 expression and purification

Cas9 purification was adapted from Paix et al. (2015). BL21 (DE3) *E. coli* were transformed with pHO4d-Cas9 (Addgene #67881) (Paix et al., 2015). The main culture was induced at a density of OD<sub>600</sub> = 0.8 with a final concentration of 0.2 mM IPTG at 18°C overnight. Cells were collected by centrifugation and 6 ml Buffer A (20 mM Tris pH 8.0, 250 mM KCl, 20 mM Imidazole, 10% glycerol, 1 mM TCEP, 1x EDTA-free protease inhibitor) was added per gram of wet culture. Lysozyme was added to a final concentration of 1 mg/ml (Sigma L6876). The suspension was lysed by sonication on ice (10% amplitude, 1.5 s pulse, 5 s pause) for a total time of 45 min. The lysate was clarified by centrifugation at 16,000 x g and the supernatant transferred to a fresh tube. Clarified lysate was passed over a 5 ml HisTrap Hp column (GE Healthcare) at a flowrate of 0.5 ml/min and washed with 100 ml of buffer B (20 mM Tris pH 8.0, 800 mM KCl, 20 mM imidazole, 10% glycerol, 1mM TCEP). The bound protein was eluted with 20 column volumes of a gradient from 0-100% buffer C (20 mM Hepes pH 8.0, 500 mM KCl, 250 mM imidazole, 10% glycerol). Eluent was passed over a MonoQ column to remove Cas9-bound DNA and the flowthrough was collected. To remove any aggregated Cas9 protein, the flowthrough was separated on a 26/60 Sephacryl S-200 column (GE Healthcare #17Z1195Z01) with Buffer D (20mM Hepes pH 7.5, 500 mM KCl, 20% glycerol). Fractions containing monomeric Cas9 were pooled and concentrated to 10 mg/ml by centrifugation through a 100K filter (Milipore, UFC910024).

### CRISPR/Cas9-mediated homologous recombination

Generation of transgenic animals was performed as previously described with adaptations (Paix et al., 2015). An aliquot of 5 µl purified Cas9 was thawed on ice and incubated with a 100mer sgRNA (Synthego) targeting the gene of interest and *dpy-10* as an injection control for 10 min at room temperature (RT). For deletions/knockouts ssODNs (synthetic single-stranded oligodeoxynucleotide donors) were ordered from Integrated DNA Technologies (IDT) as a repair

template and reconstituted to a concentration of 1 mg/ml for the gene of interest and 0.5 mg/ml for *dpy-10*. After incubation, 2.2  $\mu$ l of ssODN for the gene of interest and 0.55  $\mu$ l of ssODN against *dpy-10* was added to the injection mix. To keep Cas9 soluble, 0.5  $\mu$ l of 1 M KCL and 0.75  $\mu$ l of 200 mM Hepes pH 7.4 was added. The injection mix was topped up to 20  $\mu$ l with water and centrifuged at 20,000 x g for 2 min before injecting it into the gonads of the nematodes. The injection mix or ribonucleoprotein complexes (protein Cas9, tracrRNA, crRNA) and ssODN were microinjected into the gonad of young adults using standard methods. Single injected worms were placed at 20°C. Integrated lines were identified by screening for rollers and singled out on individual plates.

### Immunoblotting

Synchronized D1 adult worms were lysed using a Biorupter (Diagenode) (7 cycles of 30s on with 30s pause) at 4°C. Lysate was clarified by centrifugation at 400 x g for 10 min at 4°C. Proteins were transferred from polyacrylamide gels to nitrocellulose membranes (GE Healthcare) at a constant voltage of 75 V, limiting the current to 200 mA for 2 h. Membranes were washed in TBS-T buffer (10 mM Tris-HCl pH 7.5, 150 mM NaCl, 0.05% Tween-20) and blocked with 5% skim milk for 1h at RT. Membranes were incubated with primary antibody in TBS-T with 5% skim milk overnight at 4°C. The blot was then washed 4 times with TBS-T for 10 min each time at RT and incubated with secondary antibody for 1h at RT. After 4 washes the blot was developed either on an ImageQuant LAS 4000 or ImageQuant 800 system. Images were analyzed in FIJI.

### LC-MS/MS analysis

For mass spectrometry analysis, tryptic peptides were loaded on a reverse phase column with an inner diameter of 75  $\mu$ m packed with 1.9  $\mu$ m C18 beads using the autosampler of the Thermo Easy LC system (Thermo Scientific). Temperature of the column was kept at a constant 50°C in a column oven (Sonation). Peptides were loaded in buffer A (0.1% formic acid), separated with a 130 min gradient of 5%–30% buffer B (80% ACN and 0.1% formic acid) at a flowrate of 300 (or 250) nl/min and directly applied onto a benchtop Orbitrap Q Exactive HF mass spectrometer (Thermo Scientific) via electrospray. The Q-Exactive HF was operated in data-dependent mode with survey scans at mass range of 300 to 1650 m/z. Up to the 10 or 15 most abundant precursor patterns from the survey scan were selected and fragmented by

higher energy collisional dissociation. MS/MS spectra were acquired with a resolution of 15,000 (FWHM), at a maximum injection time of 50 ms, and a target value of 1e5 charges.

### MS data analysis

Raw data was processed using MaxQuant version 1.5.0.25 with a false discovery rate (FDR) of 0.01 for peptides and proteins. MS/MS peaks were searched against the Uniprot reference proteome list of either *Caenorhabditis elegans* or *Homo sapiens*. Cysteine carbamidomethylation was set as a constant modification, whereas methionine oxidation and N-terminal acetylation were selected as variable modifications. Depending on the experiment, the match-between-run option was enabled, and proteins were quantified using the label-free quantification (LFQ) algorithm. LFQ values were further processed using the Perseus software.

### mRNA pulldown

3'-Biotin-TEG 20 nt antisense oligonucleotides targeting the coding region of YFP were designed as previously described (Chu et al., 2012). Probes were adjusted to a final concentration of 100  $\mu$ M (10  $\mu$ M each). Immunoprecipitation was performed as previously described with adaptations (Theil et al., 2019). Standard nematode growth medium (NGM) plates were seeded with 300  $\mu$ l of an overnight OP50 bacteria culture. The bacterial lawn was grown for 4-6 days before 20 L4 hermaphrodites were transferred. Worms were cultured at 20°C and monitored till the bacterial lawn was fully consumed (6-7 days). The plates were washed with M9 buffer and synchronized worms were transferred to 500 mL S-Basal. The culture was grown for 3 days with shaking at 120 rpm at 20°C. Worms were pooled in 50 mL Falcon tubes and washed several times with M9 buffer. The worm suspension was then transferred to unseeded 15 cm plates and exposed to 254 nm UV light (1J/cm<sup>2</sup>) using a Stratalinker 1800 to crosslink interactions of RNA with proteins. The worm pellet was washed with lysis buffer (25 mM Hepes-KOH pH 7.4, 100 mM KoAC, 10 mM MgCl<sub>2</sub>, 0.5 mM DTT, 2 tablets EDTA free protease inhibitor, 0.1 U/ $\mu$ L SUPERase\*In) and frozen by dripping small droplets into liquid nitrogen.

Frozen worms were lysed using a Retsch Cryomill MM400 at 30 Hz (3 times 90 s with cooling between cycles). Lysate was thawed on ice and clarified at 2000 x g for 10 min at 4°C. Samples were adjusted to a concentration of 10 mg/ml protein and 250 pmol of probe (see Key Resource Table) was added per 100 mg protein. Formamide was added to a final concentration of 7.5%

and samples were incubated at 20°C by vertical rotation for 2 h. 200 µL of Dynabeads MyOne Streptavidin C1 (Thermo Fisher Scientific) were added to the lysate and incubated for 1 h at 20°C. The beads were washed 5 times and mRNA-bound proteins were digested on-bead using trypsin using the iST 8x kit (PreOmics), followed by analysis by mass spectrometry.

### Human cell culture and transfection

HEK293T cells were cultured in DMEM (Thermo Scientific, 11995073) supplemented with 10% FBS (Gibco, 10270106) at 5% CO<sub>2</sub> and 37°C. Cells were transfected using lipofectamine 3000 (Thermo Fisher Scientific) following the manufacturer's instructions. Cells were analyzed 48 h after transfection by flow cytometry.

### CRISPR knockout cell lines

HEK293T cells were seeded at a density of 250,000 cells in a 12-well plate. After 24 h the cells were transfected with px459 v2 plasmids encoding gene specific sgRNAs (Ran et al., 2013). At 48 h post transfection, DMEM containing 2 µg/ml puromycin was added to cells. 4-5 days after selection, surviving cells were passaged and tested for knockouts by immunoblotting. For generating GCN1 knockout monoclonal lines, single cells were sorted into 96 well plates and individual colonies were screened by immunoblotting.

### siRNA treatment

HEK293T cells were split at a density of 750,000 cells in a 6-well plate. After 24 h the cells were transfected with 100 pmol of ON-TARGETplus Human CNOT1 siRNA (Dharmacon) using Lipofectamine 3000 following the manufacturer's instructions. After 48 h post transfection, the cells were split into a 12-well plate (250,000 cells/well). 24 h later (72 h after siRNA transfection), the cells were transfected with the reporter plasmids using Lipofectamine 3000. The effects of siRNA-mediated knockdown on the reporters was assessed 24 h later (96 h after siRNA transfection), using flow cytometry (see below).

### Flow cytometry

HEK293T cells were transfected with various reporter plasmids 48h prior to measurement using Lipofectamine 3000 following the manufacturer's instructions. 100,000 single cells per

replicate were measured on a Thermo Scientific Attune NxT analyser, using lasers at 405 nm (mTurquoise2), 488 nm (EYFP), 561 nm (mScarlet). Representative histograms were generated using FlowJo (v.10), ratiometric analysis was done using custom scripts written in Matlab (2019b), as previously described (Sitron and Brandman, 2019). Signal bleedthrough from the red and blue channels (mScarlet and mTurquoise2, respectively) into the green channel (EYFP) was calculated using an 'RedBlue' control expressing a mScarlet and mTurquoise2 dual-CMV plasmid. Likewise, signal spillover from green and red channels (EYFP and mTurquoise2, respectively) was accounted for by expressing a 'GreenBlue' control (YFP and mTurquoise2 dual-CMV plasmid). The signal bleeding effects were subtracted before additional calculations.

### Aggregate fractionation

HEK293T cells were washed with PBS and transferred to 1.5 ml tubes. The cells were counted, and  $10^6$  cells pelleted by centrifugation at  $400 \times g$  for 3 min at  $4^\circ\text{C}$ . The cell-pellet was resuspended in 200  $\mu\text{l}$  RIPA (Thermo) buffer and incubated for 20 min on ice, followed by sonication using a Biorupter (Diagenode) (7 cycles of 30 s with 30 s pause between cycles) at  $4^\circ\text{C}$ . The same number of cells was analyzed as input control. The cell lysate was then transferred to 0.5 ml open-top thickwall polycarbonate tubes (Beckman, #343776) and centrifuged at  $100,000 \times g$  for 1h at  $4^\circ\text{C}$  in a TLA-120.1 rotor (Beckman, #362224). The supernatant was transferred to a 1.5 ml tube and the pellet was resuspended in 250  $\mu\text{l}$  1x HU buffer (8 M urea, 5% SDS, 200 mM Tris-HCL pH 6.8, 1 mM EDTA, 0.01% bromphenol blue, 2%  $\beta$ -mercaptoethanol). The supernatant and input were TCA-precipitated and resuspended in 250  $\mu\text{l}$  1x HU buffer for subsequent immunoblot analysis.

### Protein pulldown

Worms were prepared as described for the mRNA pulldown and lysed in lysis buffer (25 mM HEPES-KOH pH 7.4, 100 mM KOAC, 10 mM  $\text{MgCl}_2$ , 0.5 mM DTT, 2 tablets EDTA free protease inhibitor) using a Biorupter (Diagenode). The lysate was clarified by centrifugation at  $2000 \times g$  for 10 min at  $4^\circ\text{C}$ . For each sample, 50  $\mu\text{l}$  of GFP-Trap Magnetic Agarose beads (Chromotek) were prepared by washing the beads twice in 1 ml lysis buffer. Worm lysate (50 mg protein total) was adjusted to 10 mg/ml and added to the equilibrated beads. The suspension was then incubated for 2 h at  $4^\circ\text{C}$  with vertical rotation. The beads were washed once with 2 ml of lysis buffer and

twice with 1 ml lysis buffer containing 0.1% NP-40. After transferring the beads to a fresh 1.5 ml tube, the beads were washed 3 times with lysis buffer without detergent. The bound protein was digested on beads using the iST 8x Kit (PreOmics) following manufacturer's instructions.

### Preparation of total protein extracts for immunoblot analysis

Synchronized D1 adult worms were collected in M9 and OP50 bacteria were washed off with water until the supernatant was clear. Excessive water was aspirated without disrupting the worm pellet and an equal amount of lysis buffer was added (25 mM Hepes-KOH pH 7.4, 100 mM KoAC, 10 mM MgCl<sub>2</sub>, 0.5 mM DTT, 2x EDTA free protease inhibitor). Nematodes were lysed by sonication in a Biorupter (Diagenode) as above. The lysate was clarified by centrifugation at 2,000 x g and the supernatant transferred to a fresh tube. Protein concentration was estimated by Bradford assay and adjusted to 1 mg/ml. 100 µl lysate was transferred to a fresh tube and 4 µl of 0.5% Na-deoxycholate was added. After 15 min incubation on ice, 10 µl of 100% TCA was added, followed by incubation for another hour on ice. The sample was centrifuged at 18,000 x g at 4°C for 30 min and the supernatant was discarded. The pellet was washed with 700 µl of ice-cold acetone and centrifuged for another 10 min at 18,000 x g at 4°C. The pellet was air dried and resuspended in 100 µl of 1x HU buffer (8 M urea, 5% SDS, 200 mM Tris-HCL pH 6.8, 1 mM EDTA, 0.01% bromphenol blue, 2% β-mercaptoethanol).

### Total RNA isolation

Worms were synchronized by bleaching and grown up to D1 adult stage. The nematodes were then washed off the plate with M9 buffer and transferred to a 1.5 ml tube. Following 3 washes with M9 and 1 wash with water, 5 pellet volumes of TRIzol reagent (Invitrogen) was added. The worms were lysed by 3 cycles of freezing in liquid nitrogen (30 s) and thawing at 37°C. The suspension was then vortexed and left at RT for 5 min. Afterwards, 1 pellet volume of chloroform was added and the reaction shaken vigorously. After centrifugation at 12.000 x g for 15 min at 4°C the supernatant was transferred to a fresh tube and the RNA was precipitated using 2.5 volumes isopropanol. The pellet was washed in 70 % ethanol and air dried. Finally, the pellet was resuspended in RNase-free water.

## Quantitative real-time PCR

A quantity of 500 ng RNA was used for reverse transcription using random primers according to the manufacturer's protocol (Qiagen Quantitect Reverse Transcription Kit). qPCR reactions on cDNA contained Power SYBR green master mix (Applied Biosystems). Relative mRNA levels were determined using the  $\Delta\Delta$ CT method, normalizing to *pmp-3* and *tba-1* (Livak and Schmittgen, 2001). For YFP quantification, results were normalized to the copy number using gDNA for each qPCR against YFP, normalizing to *tba-1*.

## mRNA sequencing

mRNA sequencing libraries were prepared with 200 ng or 1 mg of total RNA of each sample using the NEBNext Ultra™ II Directional RNA Library Prep Kit for Illumina® (E7765, NEB) with NEBNext® PolyA mRNA Magnetic Isolation Module (E7490, NEB), according to standard manufacturer's protocol. Quality control of total RNA input and final libraries were performed using the Qubit™ Flex Fluorometer (Q33327, Invitrogen) and 4200 TapeStation System (G2991BA, Agilent). Paired-end sequencing was performed on an Illumina NextSeq 500. The samples were multiplexed and sequenced on one High Output Kit v2.5 to reduce a batch effect. BCL raw data were converted to FASTQ data and demultiplexed by bcl2fastq Conversion Software (Illumina).

## Preparation of total ribosome fraction for Ribo-seq

### C. elegans

Synchronized nematodes were transferred to 1 l S-Basal and grown in liquid culture until D1 of adulthood or until D6, when indicated. FUdR (200  $\mu$ M) was added when the culture had reached the L4/young adult stage. After thorough washing in M9, the nematodes were frozen in lysis buffer (25 mM HEPES-KOH pH 7.4, 100 mM KOAC, 10 mM MgCl<sub>2</sub>, 0.5 mM DTT, 2x EDTA free protease inhibitor, 0.1 U/ $\mu$ L SUPERase\*In, 100  $\mu$ g/mL cycloheximide) by dropwise transfer into liquid nitrogen. The nematodes were lysed with a Retsch Cryomill MM400 at 30 Hz for 3 times 90 s with cooling between cycles. The lysate was cleared for 10 min at 20,000 x g and 4°C. Ribosome protected fragments (RPFs) were recovered, and libraries were prepared as previously described (McGlincy and Ingolia, 2017).

### HEK293T cells

HEK293T cells were seeded into 15 cm plates 24 h prior to treatment. The cells were treated with 10 nM CC-885 and 20 µg/ml G418 for 4 h. Ribosome protected fragments (RPFs) were recovered, and libraries were prepared as previously described (McGlincy and Ingolia, 2017).

### Preparation of ribosome fractions for GCN-1-IPed Ribo-seq

#### C. elegans

The procedure for immunoprecipitation (IP) of GCN-1 bound ribosomes was adapted from (Matsuo and Inada, 2021). Nematodes were synchronized by bleaching. L1 larvae were transferred to 1 L S-Basal. The animals were harvested at D1 of adulthood. Bacteria were removed by repeated washes in M9. In the last washing step, M9 was replaced by lysis buffer (25 mM Hepes-KOH pH 7.4, 100 mM KoAC, 10 mM MgCl<sub>2</sub>, 0.5 mM DTT, 2x EDTA free protease inhibitor, 0.1 U/µL SUPERase\*In, 100 µg/mL cycloheximide). After a quick spin, the worms were flash frozen in liquid nitrogen. The frozen worms were lysed with a Retsch cryomill MM400 at 30 Hz as above. The lysate was thawed on ice and clarified by centrifugation at 4,000 x g for 10 min at 4°C. Protein concentration was determined by Bradford assay. The supernatant fraction (80 mg of total protein) was partially digested with 3 units per 1 mg RNA RNase I (Epicenter) at 4°C for 1 h. Ribosomes were pelleted through a sucrose cushion (1 M, 20 U/mL SUPERase\*In (Invitrogen)) at 55,000 rpm in a SW 55 Ti rotor (Beckman Coulter) for 2 h at 4°C and resuspended in lysis buffer supplemented with 10% glycerol. The IP was performed at 4°C for 1 h using M2 anti-FLAG magnetic agarose beads (Invitrogen). The beads were washed 10 times with lysis buffer and bound material was digested with 12.5 units of RNase I (Epicenter) at 23°C for 45 min (strong RNase I treatment). Ribosome protected mRNA fragments were eluted by adding TRIzol reagent (Invitrogen). For disome analysis the sizes between 54 to 68 nt were excised from the gel, using oligo markers previously described (Meydan and Guydosh, 2020). Monosome and disome libraries were prepared (McGlincy and Ingolia, 2017) and sequenced on an Illumina NextSeq 500 or NovaSeq 6000 system.

#### HEK293T cells

Cells (treated with CC-885 or untreated) were harvested, washed with PBS, and lysed by trituration through a 26 G needle for 10 times in lysis buffer (20 mM Tris, pH 7.4, 150 mM NaCl, 5 mM MgCl<sub>2</sub>, 1 mM DTT, 100 µg/ml cycloheximide, 1 % Triton-X 100). The lysate was cleared at 4,000 x g for 10 min and an equivalent of 5 mg RNA input was digested with 15 units of RNase I. The digested lysate was then layered over a sucrose cushion (1 M, 20 U/mL SUPERase\*In

(Invitrogen)) and centrifuged at 55,000 rpm in a SW 55 Ti rotor (Beckman Coulter) for 2 h at 4°C. The pelleted ribosomes were resuspended in lysis buffer supplemented with 10 % glycerol and incubated with GCN1 antibody (A301-843A, Thermo Fisher) coupled to protein G Dynabeads (10003D, Invitrogen) (5 µg antibody per 50 µl of protein G beads) for 2 h at 4°C. The beads were washed 10 times and digested with 4 units RNase I for 45 min at 23°C. RPFs were isolated by TRIzol, and libraries were prepared as previously described (McGlincy and Ingolia, 2017).

### SLAM-seq

mRNA libraries for SLAM-seq analysis were prepared using the SLAM-seq Kinetics Kit (Lexogen), following the manufacturer's instructions. Briefly, to label the pre-existing mRNA, HEK293T cells were incubated with 100 µM 4sU for 24 h, changing the media every 3 h, keeping the cells in the dark. At the onset of the chase, the 4sU-containing media was removed and changed to media supplemented with 10 mM UTP (100x excess over 4sU). The cells were collected at timepoints 0, 2, 4, and 8 h after the onset of the chase. The library preps were performed using the QuantSeq 3'mRNA-seq kit (Lexogen). All subsequent steps during library preparation were performed under red light to avoid crosslinking. Libraries were sequenced on a NovaSeq 6000 system, and the data processed using the SLAM-dunk pipeline (Neumann et al., 2019).

### Polysome gradient analysis

Sucrose density gradients (10% - 50%) were prepared in SW41 ultracentrifuge tubes (Steton) using a BioComp Gradient Master (BioComp Instruments) according to manufacturer's instructions. The individual 10% and 50% sucrose solutions were prepared in polysome buffer (20 mM Tris, pH 7.4, 150 mM NaCl, 5 mM MgCl<sub>2</sub>, 1 mM DTT, 100 µg/ml, 20 U/ml SUPERase\*In). The lysate concentration was assessed by Bradford assay and a total protein amount of 5 mg was loaded onto the gradients. The gradients were centrifuged for 2 h at 40,000 rpm at 4°C. The gradients were fractionated using a piston gradient fractionator coupled to an A254 nm spectrophotometer (Biocomp). Polysome fractions were pooled and precipitated using 10% TCA. The protein pellets were processed for mass spectrometry using the iST 8x kit (PreOmics) following the manufacturer's protocol.

## SDS-PAGE

Proteins were separated on NuPAGE 4%–12% Bis-Tris SDS gels (Invitrogen) using NuPAGE MOPS SDS running buffer (Invitrogen) or NuPAGE MES SDS running buffer (Invitrogen) at 120 V for 1.5 h.

## Microscopy

Worms were picked from plates, placed on 4% agarose pads, and immobilized using polystyrene beads and a coverslip. Images for 3 color analysis were obtained using a Zeiss Axio Zoom.V16 microscope equipped with filtersets 46 (YFP), 47 (CFP) and 63 (RFP) and a Hamamatsu Orca Flash 4.0 camera. Confocal fluorescence images were obtained with an Olympus (Tokyo, Japan) FV1000 confocal microscope setup equipped with an Olympus PLAPON 60x/NA1.42 oil immersion objective or on a Leica SP8 FALCON confocal laser scanning microscope equipped with a LEICA HC PL APO 63x/NA 1.4 oil immersion objective. YFP was excited at 488 nm and emission detected at 505–540 nm. For red fluorophores, an excitation wavelength of 559 nm was used, and emission detected at 575–675 nm. Images were visualized using Fiji.

## Image analysis

Expression of 3-color reporter constructs for hydrophilic or hydrophobic 3'UTR fusion proteins was assessed in young (D0) nematodes. Fluorescence microscopy images of either YFP:mScarlet (protein) or mScarlet:CFP (mRNA/translation) were analyzed using a custom Fiji script. Briefly, the mScarlet channel was used to outline the muscle cells of the worm. Next, the channel intensities (pixel-wise) within the selected region were extracted. Pixels below an intensity threshold of 200 were excluded from downstream analysis. Linear regression analysis was applied to values of each pixel (for the corresponding channel). The resulting slope was used to express the ratios (normalized to respective STOP controls) depicted in the final data representation.

## Analysis of Ribo-seq and mRNA-seq data

Sequencing reads were demultiplexed and trimmed using a custom awk script. The UMI were extracted using UMI-tools using the option `'--extract-method=regex --bc-pattern="^(?P<umi_1>.{2}).+(?P<umi_2>.{6})$"'`, which serves to remove duplicated reads arising from library amplification. The clipped reads were then mapped against ncRNA/rRNA

indices using Bowtie2 (v2.4.2) with the parameters '-N 1 -L 15'. Unaligned reads were mapped against the genome using STAR (v2.7.10a) with parameters '--outFilterMismatchNmax 2 --quantMode TranscriptomeSAM GeneCounts --outSAMattributes MD NH --outFilterMultimapNmax 1'. The P-site offset and metagene plots were computed using the R package "riboWaltz" (Lauria et al., 2018). Transcript enrichment was calculated with the R package "DESeq2" (Love et al., 2014) or "DEBrowser" (Kucukural et al., 2019). Enrichment plots around the first TMD, pause scores, tAI scores, and A-site occupancy (using offsets calculated with riboWaltz) were computed using "RiboMiner" (Li et al., 2020). For disomes the A-site offset was assigned to the leading ribosome using the stop codon peak for the offset calculation. Pause scores are defined as the sum of normalized ribosome densities (AU) on each tripeptide motif. Motifs with a pausing score of < 5 (low confidence) in aged wild-type animals were excluded from downstream analysis. Read count matrices of reads mapping into the 3'UTRs of transcripts were generated using featureCounts (v2.0.1) (Liao et al., 2014). Metagene plots around polyproline stretches were analyzed as previously described (Stein et al., 2022). Reads were aligned at the A-site around the onset of the polyproline stretch. The polyproline stretch was defined as a 12 amino acid window with at least 8 of the 12 residues being proline. Next, the mean was calculated and the 95% confidence intervals at each position. Transcripts with average reads per codon within the analyzed window of less than 0.5 were discarded. mRNA half-lives were calculated as described (Herzog et al., 2017). Briefly, T>C conversions were normalized to the chase-onset. Curve fitting (non-linear regression) was performed in R using the minpack.lm package. Only RNAs that met an  $R^2 > 0.6$  (goodness of fit) cutoff were used for downstream analysis. Codon stability coefficients (CSC) were calculated as the Pearson's correlation coefficient between codon content and mRNA half-lives. Similarly, codon recruitment coefficients (CRC) were calculated as the Pearson's correlation coefficient between codon occurrence and GCN-1 recruitment.

## Statistics

Preparation of graphs and statistical analyses were performed using GraphPad Prism 8 or R (v4.1.0). The statistical tests applied are indicated in the corresponding figure legends. For multiple comparisons, one- and two-way ANOVA were used with the following corrections: Dunnett and Holm-Sidak. When two groups were compared, statistical significance was

computed using Student's t-tests and Mann-Whitney tests. *P*-Values < 0.05 were considered significant.

## Results

### The BAG6 complex degrades hydrophobic readthrough products

Translation through stop codons into polyA-tails of mRNAs leads to the clearance of both protein and mRNA via the RQC machinery (Sitron and Brandman, 2020). However, in metazoans most 3'UTRs have additional stop codons in-frame prior to the polyA-site and therefore ribosomes would terminate translation before reaching polyA-tails of mRNAs.

While previous studies identified a general clearance mechanism of aberrant protein species resulting from stop codon readthrough in *C. elegans* and human cells (Arribere et al., 2016), it remained unclear which cellular pathways are involved.

To study the mechanism underlying the clearance of readthrough translation products, we used the nematode *C. elegans*. We generated strains expressing YFP constructs with and without stop codon (YFP-STOP and YFP-UTR, respectively) in muscle cells. In YFP-UTR strains 115 residues of the *unc-54* 3'UTR are translated up to a stop codon before the polyA-site (Figure 17).

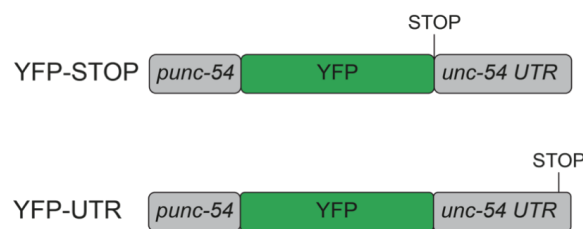


Figure 17: Translational readthrough and control constructs for muscular YFP expression.

In accordance with previous studies, we observed that YFP-UTR expression is strongly reduced compared to YFP-STOP. Interestingly, we found that the residual YFP-UTR formed inclusions, consistent with aggregate formation, which were absent in YFP-STOP expressing animals (Figure 18).

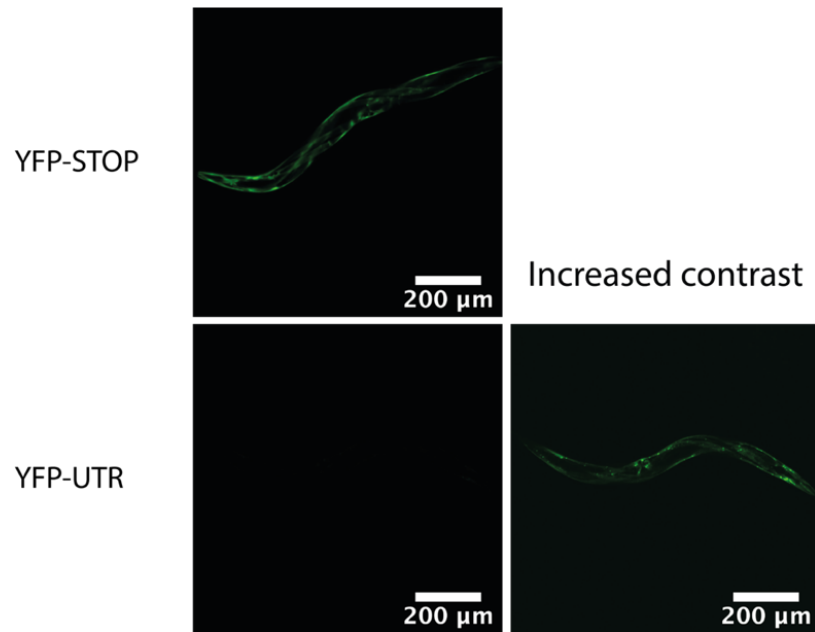


Figure 18: Representative fluorescence microscopy images of animals expressing YFP-STOP or YFP-UTR proteins (exposure 4 ms). While a clear fluorescent signal is observed in animals expressing YFP-STOP (top panel), the fluorescence in YFP-UTR expressing animals is barely visible (bottom row; left panel). Only upon increasing the contrast, the YFP signal becomes visible (bottom row; right panel).

Immunoblot analysis of YFP-UTR expressing animals confirmed the reduction in protein levels (Figure 19A). We observed an increased expression of YFP-UTR in proteasome impaired  $\Delta$ RPN-10 animals, suggesting that readthrough proteins are being cleared via the ubiquitin-proteasome pathway (Figure 19B), as previously suggested for similar constructs (Dhamija et al., 2020; Hashimoto et al., 2019; Shibata et al., 2015).

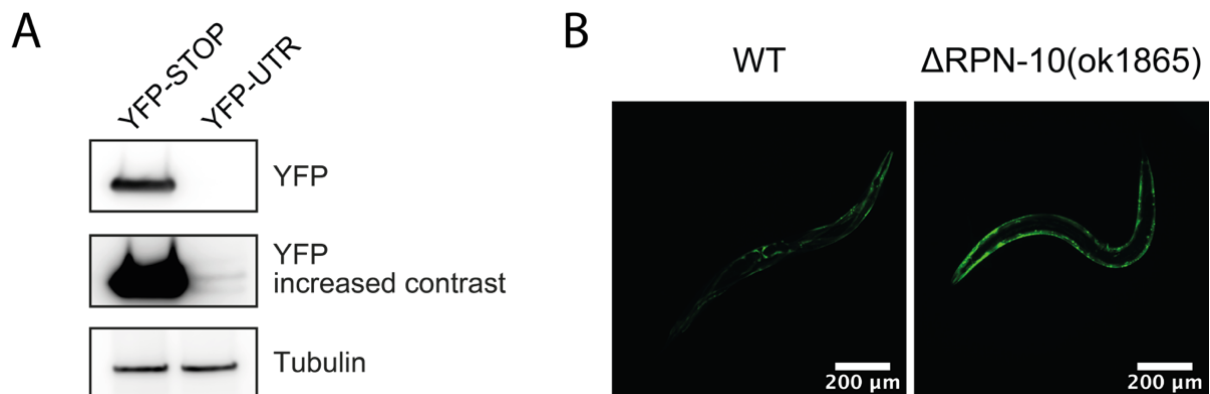


Figure 19: Readthrough into the (*unc-54*) 3'UTR region has a destabilizing effect on the protein. (A) Immunoblot analysis of YFP-Stop and YFP-UTR (B) microscopy images of worms expressing YFP-UTR in wild-type or RPN-10 mutant background.

To uncover possible factors that facilitate the degradation of readthrough products, we investigated the interactome of YFP-UTR by YFP pulldown and label-free mass spectrometry, using YFP-STOP as a control. We found the BAG6 chaperone complex, known for its function in quality control of tail-anchored (TA) membrane proteins (Guna and Hegde, 2018; Hessa et al., 2011), to be strongly interacting with YFP-UTR (Figure 20), including BAG-6, the chaperone SGT-1 (SGTA in mammals), the E3 ubiquitin ligase RNF-126, as well as UBQL-1, ASNA-1 (GET3 in mammals), and CEE-1 (GET4 in mammals). Additionally, we identified subunits of the 20S and 19S proteasome and molecular chaperones, including small HSP (HSP-16) family members, the Hsp70 protein HSP-1 and the chaperonin TRiC/CCT. Ribosomal subunits were borderline enriched, suggesting that both ribosome-associated and completely synthesized YFP-UTR were analyzed.

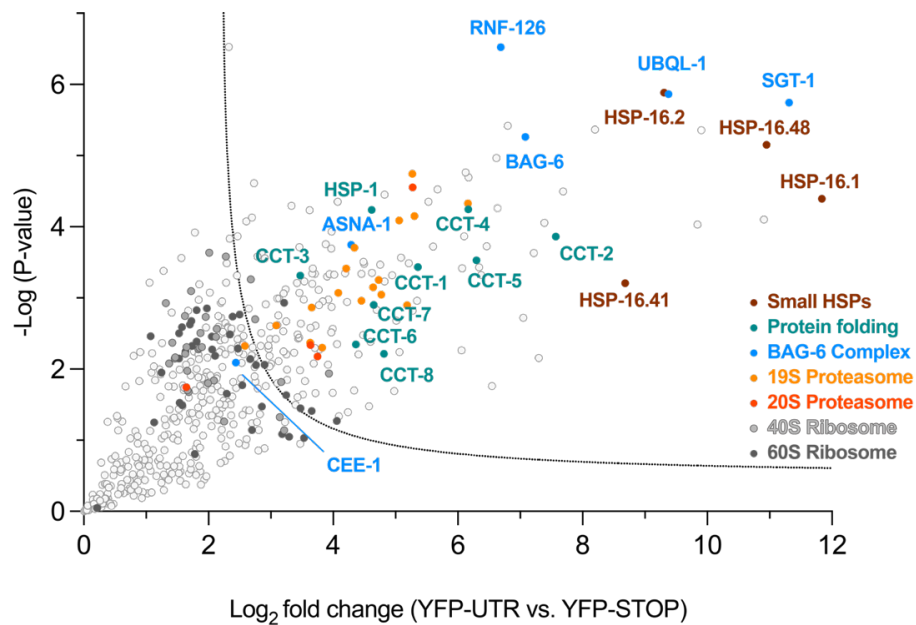
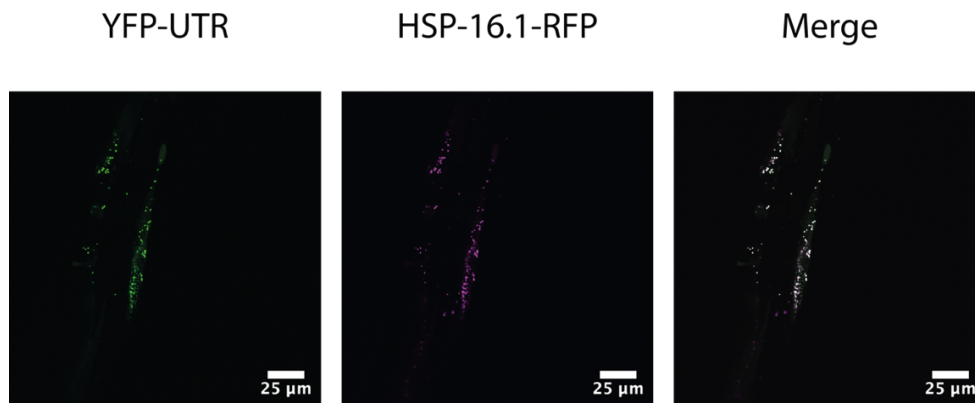


Figure 20: Volcano plot representation of label-free proteome analysis of YFP pulldown fractions from worm lysates. Components of the BAG6 quality control complex, proteasomes, TRiC/CCT chaperonin and molecular chaperones such as sHSPs and HSP-1 are significantly enriched on YFP-UTR. Selected proteins are annotated.

We confirmed the interaction of YFP-UTR with sHSPs by microscopy using an HSP-16.1-RFP expressing reporter strain (Figure 21).

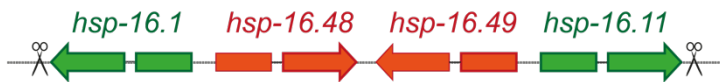


*Figure 21: HSP-16.1 colocalizes with YFP-UTR. Expression of YFP-UTR in the muscles results in puncta formation (left panel) and induces the expression of HSP-16.1 (middle panel). Merging the two channels reveals a strong colocalization of YFP-UTR with HSP-16.1 (right panel).*

sHSPs are an ancient class of ATP-independent molecular chaperones that bind to misfolded proteins and prevent them from forming irreversible protein aggregates (Horwitz, 1992; Jakob et al., 1993; McHaourab et al., 2002). sHSPs have been described to actively sequester proteins, thereby preventing the formation aberrant interactions. We therefore hypothesized that the sequestration of YFP-UTR into inclusions may be an active process mediated by the sHSPs. To test this idea, we deleted all 6 copies of the hsp-16 family (Figure 22A). Interestingly, we observed that the large inclusions were no longer visible in the deletion strain and the protein appeared dispersed instead (Figure 22B), which agrees with the function of sHSPs in actively sequestering aberrant proteins. The smaller inclusions of YFP-UTR that remained after deleting sHSPs associated with the dense bodies inside the muscle cells. Dense bodies are structural elements inside muscle cells, serving as an anchor of actin filaments to the extracellular matrix (ECM). In addition to its structural role, dense bodies fulfill important stress signaling functions (Lecroisey et al., 2007).

A

V: 1,92 +/- 0,001 cM



V: 17,58 +/- 0,044 cM



B

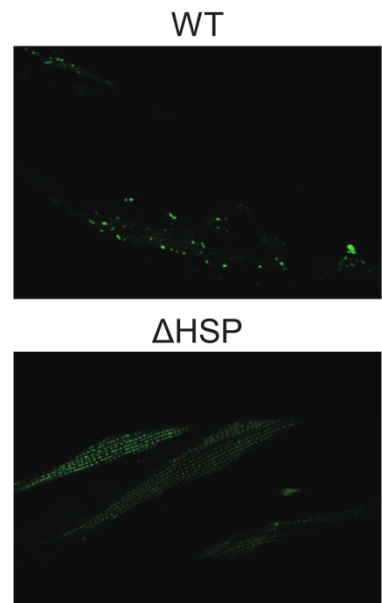


Figure 22: The hsp-16 family is actively sequestering YFP-UTR in larger inclusions. (A) schematic overview of CRISPR/Cas mediated knockout. (B) microscopy images of YFP-UTR expressing worms either in the wild-type or sHSPs mutant background.

HSP-16s are known to be highly upregulated under stress conditions (compared to unstressed animals) and during aging (compared to young animals) (Hsu et al., 2003; Morley and Morimoto, 2004; Walker and Lithgow, 2003; Walther et al., 2015). We speculated that translational readthrough, like heat stress, is sensed by the organism and is met by increased sHSPs expression. Indeed, a proteome analysis of YFP-UTR expressing worms compared to YFP-STOP showed a ~30-100-fold increase in the expression of hsp-16 family members (Figure 23).

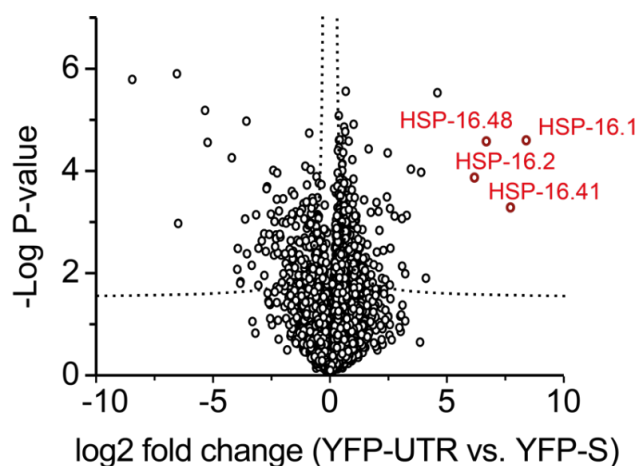


Figure 23: Total proteome analysis by mass spectrometry of worms expressing YFP-UTR compared to animals expressing YFP-STOP reveals a robust heat shock induction. Small heat shock proteins (sHSPs) are highlighted in red.

During heat stress, the induction of sHSPs is transcriptionally driven by heat shock factor 1 (HSF1). To investigate whether the same mode of induction occurs in the case of translational readthrough, we performed qPCR on YFP-STOP and YFP-UTR worms and compared the extent of induction to acute heat stress. We found that translational readthrough can induce the expression of sHSPs, however, the extent of induction is considerably lower than observed upon heat stress (Figure 24).

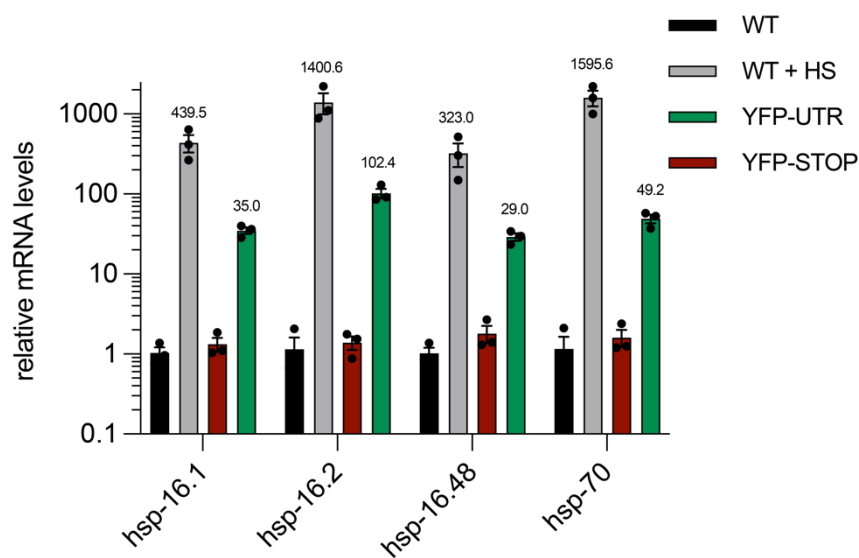


Figure 24: qPCR analysis of genes induced by heat shock either after heat shock or expressing YFP-STOP/YFP-UTR relative to unstressed wild-type animals. Black bars indicate expression of indicated genes at basal conditions (wild-type), gray bars represent heat-shocked animals (wild-type + heat shock), red for YFP-STOP expressing worms and green bars were chosen for YFP-UTR expressing animals.

As sHSPs have been attributed a role in keeping proteins in a more soluble, folding competent state, we hypothesized that they may also aid in the clearance of readthrough products. We therefore analyzed the protein levels of YFP-UTR in wild-type and sHSPs deficient worms. However, we did not observe any changes in the efficiency of protein degradation in the absence of sHSPs (Figures 25A and 25B).

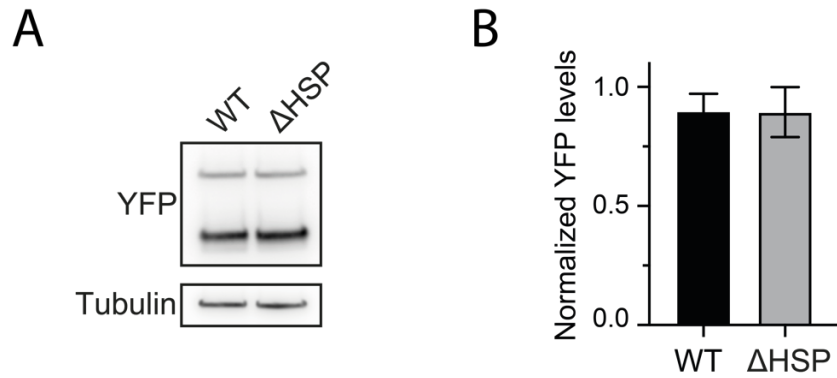


Figure 25: Deletion of small heat shock proteins (sHSPs) does not affect protein clearance of readthrough products. (A) Immunoblot analysis of YFP-UTR in wild-type or sHSPs ( $\Delta$ HSP) deficient animals (B) quantification by densitometry of western blot analysis in A).

Next, we investigated whether overall aggregation dynamics could be affected by the presence of sHSPs. To investigate this possibility, we performed a filter trap assay, whereby large inclusions are being retained on a filter paper, whereas smaller oligomeric species are allowed to pass through. Surprisingly, we did not observe any changes in the amount of YFP-UTR captured on the filter in the absence of SDS, whether sHSPs are present or not. Unlike amyloidogenic species or the aggregates of CAT-tailed proteins, known to be SDS-resistant, the inclusions formed by YFP-UTR were sensitive to mild detergent treatment with 0.1 % SDS (Figure 26).

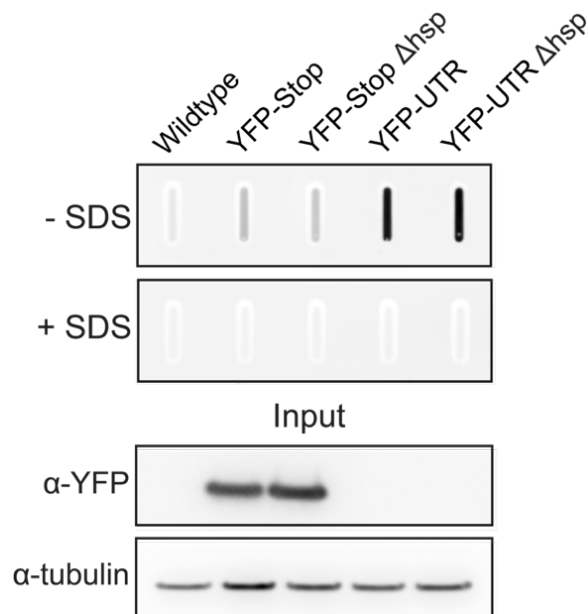


Figure 26: Formation of YFP-UTR oligomers are not dependent on sHSPs and sensitive to SDS. Immunoblot analysis of filter-retained material from lysates prepared of wild-type, YFP-STOP

and YFP-UTR expressing animals in either *sHSPs* deletion strains or wild-type backgrounds washed with buffer lacking SDS (top blot) or containing SDS (bottom blot). In the lower panel the loading for each lane of the filter trap is analyzed by SDS-PAGE followed by an immunoblot analysis, probed against YFP and tubulin. YFP-UTR without adjusted contrast is not visible in the input, as it is rapidly degraded (see Figure 19A).

YFP-UTR copurified with the BAG6 complex, a chaperone complex that triages mislocalized TA proteins in the cytosol for degradation. The identification of the BAG-6 complex as a direct interactor of YFP-UTR suggested that this mechanism has been coopted to clear readthrough proteins. We therefore investigated whether YFP-UTR shows similarities to TA-proteins. Indeed, the *unc-54* 3'UTR, when translated, has a strong bias towards hydrophobic amino acids (Figure 27).

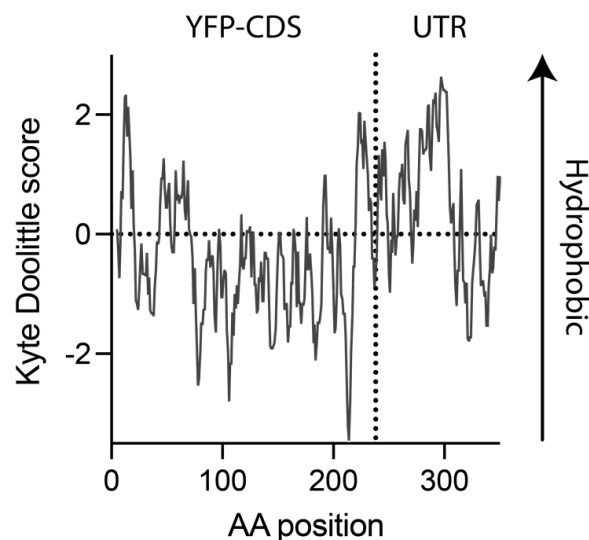


Figure 27: Kyte Doolittle score as a measurement for hydrophobicity across the YFP-UTR construct reveals a strong bias towards hydrophobic amino acids in the 3'UTR region.

Interestingly, we found that such a bias applies to most 3'UTRs in *C. elegans* (Figure 28). Average hydrophobicity of these sequences is significantly higher than that of coding (CDS) regions and similar in hydrophobicity to bona fide TA proteins, and transmembrane domains (TMDs) of TMD-containing transcripts.

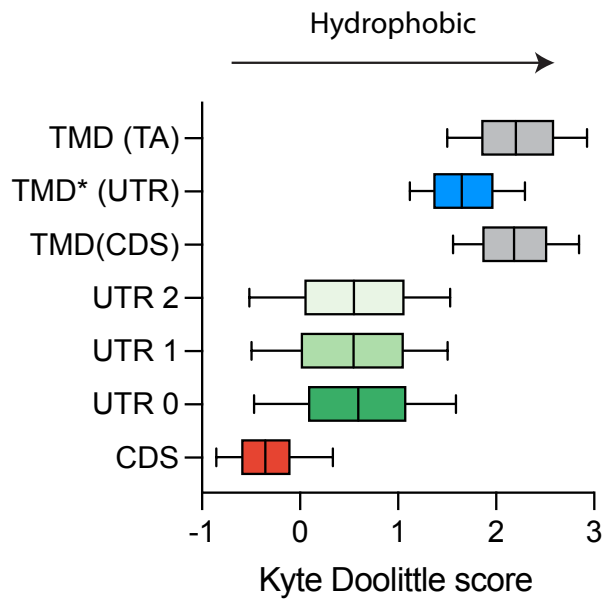


Figure 28: 3'UTRs show a bias towards hydrophobic amino acids. The Kyte Doolittle Score, a measure for hydrophobicity, is increased in 3'UTRs if translated into the corresponding amino acids.

While global hydrophobicity appears to be weaker in human 3'UTRs compared to *C. elegans*, human 3'UTRs encode similar hydrophobic stretches (~21 aa in length, corresponding to an average TA transmembrane span) (Figure 29A). To understand sequence features that may contribute to these patterns, we analyzed the nucleotide content of 3'UTRs in *C. elegans*. The hydrophobicity observed in *C. elegans* 3'UTRs arises from their relatively high U-content in comparison to the CDS regions of transcripts (Figures 29B and 29C). Interestingly, a higher U-content is associated with a lower tRNA adaptation index, a proxy for codon optimality (as measured by the tRNA adaptation index (tAI)), a feature that suggests that translation into the 3'UTRs may alter ribosome kinetics (Figure 29D).

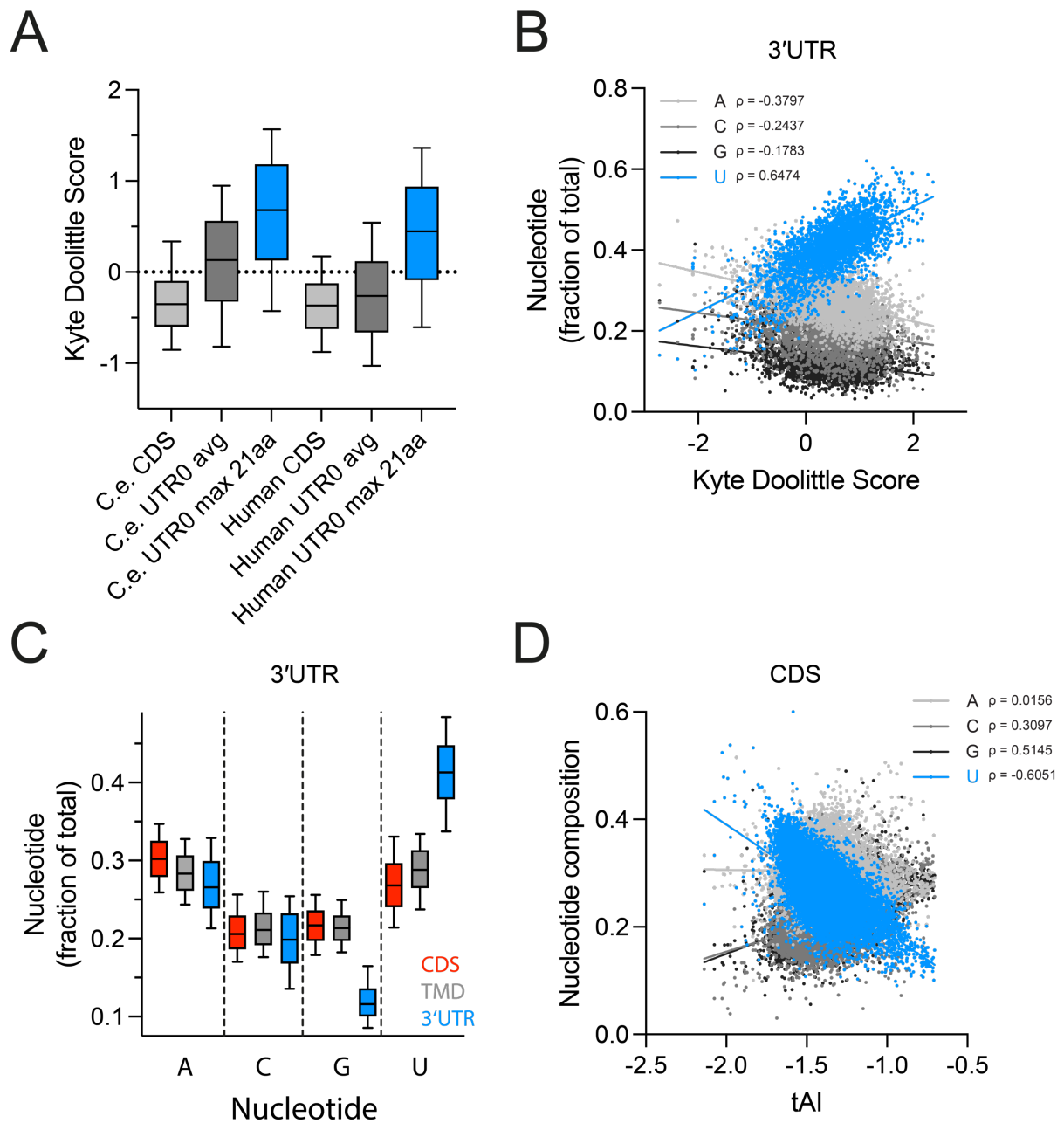
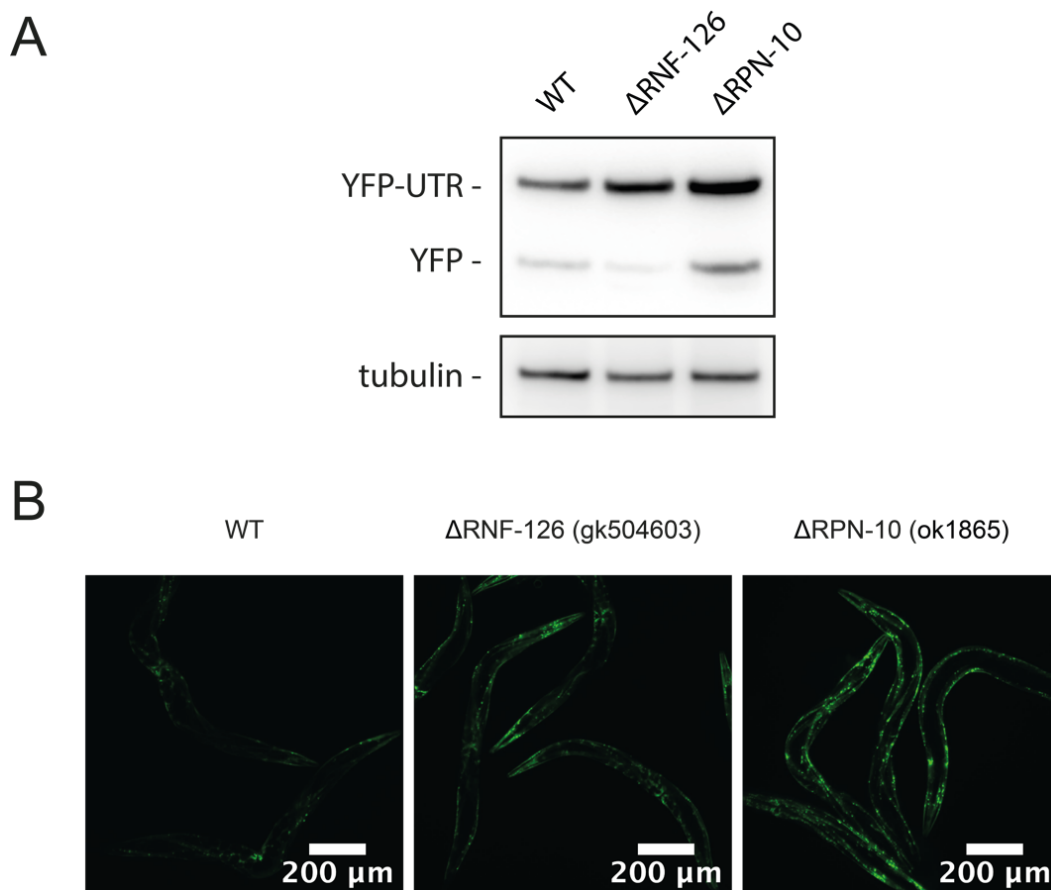


Figure 29: Feature analysis of 3'UTRs. (A) Kyte Doolittle Score of *C. elegans* and *H. sapiens* 3'UTR-derived peptides of at least 21 AA length in reading frame 0 compared to the CDS regions. (B) Pearson's correlation coefficients of nucleotide content and KDS, reveals a positive correlation between U-content and increased hydrophobicity of 3'UTR-derived peptides. (C) 3'UTRs have a general increased frequency of U, whereas G is reduced compared to the CDS and TMD containing transcripts. (D) Higher U content in the CDS is associated with a lower tAI score.

The identification of the BAG6 complex as an interactor of YFP-UTR (Figure 20), suggested that readthrough products are cleared by the same machinery as orphaned TA proteins. In that mechanism, mislocalized TA proteins are captured by SGT-1 (SGTA in mammals) and handed over to BAG6, where they are triaged for either membrane insertion or if recognized as faulty,

ubiquitylated by RNF126 for degradation (Hegde and Keenan, 2022). Indeed, we observed that the E3 ligase RNF-126 is involved in the clearance of the YFP-UTR reporter to a similar extent as the proteasome (Figures 30A and 30B).



*Figure 30: RNF-126 is involved in the clearance of readthrough products. (A) Western blot analysis reveals a stabilization of YFP-UTR in the absence of RNF-126, comparable to the stabilization observed in proteasome impaired worms. (B) Similar observations can be made by microscopy.*

We also observed that the vast majority of the 3'UTRs contain an in-frame stop codon before the polyA sequence, irrespective of the reading frame (Figure 31). This implies that most of the readthrough events would not be subject to the classical RQC mediated clearance of non-stop mRNA.

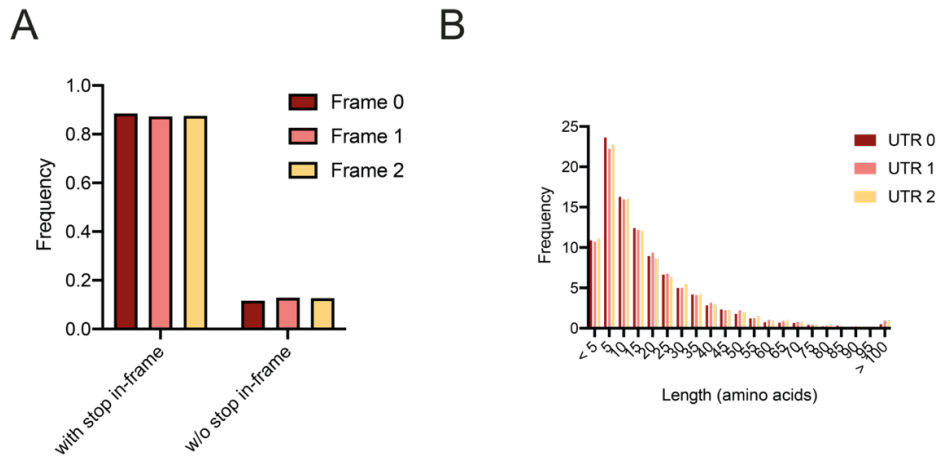


Figure 31: Most 3'UTRs code for a stop codon before reaching the polyA signal sequence, irrespective of the reading frame. (A) Frequency of 3'UTRs with stop codon in frame versus transcripts allowing translation into the polyA-tail. (B) Theoretical length distribution of 3'UTR-derived peptides.

To investigate whether the BAG6 pathway preferentially degrades hydrophobic readthrough sequences, we generated a tricolor expression construct encoding CFP and mScarlet-T2A-YFP expressed from individual promoters. Since a T2A site is present, the resulting reporter expresses mScarlet and either YFP-STOP or YFP-3'UTR as individual proteins derived from the same mRNA, therefore allowing the assessment of protein stability by YFP:mScarlet ratios. On the other hand, CFP is expressed from a separate mRNA, thereby serving as a copy number control (Figures 32).

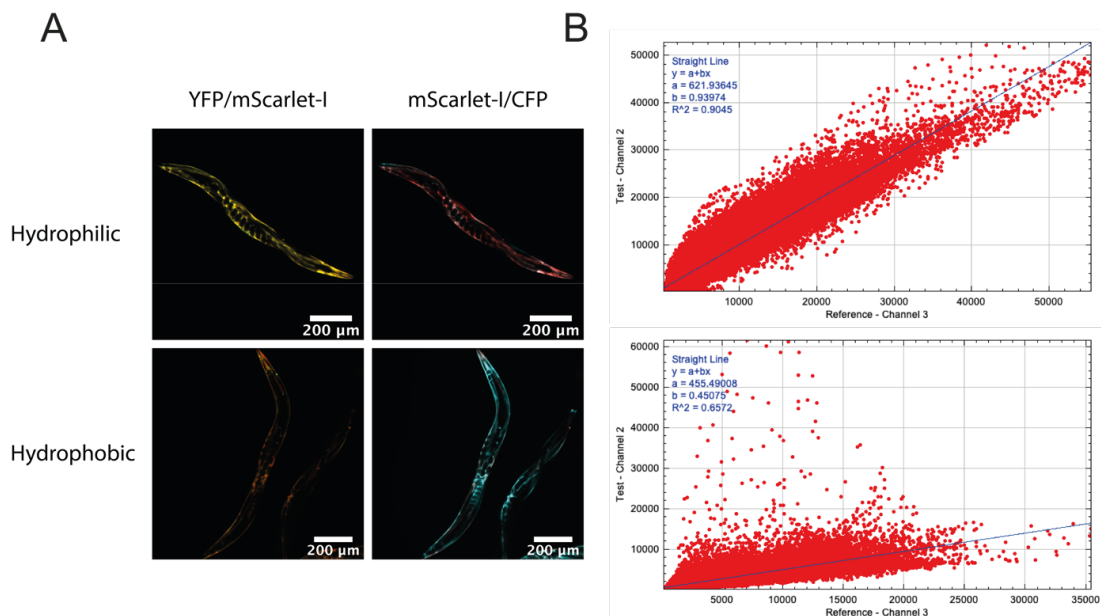


Figure 32: (A) Overlay of YFP/mScarlet-I or mScarlet-I/CFP for hydrophobic and hydrophilic 3'UTRs reveal a colour shift reflective of protein and mRNA destabilization. (B) Examples for

the computational assessment of the ratio change. The value for each pixel was plotted for their value in the corresponding channel. The resulting points were fitted by a linear regression and the slope reflecting the ratio between the 2 channels.

Using ratiometric microscopy imaging (Figures 32A and 32B), we compared the effects on protein stability upon translation of two length-matched hydrophobic (SLC-17.5 and R160.3) or hydrophilic (F40D4.17 and T21C12.3) 3'UTR sequences (Figure 33).

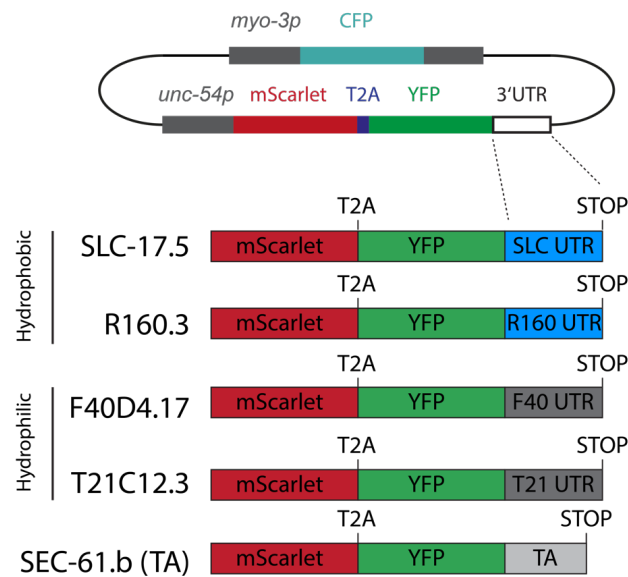


Figure 33: Schematic overview of 3 color constructs of two length matched hydrophobic (SLC-17.5 and R160.3) and hydrophilic (F40D4.17 and T21C12.3) 3'UTRs, as well as the tail-anchor region of a bona fide TA protein (SEC-61.b (TA)).

By comparing the length matched hydrophobic and hydrophilic candidates, we observed that readthrough resulted in protein destabilization only in the case of hydrophobic 3'UTRs (Figure 34A). Interestingly, the bona fide TA protein SEC-61.b, although containing a hydrophobic TA sequence, was not destabilized, suggesting that proper and timely targeting does not invoke this quality control pathway. Importantly, destabilization of the readthrough protein was partially rescued in RNF-126 mutant worms, suggesting that the BAG6-RNF-126 complex coevolved to detect hydrophobic readthrough products and mediate their degradation (Figure 34B).

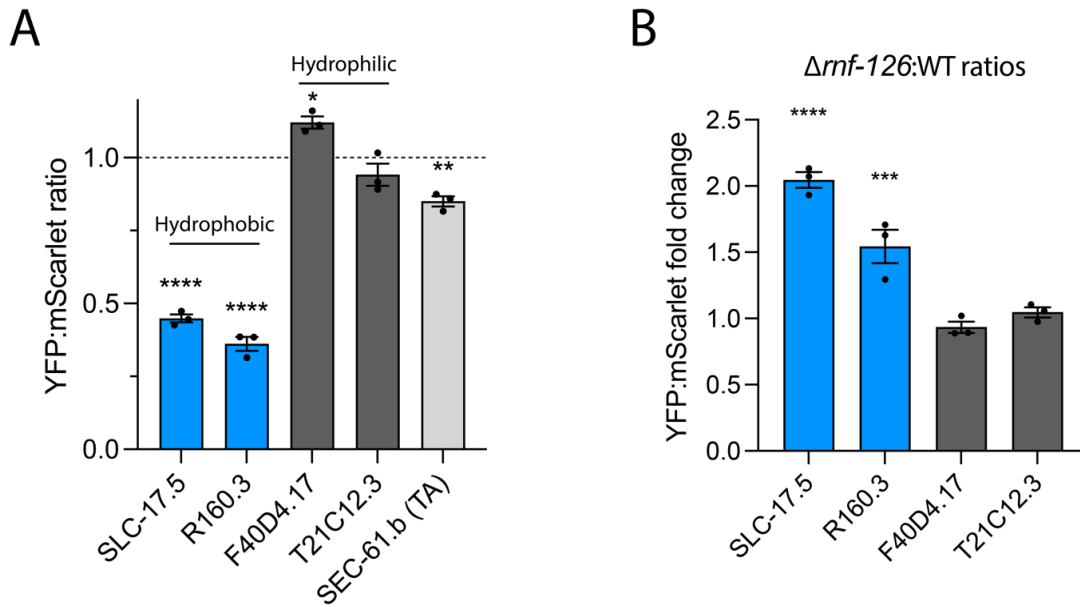


Figure 34: RNF-126 is involved in the clearance of hydrophobic readthrough products. (A) Hydrophobic 3'UTR extension destabilize the protein upon translation. (B) The destabiliation can be rescued in a RNF-126 deficient nematode. Significance was assessed by one-way ANOVA with dunnett's correction.

### Stop codon readthrough leads to mRNA decay via GCN-1-CCR4/NOT complex recruitment

It remained unclear whether mRNA degradation contributes to mitigating stop codon readthrough. mRNA sequencing revealed a ~70% reduction in mRNA abundance of YFP-UTR relative to YFP-STOP. These results were confirmed by qPCR analysis of mRNA levels, corrected for copy numbers of the transgene. Importantly, this reduction in mRNA level did not rely on SKIH-2 (RNA helicase component), pointing towards an RQC-independent mechanism (Figures 35A-C).

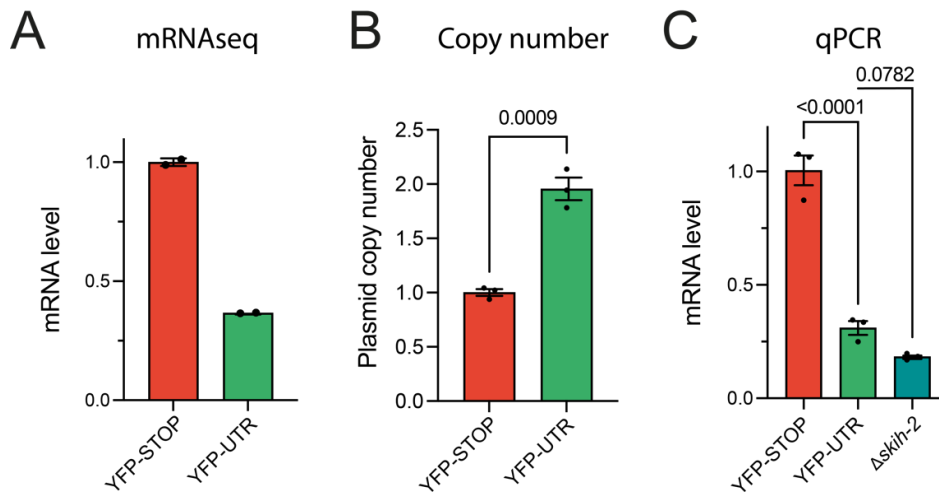


Figure 35: Translational readthrough into hydrophobic 3'UTRs is destabilizing the mRNA in a mechanism independent of RQC. (A) Relative copy number of plasmid integrated into the genome. (B) Copy-number corrected qPCR experiment. (C) mRNAseq results of YFP-STOP and YFP-UTR expressing animals. Significance was assessed by Student's t-test or one-way ANOVA.

Using Ribo-seq, we observed a ~25% decrease in translational efficiency of YFP-UTR, suggesting that additional to mRNA decay, translational repression may also contribute to the total reduction in protein levels (Figure 36).

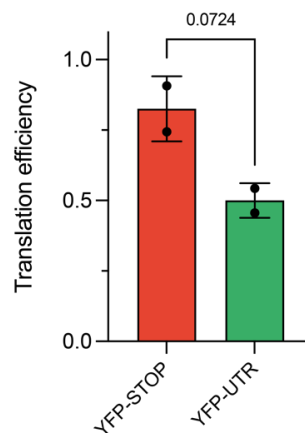


Figure 36: Translational efficiency is reduced in YFP-UTR compared to YFP-STOP. P-values were obtained by Student's t-test analysis.

To identify factors mediating this mRNA decay, we performed a crosslinking-RNA-immunoprecipitation-mass-spectrometry (CLIP-MS, see Methods) experiment against the mRNA of YFP-STOP and YFP-UTR. Interestingly, we found components of the BAG6 complex and sHSPs to be associated with YFP-UTR, indicating a cotranslational recruitment of these protein quality control factors. Additionally, we identified GCN-1, a ~2600 amino acid protein rich in HEAT domains that was recently found to bind to collided and stalled ribosomes

(Meydan and Guydosh, 2020; Pochopien et al., 2021; Wu et al., 2020; Yan and Zaher, 2021). Several components of the CCR4/NOT complex, involved in mRNA surveillance and homeostasis, were likewise enriched, including the catalytically active exonuclease component CCF-1 and CCR-4 (Figure 37A). While the role of CCR4/NOT in mRNA degradation is well established (Buschauer et al., 2020; Webster et al., 2018), GCN-1 has no known function in mRNA turnover. To explore a possible function of GCN-1 in mRNA decay upon translational readthrough, we utilized nematodes carrying a hypomorphic *gcn-1(nc40)* mutant allele, lacking 244 amino acids near the N-terminus of GCN-1. We noted that YFP-UTR mRNA was partially restored in the *gcn-1(nc40)* mutant (Figure 37B).

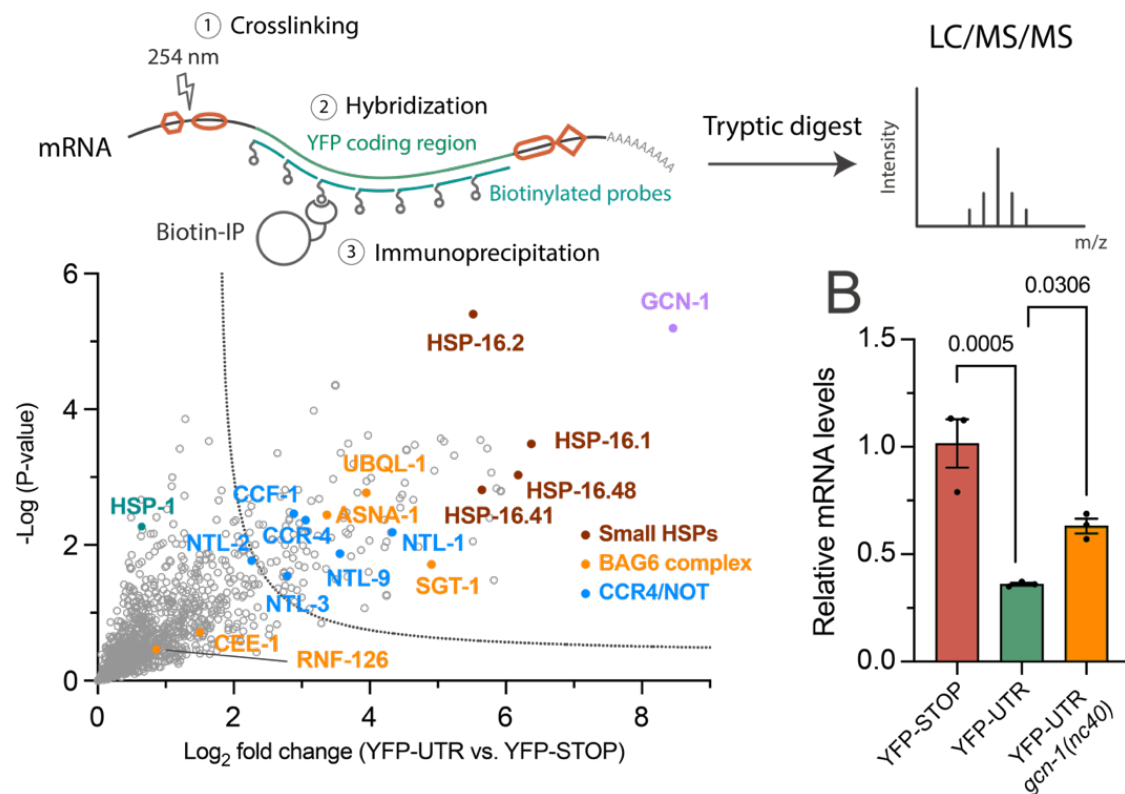


Figure 37: GCN-1 and the CCR4/NOT complex are strong interactors of YFP-UTR mRNAs. (A) Upper panel: Schematic representation of mRNA pulldown of YFP-UTR and YFP-STOP constructs. Lower panel: Interactome analysis of YFP-UTR mRNA (vs. YFP-STOP). Volcano plot representation of label-free proteome analysis of pulldown fractions showing enrichment of GCN-1, BAG6 complex, CCR4/NOT and sHSPs on YFP-UTR. (B) qPCR analysis of YFP-STOP and YFP-UTR mRNA levels in wild-type *C. elegans* and in *gcn-1(nc40)* mutant animals ( $n = 3$ ). Data was analyzed using the  $2(-\Delta\Delta Ct)$  formula and  $p$ -values were calculated using Fisher's LSD test (see STAR Methods). Error bars represent mean  $\pm$  SEM.

Additionally, the increased mRNA levels of YFP-UTR observed in the *gcn1(nc40)* worms resulted in higher protein levels (Figure 38).

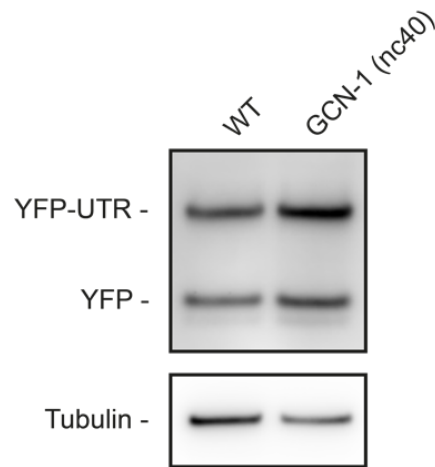
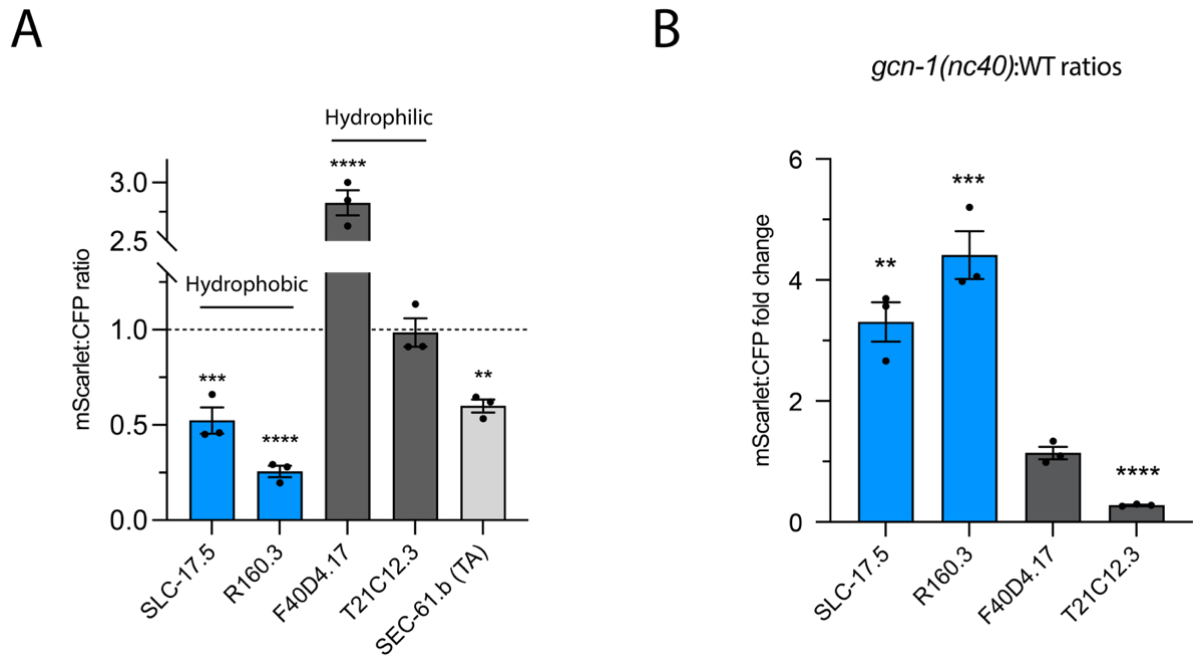


Figure 38: Immunoblot analysis of wild-type and *GCN-1(nc40)* mutant worms expressing YFP-UTR reveal increased YFP-UTR levels in the mutant nematodes.

To further elucidate the effects of GCN-1 dysfunction upon translation of proteins with hydrophobic or hydrophilic C-terminal extensions (CTEs), we next utilized the tricolor expression constructs introduced above (Figure 33). Based on mScarlet:CFP ratios, wild-type animals exhibit reduced mRNA levels upon translation of hydrophobic CTEs, while the mRNAs for proteins with hydrophilic CTEs either were unchanged or even stabilized further (Figure 39A). Interestingly, we observed a destabilization for the mRNA of the SEC-61.b TA-protein (see Figure 33), suggesting that without the full-length mRNA and protein context, the TA-region triggers mRNA degradation as for readthrough proteins. In the *gcn-1(nc-40)* animals, the mRNA levels of hydrophobic readthrough proteins were increased 3-5-fold (Figure 39B), while the mRNAs of hydrophilic readthrough proteins were unaffected or even reduced (as in the case of T21C12.3). Together, these results indicate that GCN-1 facilitates mRNA decay of readthrough reporters when they encode for hydrophobic CTEs.



**Figure 39: Translation of hydrophobic 3'UTRs initiates GCN-1-mediated mRNA decay. (A)** Ratiometric analysis of relative mRNA levels (mScarlet:CFP ratios) of the indicated hydrophilic and hydrophobic readthrough constructs (Figure 56) from fluorescence microscopy images of worms. Experiments were performed in triplicates with at least 5 images per replicate. \*,  $p < 0.05$ ; \*\*,  $p < 0.01$ ; \*\*\*,  $p < 0.001$ ; \*\*\*\*,  $p < 0.0001$  by Dunnett's test. Error bars represent mean  $\pm$  SEM. Dotted line indicates STOP controls. **(B)** Selective stabilization of mRNA levels of hydrophobic readthrough constructs in *gcn-1(nc40)* mutant animals. Experiments were performed in triplicates with at least 5 images per replicate. \*,  $p < 0.05$ ; \*\*,  $p < 0.01$ ; \*\*\*,  $p < 0.001$ ; \*\*\*\*,  $p < 0.0001$  by Dunnett's test. Error bars represent mean  $\pm$  SEM.

As GCN-1 has a role in sensing collided ribosomes, we speculated that hydrophobic amino acid stretches could induce ribosomal collisions. Although previous reports suggested that hydrophobic sequences lead to ribosomal stalling (Hashimoto et al., 2019), utilizing Ribo-seq we failed to identify a defined translational pause site in the CTE of YFP-UTR (Figure 40A). Similarly, using a stalling reporter did not suggest a persistent translational arrest (Figure 40B), whereas an established stalling sequence (K(AAA)<sub>20</sub>) was reliably detected with our reporter (Figure 40C). These results suggest, that in the context of translational readthrough, GCN-1 may sense transient translational slowdown, rather than persistent disome formation.

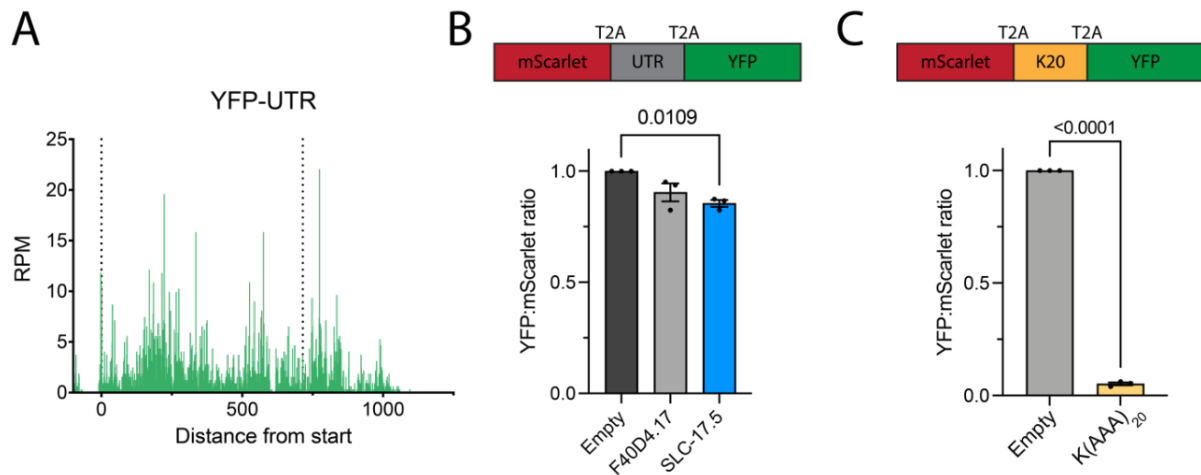


*Figure 40. Hydrophobic stretches do not induce stable disome formation. (A) Ribo-seq analysis of *C. elegans* YFP-UTR reporter strain. Dotted lines indicate start and annotated stop codon (present in YFP-STOP) of YFP-UTR. Y-axis indicates reads per million (RPM) along the YFP-UTR transcript. (B) Ratiometric analysis of fluorescence microscopy images of nematodes expressing the indicated translational stalling reporters. The construct shown schematically on top carries either no sequence between mScarlet and YFP or the 3'UTR of the indicated transcripts. Stalling in the 3'UTR would result in low YFP:mScarlet ratios. Error bars represent mean  $\pm$  SEM ( $n = 3$ ) p-Values by Dunnett's test. (C) Ratiometric analysis of fluorescence microscopy images of nematodes expressing the K(AAA)<sub>20</sub> reporter constructs shown schematically on top (as in (B)). Error bars represent mean  $\pm$  SEM ( $n = 3$ ). p-Values by Student's t-test.*

As GCN-1 has no reported mRNA degradation activity, it is unlikely that it directly acts on mRNAs but rather functions as a recruitment platform for other quality control factors (Oltion, 2022). To identify possible protein-protein interactions and ribosome recruitment modes, we performed an IP on 3xFLAG-tagged GCN-1 followed by mass spectrometry. Besides factors that have been previously described as direct interactors of GCN-1, such as ABCF-3 (ABCF3), GIR-2 (RWDD1), RBG-2 (DRG2) and MBF1 (EDF1) (Pochopien et al., 2021), we found multiple components of the CCR4/NOT complex (CCR-4, CCF-1, NTL-1) as well as the BAG-6 complex (SGT-1, UBQL-1, CEE-1, ASNA-1) to be enriched in the GCN-1 interactome (Figure 41).

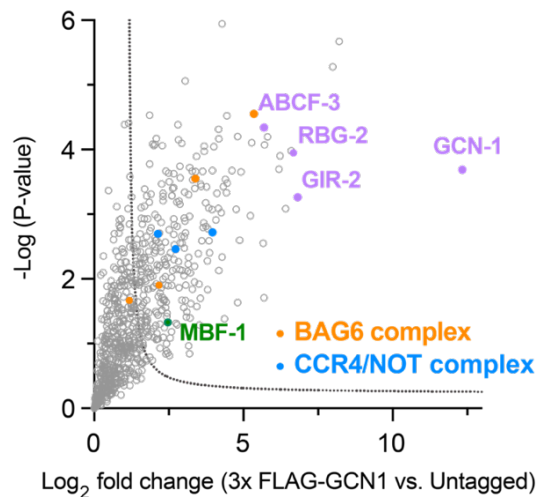


Figure 41: GCN-1 IP reveals a direct interaction of GCN-1 with the CCR4/NOT complex. Immunoprecipitation coupled to mass spectrometry from lysate of nematodes 3x FLAG-tagged GCN-1 from its endogenous locus compared to untagged animals. Previously GCN-1 associated proteins are highlighted in pink, BAG-6 components in yellow and proteins of the CCR4/NOT complex in blue. MBF-1, homolog of the mammalian EDF1, is highlighted in green.

As the previous result would suggest that GCN-1 initiates mRNA decay via the recruitment of CCR4/NOT, we hypothesized that in GCN-1 mutant animals CCR4/NOT recruitment to translating ribosomes would be reduced. To test this idea, we performed mass spectrometry on fractionated polysomes by sucrose gradient fractionation of young (day 0) wild-type and *gcn-1(nc40)* mutant nematodes. As expected, GCN-1 recruitment to translating ribosomes was reduced in the mutant worms. Similarly, we observed a decreased recruitment of CCR4/NOT complex in *gcn-1(nc40)* nematodes (Figure 42).

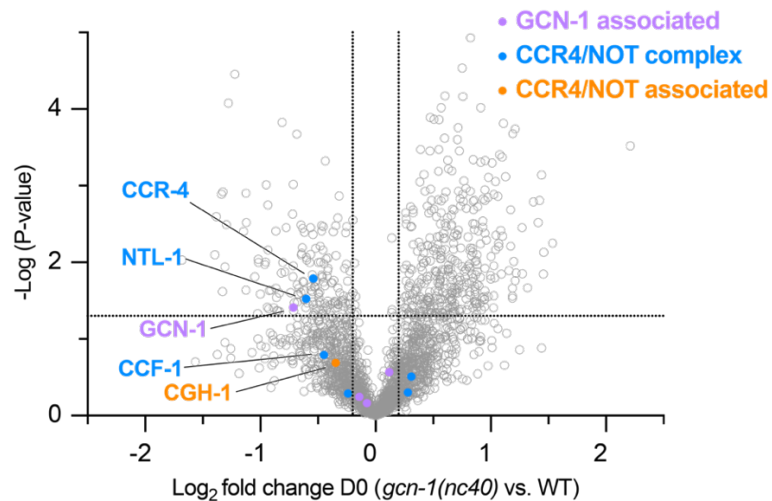


Figure 42: Polysome fractionation coupled to mass spectrometry reveals the role of GCN-1 in recruiting the CCR4/NOT complex to translating ribosomes. Polysome fractions were isolated by sucrose cushion fractionation from either wild-type animals or *gcn-1(nc40)* mutant nematodes and analyzed by mass spectrometry. GCN-1 associated genes are highlighted in pink, CCR4/NOT components in blue and CCR4/NOT associated proteins in yellow.

### Mechanism of readthrough mitigation is evolutionarily conserved

Is the pathway of translational readthrough mitigation evolutionarily conserved? To answer this question, we chose the 32 residue, hydrophobic 3'UTR of TCEAL1 and expressed it as a YFP fusion protein in human HEK293T cells, using YFP-STOP as a control. Next, we performed an interactome analysis by mass spectrometry, which identified components of the BAG6 and CCR4/NOT complexes as interactors of YFP-TCEAL (Figure 43), mirroring the results obtained in *C. elegans*.

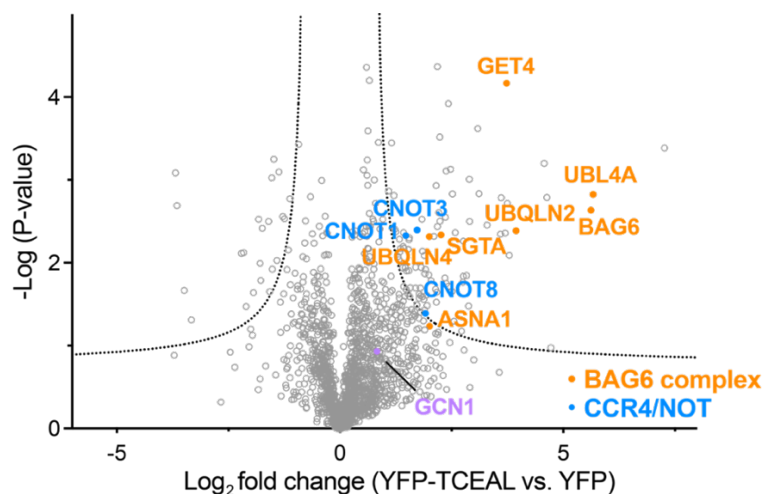
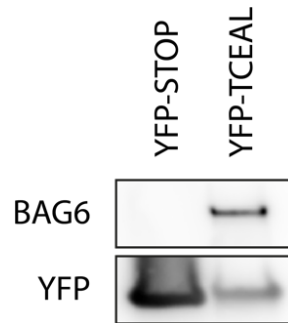


Figure 43: Volcano plot representation of label-free interactome analysis of YFP-TCEAL from HEK293T cells expressing YFP-TCEAL readthrough construct and YFP-STOP as control.

*Components of the BAG6 and CCR4/NOT complexes are identified as interactors of YFP-TCEAL. Selected proteins are highlighted.*

Further, we confirmed the direct and specific interaction of the readthrough product by immunoprecipitation followed by immunoblot analysis (Figure 44).



*Figure 44: Immunoprecipitation of YFP-STOP and YFP-TCEAL followed by immunoblot analysis confirms the specific interaction of hydrophobic readthrough products with BAG6.*

To assess the stability of translational readthrough protein products and corresponding mRNA, we expressed two length-matched readthrough proteins with either hydrophobic (TCEAL1 and OR8D4) or hydrophilic CTEs (CNIH3 and CCK), employing ratiometric reporter constructs (Figure 45). Two individual CMV promoters induce the expression of mScarlet-2xT2A-YFP fused to the 3'UTR of interest and mTurquoise2 serving as copy number control, enabling the concurrent measurement of protein stability (YFP:mScarlet ratios) and relative mRNA levels (mScarlet:mTurquoise2 ratios) by flow cytometry.

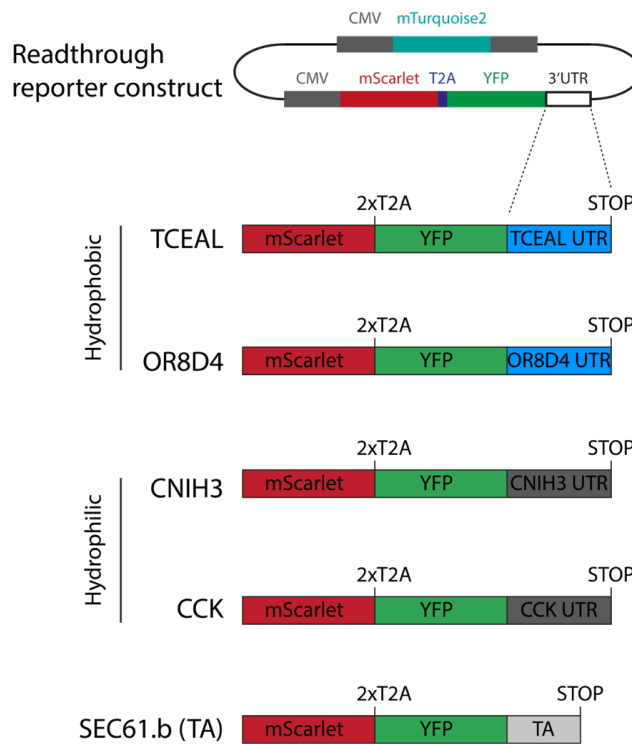


Figure 45: Constructs for ratiometric analysis by flow cytometry of the effect of readthrough into 3'UTRs encoding hydrophobic (Transcription elongation factor A protein-like 1, TCEAL, KDS = 2.07, 32 residues; Olfactory receptor 8D4, OR8D4, KDS = 1.96, 28 residues) or hydrophilic (Protein cornichon homolog 3, CNIH3, KDS = -2.21, 34 residues; Cholecystokinin, CCK, KDS = -1.89, 26 residues) CTE sequences in HEK293T cells. The TA-sequence of SEC61.b was also analyzed.

As in *C. elegans*, the presence of hydrophobic CTEs destabilized the readthrough model protein in human cells and resulted in reduced mRNA levels (Figures 46A-D). The TA sequence of SEC61.b had also a negative effect on both protein and mRNA stability.

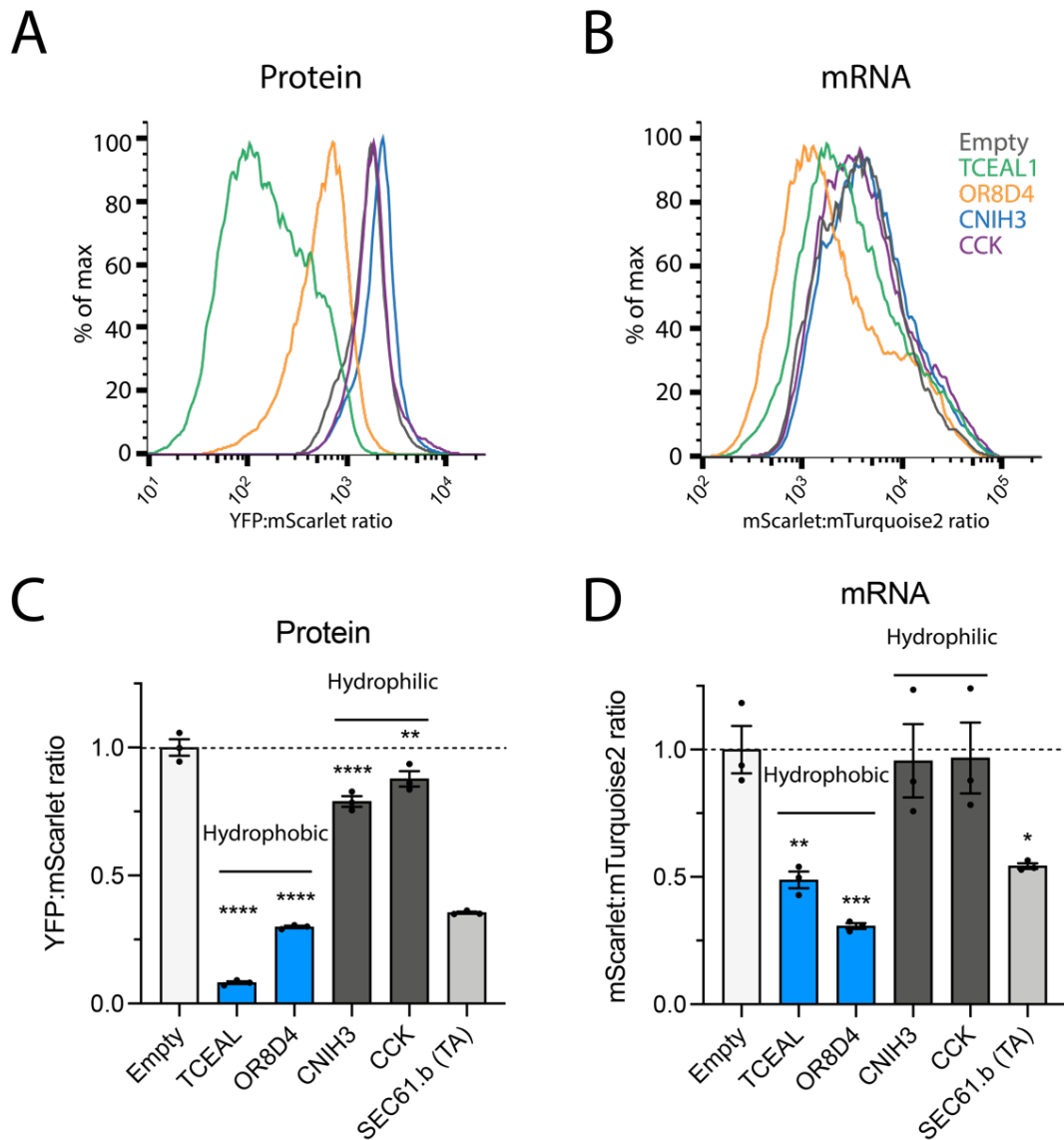


Figure 46: Protein and mRNA destabilization upon translation of hydrophobic UTRs is conserved in mammals. (A) and (B) Representative histograms of flow cytometry analysis indicating YFP:mScarlet and mScarlet:mTurquoise2 ratios of cells transiently transfected with the indicated reporter plasmids. (C) and (D) Ratiometric analysis in HEK293T cells of protein levels (YFP:mScarlet ratio) A) and of mRNA levels (mScarlet:mTurquoise2 ratio) B) of constructs in Figure 45. Data from flow cytometry. \*,  $p < 0.05$ ; \*\*,  $p < 0.01$ ; \*\*\*,  $p < 0.001$ ; \*\*\*\*,  $p < 0.0001$  by Dunnett's test. Error bars represent mean  $\pm$  SEM ( $n = 3$ ). Dotted line indicates Empty control ratios.

We speculated that the degradation of readthrough proteins with hydrophobic CTEs was dependent on the UPS, as observed in *C. elegans*. To formally test this idea, we treated cells with MLN-7243, an inhibitor of the E1 ubiquitin activating enzyme. Indeed, we found that inhibiting ubiquitylation selectively stabilized hydrophobic CTEs (Figure 47; left panel). In contrast, treating the cells with Bafilomycin A1 only resulted in a minor or no stabilization of the hydrophobic readthrough products, suggesting that the ubiquitin-proteasome system is the major degradation axis (Figure 47; right panel).

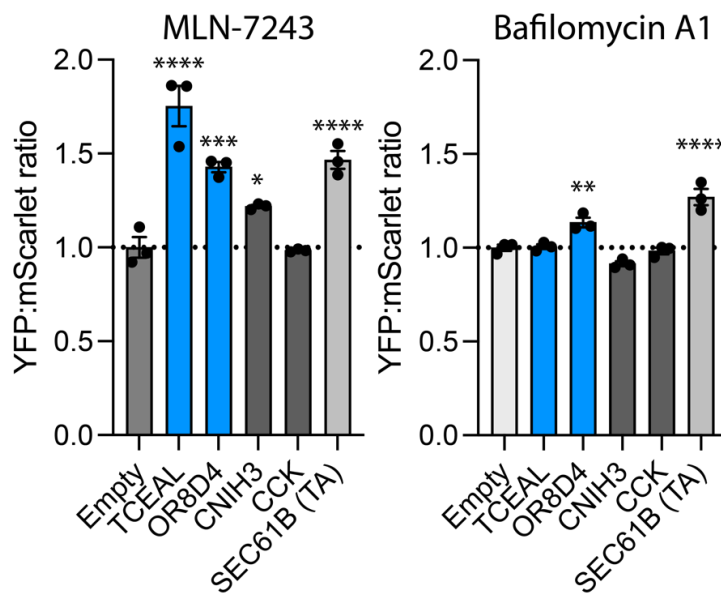


Figure 47: E1 enzyme inhibition leads to stabilization of hydrophobic readthrough products. Ratiometric flow cytometry analysis of cells expressing the indicated reporter plasmids in the presence of the E1 ubiquitin-activating enzyme inhibitor MLN-7243 or the lysosomal inhibitor Bafilomycin A1 (compared to untreated cells) ( $n = 3$ ).  $p$ -Values by Dunnett's test. \*,  $p < 0.05$ ; \*\*,  $p < 0.01$ ; \*\*\*,  $p < 0.001$ ; \*\*\*\*,  $p < 0.0001$ .

We noted that the stabilization of the reporter protein with hydrophobic CTE (TCEAL) led to the widespread formation of aggregate inclusions in HEK293 cells, as assessed by microscopy (Figure 48). In contrast, the hydrophilic CTE of CNIH3 remained soluble and diffusely distributed.

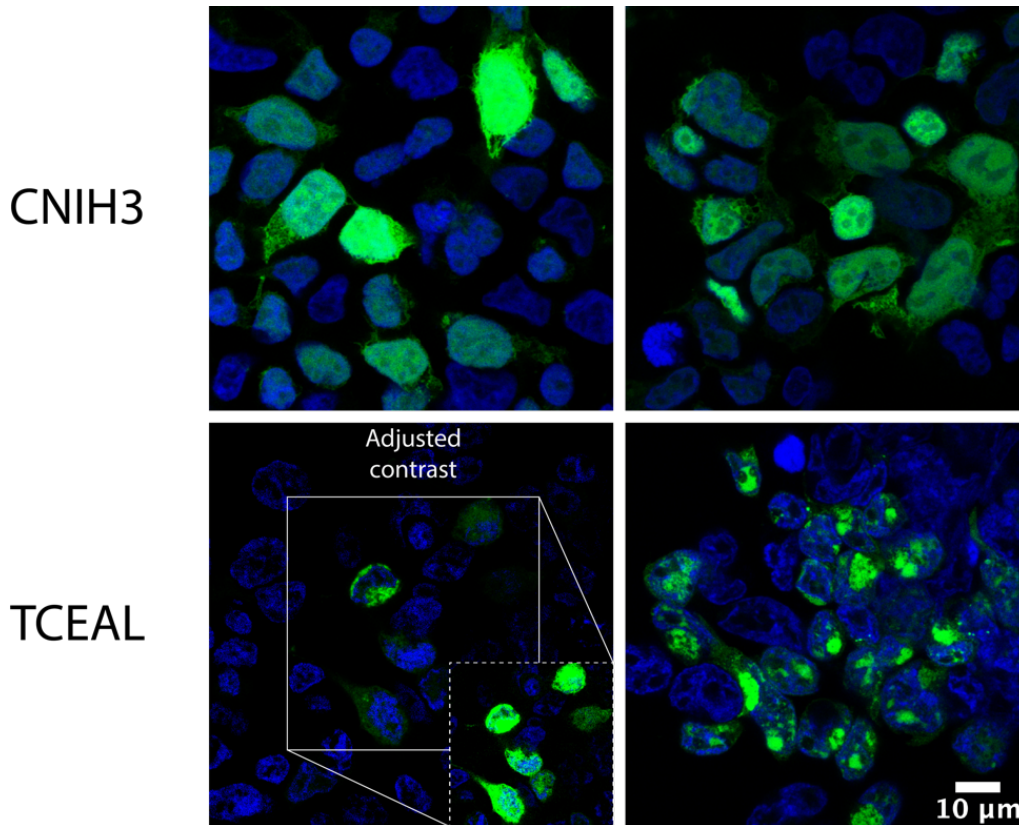


Figure 48: Representative fluorescence microscopy images of hydrophobic (YFP-TCEAL) or hydrophilic (YFP-CNIH3) readthrough reporter proteins with (right panels) or without (left panels) E1 inhibition by MLN-7243. Insert in the lower left image shows cells after contrast adjustment for the low expression level of the YFP-TCEAL readthrough reporter.

This observation was further confirmed by the increased sedimentation of TCEAL in the insoluble fraction upon E1 inhibition (Figure 49). In contrast, proteins with hydrophilic CTEs and the *bona fide* TA-protein SEC61B remained largely soluble.

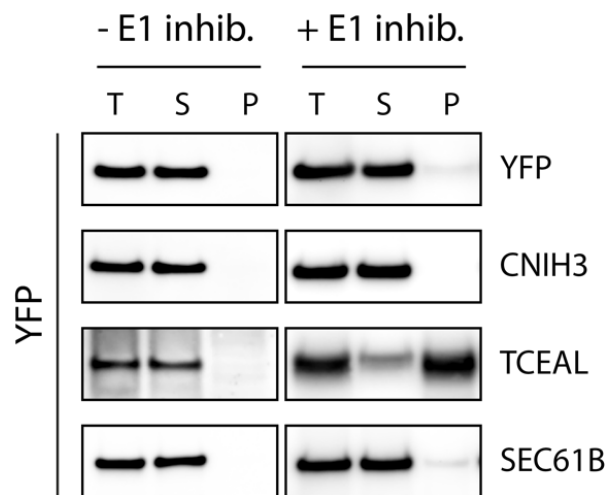


Figure 49: Representative immunoblot analysis of total (T), soluble (S) and pellet (P) fractions from cells expressing the indicated reporter constructs. YFP-TCEAL is most enriched in the pellet fraction upon E1 inhibition.

To assess if protein clearance was mediated via the BAG6/RNF126 complex, we generated knockouts of factors of this machinery (Figure 50).

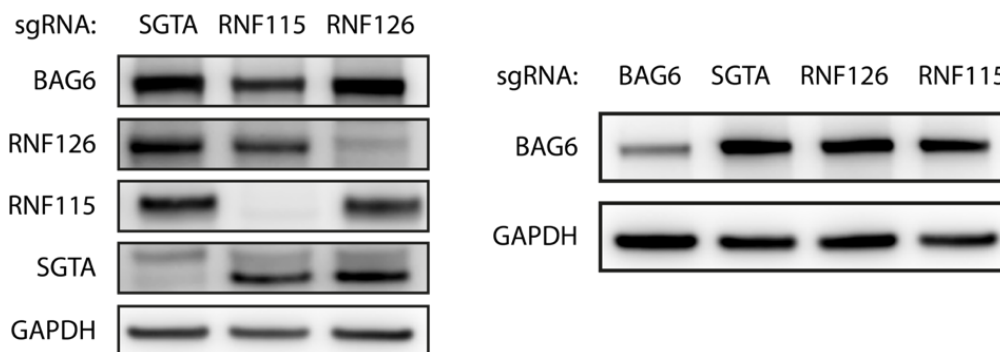


Figure 50: Representative immunoblot analysis of HEK293T depletion cell lines for components of the BAG6 complex.

Indeed, hydrophobic readthrough products were stabilized in BAG6 knockout cells (Figure 51). Human cells contain two highly similar E3 ligases found to be associated with the BAG6 complex, namely RNF126 and RNF115. While it was shown that RNF126 plays the dominant role in degrading mistargeted TA proteins in human cells (Rodrigo-Brenni et al., 2014), we found that a double knockout of RNF126 and RNF115 has a higher degree of protein

stabilization, suggesting an additive and compensatory role of the two E3 ligases (Figure 51). This effect was more pronounced with the 3'UTR of TCEAL1 than with the similarly hydrophobic 3'UTR of OR8D4, suggesting that additional chaperone machineries may operate redundantly to the BAG6 complex for proteasomal degradation of certain readthrough proteins.

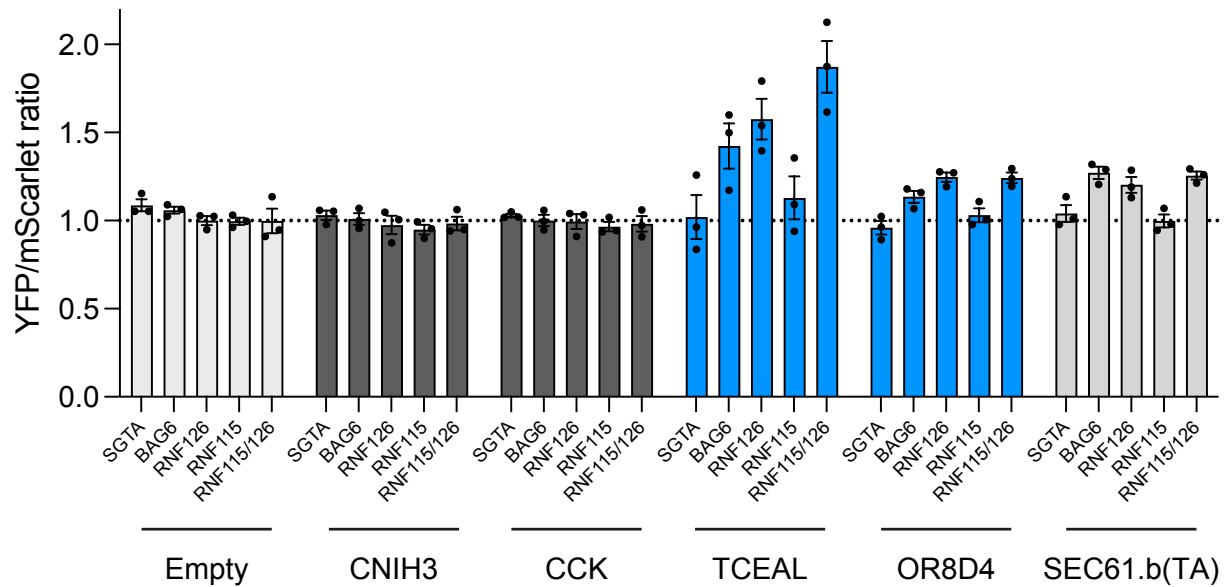


Figure 51: The BAG6 complex is involved in the degradation of hydrophobic readthrough products in mammals. Significance was determined by one-way ANOVA with Dunnett's correction  $n=3$ .

We confirmed the stabilizing effect on hydrophobic CTEs upon deletion of BAG6-associated E3 ligases by immunoblot analysis (Figure 52), showing a similar degree of stabilization as assessed by flow cytometry.

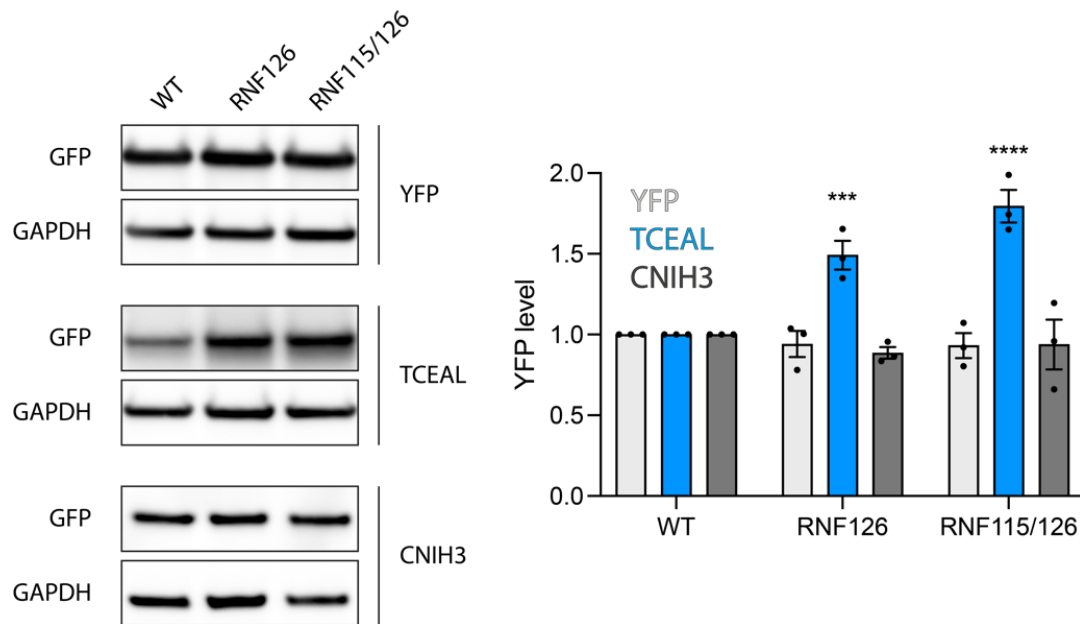


Figure 52: Immunoblot analysis confirms RNF115/126 involvement in the degradation of hydrophobic readthrough products.

We next investigated the role of the CCR4/NOT complex in readthrough mRNA decay. Since CCR4/NOT complex members are largely essential, we used siRNA mediated depletion of CNOT1, a core scaffolding subunit, resulting in a ~75% protein reduction (Figure 53).

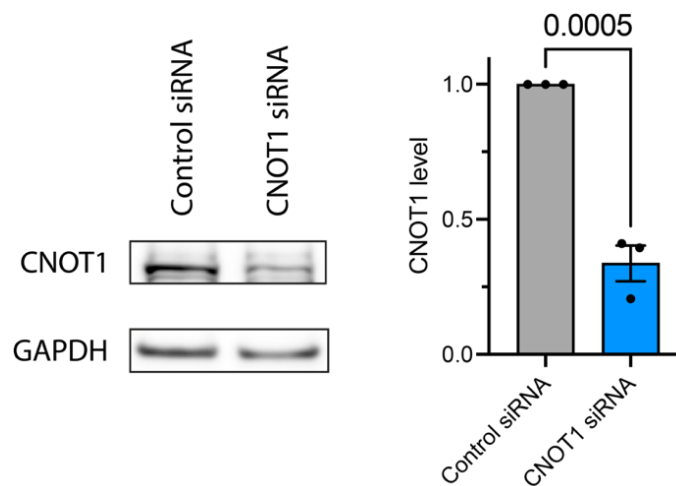


Figure 53: Representative immunoblot analysis of downregulation efficiency using siRNA against CNOT1 compared to control siRNA and corresponding quantification by densitometry. Error bars represent mean  $\pm$  SEM (n = 3). p-Value by Student's t-test.

We found a modest, but reproducible increase in the mRNA levels for the hydrophobic 3'UTR constructs (Figure 54). We therefore conclude from these results that the two-tiered quality control pathway of readthrough events is conserved in human cells.

## CNOT1 vs. Control siRNA

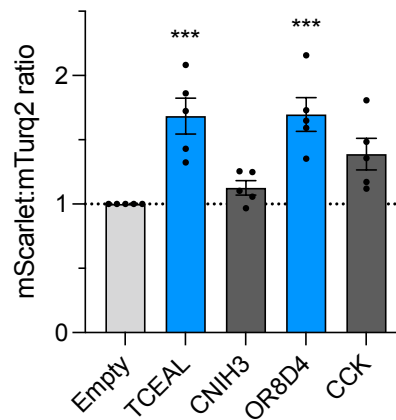


Figure 54: Effect of downregulation of CNOT1 on mRNA level of 3'UTR reporter constructs. Ratiometric analysis by flow cytometry of cells treated with siRNA against CNOT1 or control siRNA. Error bars represent mean  $\pm$  SEM ( $n = 5$ ).  $p$ -Value by Dunnett's test. \*\*\*,  $p < 0.001$ .

## GCN-1 is a general cotranslational surveillance factor for translational readthrough and transmembrane proteins

To characterize endogenous substrates of GCN-1-mediated quality control, we performed selective ribosome profiling (Ribo-seq) of GCN-1 (Becker et al., 2013; Matsuo and Inada, 2021; McGlincy and Ingolia, 2017) using nematodes expressing 3x-FLAG tagged GCN-1. Given the role of GCN-1 as a collision sensor, we performed selective Ribo-seq on GCN-1 bound monosomes and disomes. As an input control we profiled total ribosome (monosomes and disomes) from the same lysate. While GCN-1-bound footprints mainly mapped to protein coding regions (CDS), we observed a substantial (~4-fold) enrichment of footprints mapping to the 3'UTR regions compared to the total input control (Figure 55). Metagene analysis indicates that although stop codon readthrough frequency is low, GCN-1 efficiently binds to ribosomes translating into the 3'UTR. Importantly, we confirmed previous reports that ribosome collisions occur in 3'UTRs (Han et al., 2020) and established that GCN-1 can sense and bind them. Therefore, GCN-1 may actively surveil aberrant stop codon readthrough ensuring translational fidelity.

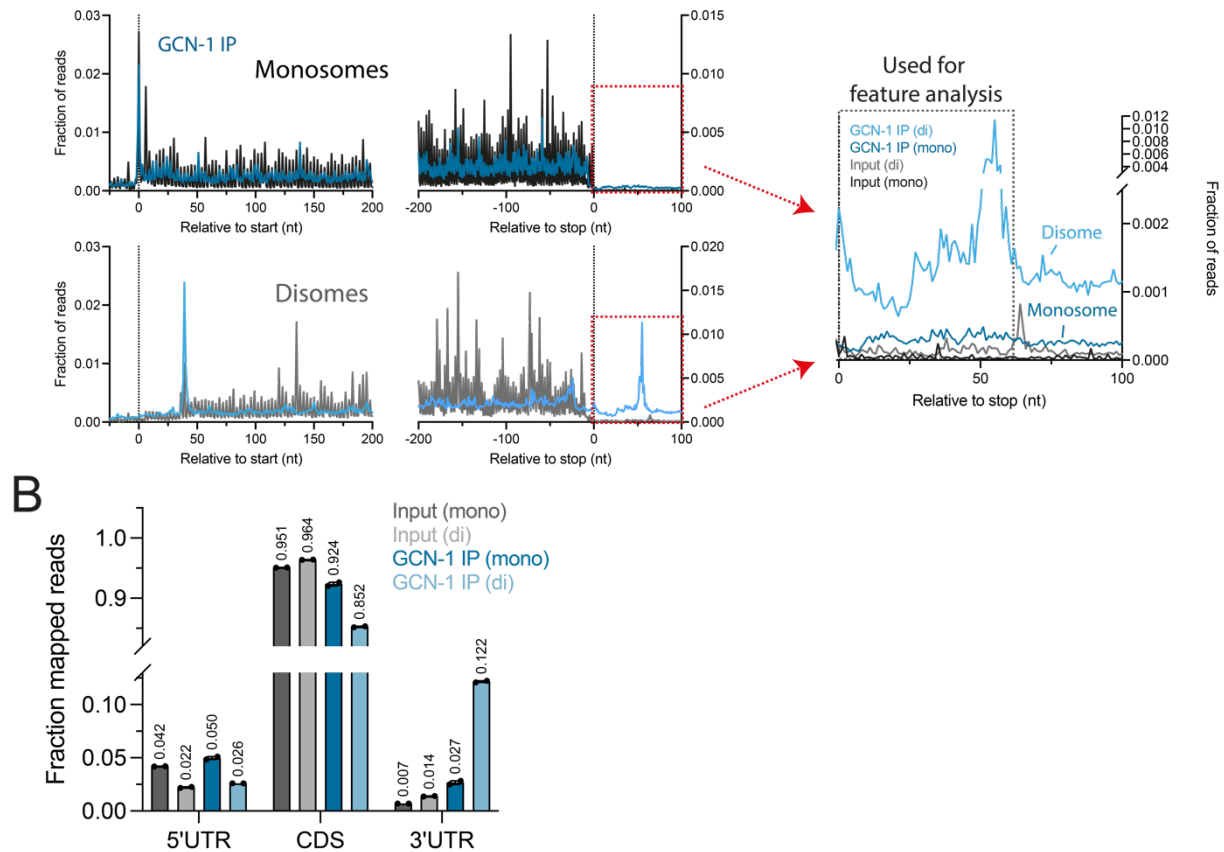


Figure 55: GCN-1-IPed ribosomes predominantly map into the coding region of transcripts, however, have an enriched density in the 3'UTR region when compared to total input. A) metagene plots represented as fraction of reads. B) Fraction of reads mapping to 5'UTR, CDS or 3'UTR for either input or GCN-1-IPed ribosomes. Significance was assessed by one-way ANOVA and corrected using Šídák method.

We noted an increased binding of GCN-1 within ~10-20 codons after the canonical stop codon (Figure 55A; right panel). The resulting protein sequences were enriched in codons for hydrophobic amino acids (phenylalanine, proline, isoleucine), while codons of polar and charged residues (arginine, threonine, glutamine) were less frequently targeted by GCN-1 (Figure 56A), supporting the previous finding that GCN-1 preferentially acts on readthrough events of hydrophobic CTEs. Further, we identified an increased occurrence of nonoptimal codons in 3'UTRs (low tRNA adaptation (tAI) scores) (Figure 56B), which suggests that GCN-1 may sense collisions induced by inefficient translation.

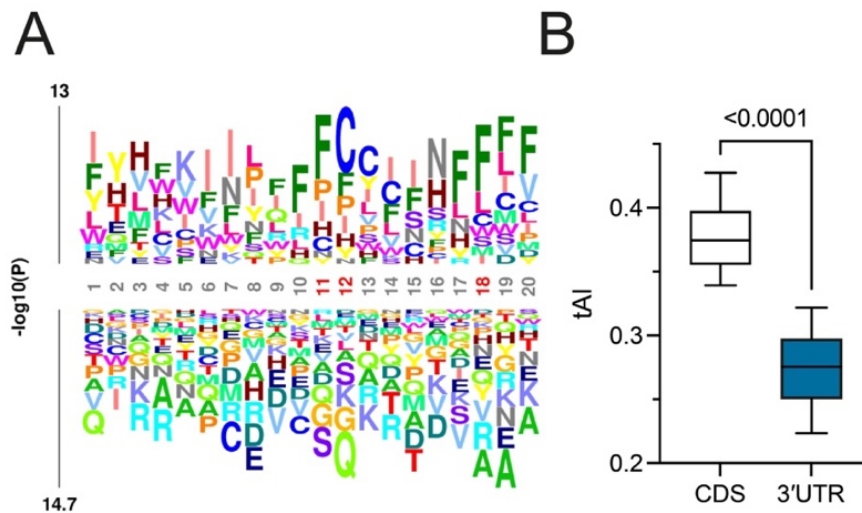


Figure 56: Logo plots of amino acid enrichment using *kplogo* analysis (Wu and Bartel, 2017). Sequences (20 aa downstream of annotated stop codon) chosen for analysis were derived from 3'UTRs bound by GCN-1 (monosomes and disomes; in frame 1). Numbers indicate the position after the stop codon. The y-axis indicates the sum of log p-values for each amino acid at a given position. Significantly enriched positions are marked in red. (B) 3'UTRs are enriched in nonoptimal codons. tRNA adaptation (tAI) index was analyzed for coding sequences (CDS) and 3'UTRs in *C. elegans*. The horizontal line in the boxplots indicates the median; boxes indicate upper and lower quartile and whisker caps 10<sup>th</sup>-90<sup>th</sup> percentile, respectively. p-Value by unpaired t-test.

Next, we investigated transcripts with increased GCN-1 recruitment upon translational readthrough. In this analysis we only considered reads that mapped to the 3'UTRs of transcripts either from GCN-1 selective Ribo-seq or input control. Gene ontology (GO) term analysis revealed transcripts involved in key functions of translation, protein, and RNA quality control, as well as biocondensate formation to be most enriched among the readthrough mRNAs targeted by GCN-1 (Figure 57).

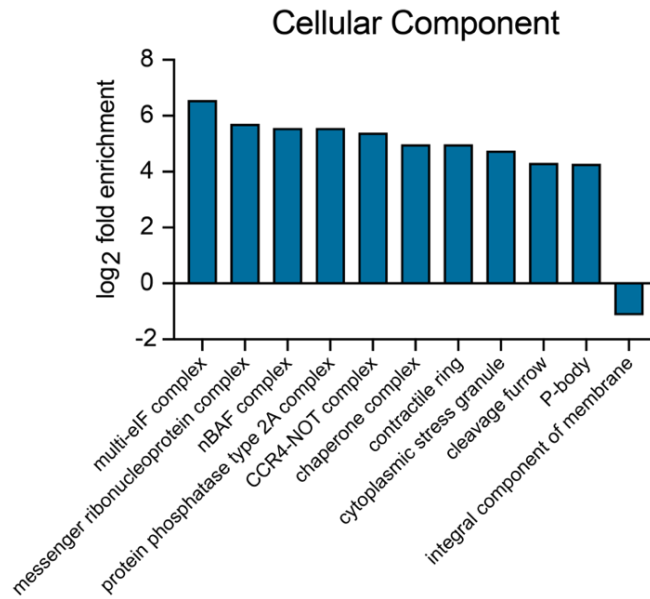


Figure 57: GO term of transcripts with enriched GCN-1-bound ribosomes in the 3'UTRs compared to total input.

We next analyzed characteristics of GCN-1-associated RPFs in coding sequences (CDSs). We observed that GCN-1 is mainly recruited to ribosomes that are engaged on mRNAs encoding for integral membrane proteins (TMD) and collagens both in GCN-1 bound mono- and disomes (Figures 58A and 58B). Interestingly, both these substrate classes have an overall higher disome occurrence compared to all detected transcripts (Figure 58C). This trend was particularly evident for collagens (Figure 58C).

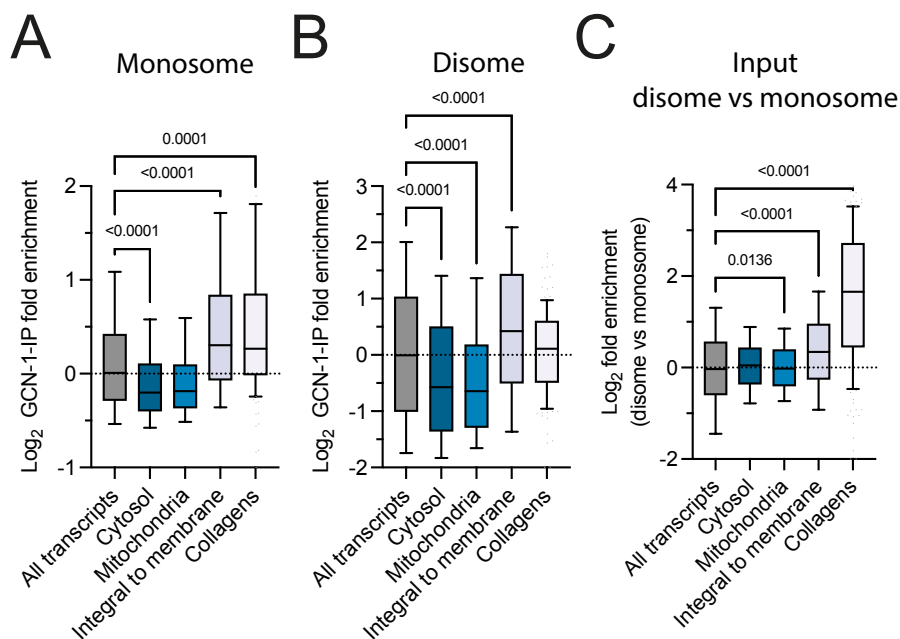


Figure 58: GO term analysis of transcripts enriched for GCN-1 reveals bias towards TMD containing transcripts.

Recently, HEL2 (homolog to human ZNF598) was shown to target TMD containing transcripts in yeast (Matsuo and Inada, 2021), making GCN-1 and HEL2 seemingly competing factors. To identify possible differences in binding preferences for TMD transcripts, we performed a polarity analysis of both GCN-1-IPed ribosomes, as well as HEL2-IPed ribosomes, based on the published yeast data for HEL2 (Matsuo and Inada, 2021). A polarity analysis reveals read distribution biases across transcripts. A skew towards the negative site of the x-axis denotes a binding preference towards the 5' end of transcripts, whereas a positive shift would indicate a higher affinity towards the 3' end. We noted that GCN-1 generally has a bias towards the 3' end of TMD transcripts, when compared to the total input (Figure 59A). This contrasts with the binding behavior of HEL2, which exhibits a binding-preference for the 5' end of TMD transcripts (Matsuo and Inada, 2021) (Figure 59B). We next asked, whether a similar bias can be observed for NOT4, a critical component of the CCR4/NOT complex which monitors and binds ribosomes on nonoptimal codons. We performed this analysis using previously published data from yeast (Buschauer et al., 2020). However, NOT4 showed no clear 3' or 5' polarity of mRNA binding bias (Figure 59C). Together these results suggest that the contrasting preferences for binding regions along the transcripts targeted by GCN-1 and HEL2 would allow them to target the same substrate classes without competing for the same ribosomes.

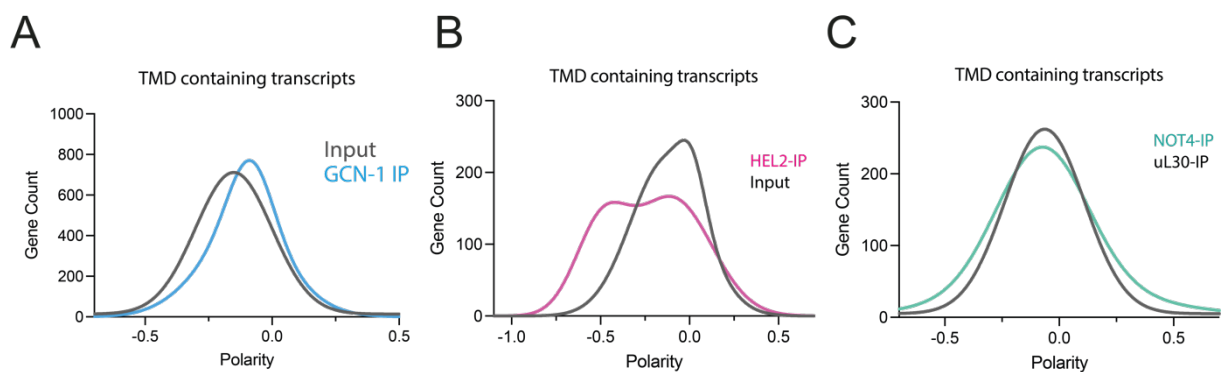


Figure 59: Comparison of (A) HEL2, (B) GCN-1 and (C) NOT4 for their binding bias across TMD transcripts using polarity plots.

To further investigate the possible role of GCN-1 in TMD biogenesis, we analyzed its binding preference around the emergence of a TMD segment. Interestingly, GCN-1 engaged the ribosome-nascent chain complexes (RNCs) of membrane proteins preferentially after emergence of a TMD from the ribosome (Figure 60), which is contrasting what has been previously reported for HEL2 (Figure 59B) (Matsuo and Inada, 2021). Importantly, profiling of total ribosomes (monosomes) from *gcn-1(nc40)* mutant animals showed a decrease in density

after TMD emergence compared to wild-type (Figure 60). Since ribosome occupancy is a proxy for elongation kinetics, reduced density would mean that in the absence of GCN-1, ribosomes traverse along these stretches faster. This would suggest that GCN-1 functions as a sensor of translational problems (disomes), and more importantly enhances the translational pause of ribosomes engaged in the TMD biogenesis particularly after the TMD segment has emerged from the exit tunnel, providing sufficient time for proper membrane insertion.

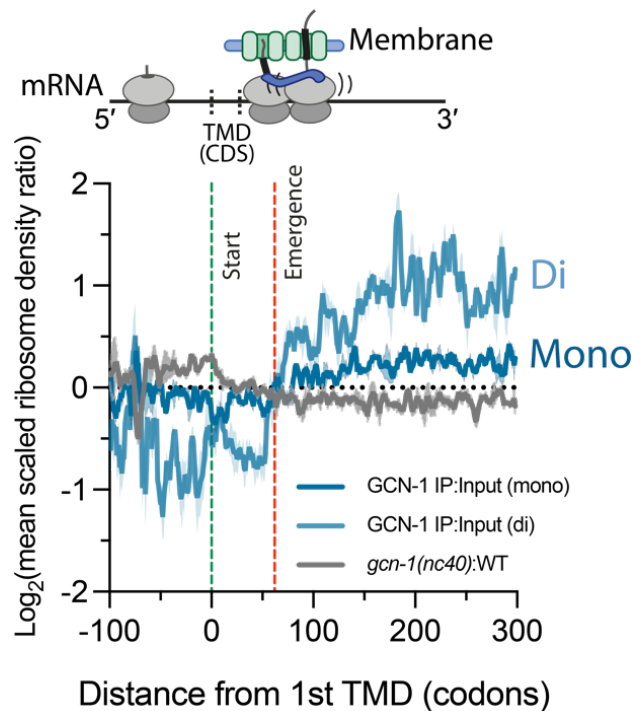


Figure 60: GCN-1 is recruited to ribosomes translating TMD containing transcripts after the TMD has emerged. The mean scaled ribosome density (normalization window of 300 codons upstream and downstream from the start of the first TMD segment) is shown with a moving average of 11 codons for GCN-IPed ribosomes (compared to input; monosomes – dark blue; disomes – light blue) and *gcn-1(nc40)* mutant (compared to wild-type; gray). The start of the TMD is indicated by a green and the emergence of the TMD from the ribosomal exit tunnel by a red vertical line.

Although mRNAs coding for TMD proteins were only mildly stabilized in young (D0) *gcn-1(nc40)* mutant animals, TMD proteins with multiple transmembrane segments, whose biogenesis is challenging, were particularly susceptible to GCN-1-mediated mRNA decay (Figure 61A). TMD transcripts have a general tendency towards containing nonoptimal codons, which is particularly evident in TMD transcripts that were susceptible to GCN-1 mediated mRNA decay. This trend is most pronounced in D6 animals (Figure 61B). GCN-1 thus

regulates the translation dynamics of TMD proteins and adjusts the levels of TMD-encoding mRNAs in an age-dependent manner. Given the concomitant change in translation dynamics and mRNA levels of GCN-1 target mRNAs observed after GCN-1 perturbation, we hypothesized that TMD proteins may misfold and aggregate in the absence of functional GCN-1. To test this hypothesis, we analyzed the detergent insoluble fraction of *gcn-1(nc40)* mutant and wild-type animals using mass spectrometry. Consistent with the age-dependence of GCN-1 effects observed above, young *gcn-1(nc40)* animals (D0) showed only a slight increase in TMD protein insolubility. However, in aged animals (D6), GCN-1 dysfunction significantly increased the sedimentation of TMD proteins in the detergent insoluble fraction (Figure 61C), suggesting that GCN-1 surveillance becomes critical as translational homeostasis undergoes age-dependent decline (Stein et al., 2022; Walther et al., 2017).

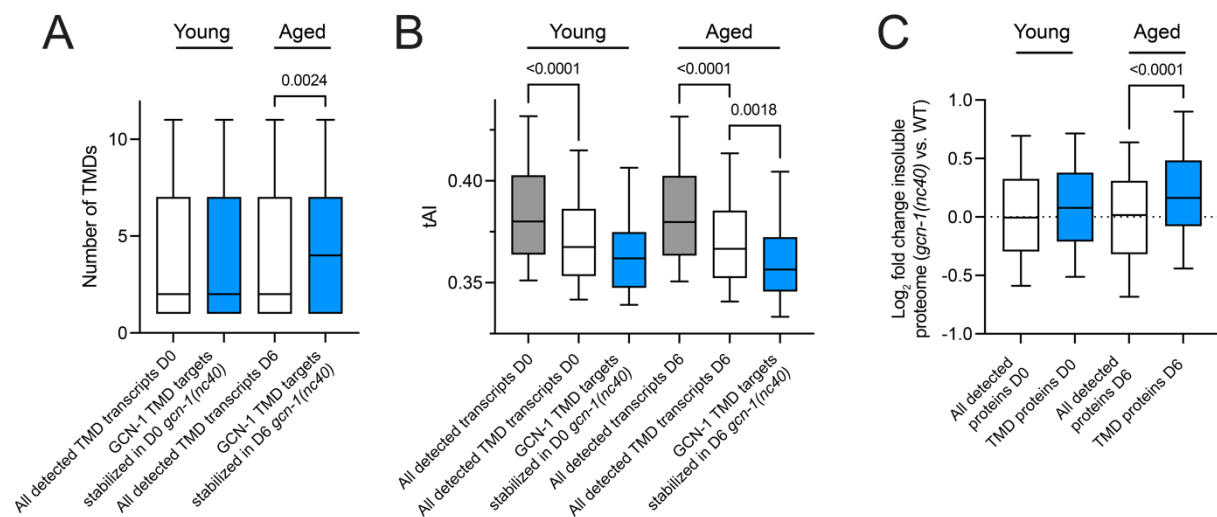


Figure 61: GCN-1 targets TMD containing transcripts with multiple TMD segments and low codon optimality. (A) GCN-1 is preferentially recruited to TMD containing transcripts with 4 or more TMD segments in aged animals. (B) TMD transcripts with a low tAI score are preferred targets of GCN-1 mediated mRNA decay. (C) Loss of functional GCN-1 leads to an increased accumulation of TMD proteins in the insoluble fraction as the worm age.

### Collagens are endogenous substrates of GCN-1

Besides transcripts coding for secreted and TMD containing proteins, our analysis identified collagens as endogenous targets of GCN-1 mediated quality control (Figure 62). Collagens are the main structural component of the extracellular matrix making up to 25% of the whole-

body protein content of mammals (Malhotra and Erlmann, 2015). Moreover, collagen homeostasis is critical for longevity in *C. elegans* (Ewald et al., 2015; Ferraz et al., 2016).

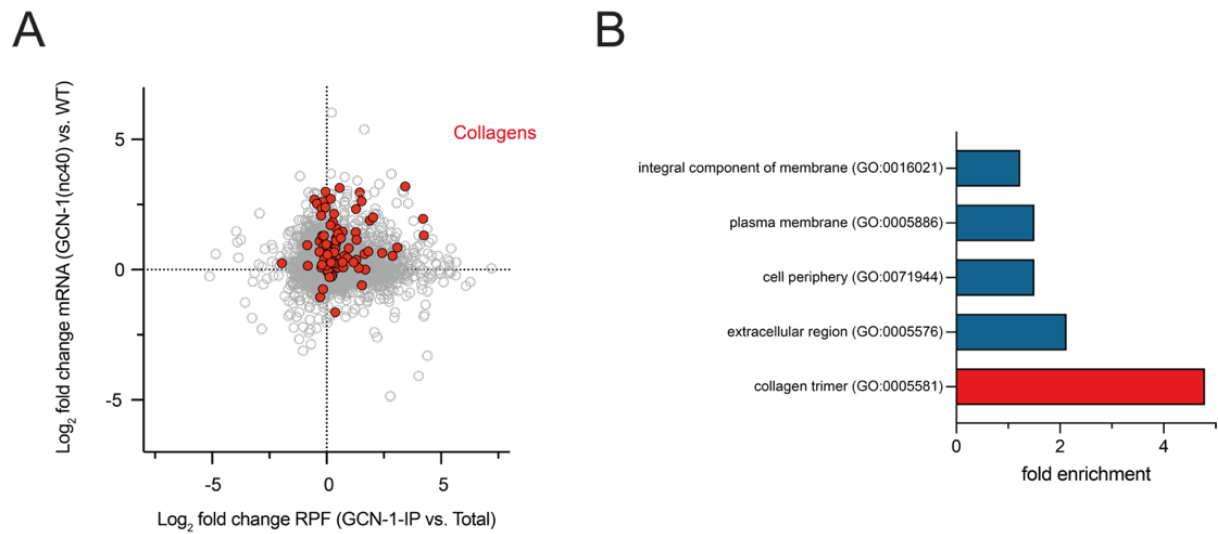


Figure 62: Collagens are an endogenous substrate of GCN-1 mediated mRNA decay. (A) Scatter plot of fold change in mRNA level (*gcn-1(nc40)* compared to wild-type [y-axis]) and GCN-1 recruitment (GCN-1-IP compared to Total[x-axis]). (B) GO term enrichment analysis of genes that are both upregulated in mRNA level and GCN-1 recruitment.

While GCN-1 is equally recruited to ribosomes translating collagens or TMD-containing proteins, the effect on mRNA decay was more pronounced for collagens (Figure 63).

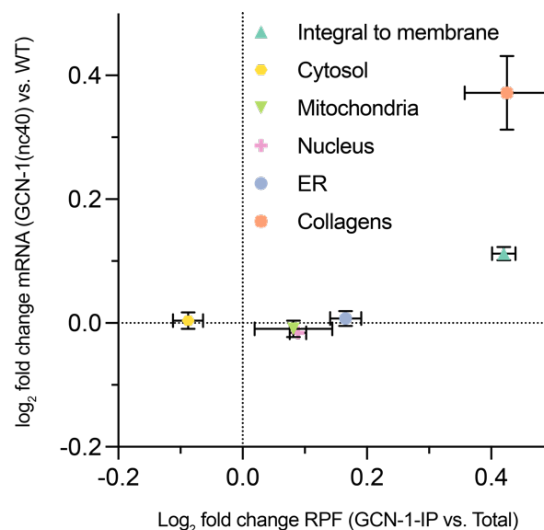


Figure 63: The bias towards GCN-1-mediated mRNA decay differs for different substrates. While transcripts of integral to membrane proteins (triangle; teal) and collagens (circle; salmon) have an equal recruitment of GCN-1, the effect of mRNA stabilization in the GCN-1(nc40) mutant differs. mRNAs of other classes, such as transcripts of cytosolic (hexagon;

yellow), mitochondria (inverted triangle; green), nucleus (cross; purple) and endoplasmic reticulum proteins are not generally affected by the loss of functional GCN-1.

The observed higher mRNA levels of collagens also result in higher protein levels in young (day 0) *gcn1-1(nc40)* mutants (Figure 64A). This increase in protein abundance is likely driven by the higher mRNA levels and not by increased translation of collagen mRNAs, as RPFs and mRNA fold changes are correlating (Figure 64B; n = 117).

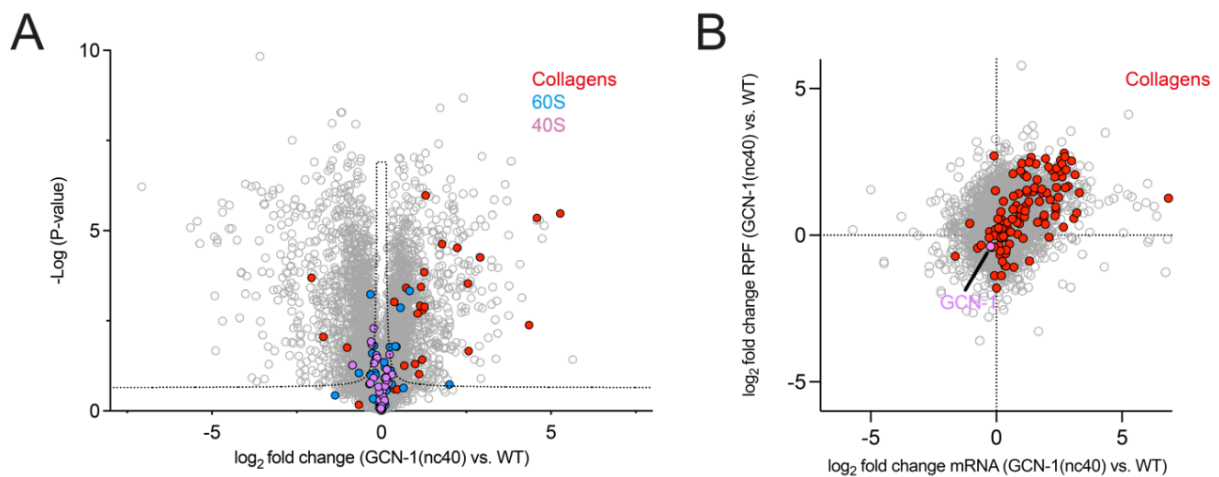


Figure 64: *GCN-1* modulates collagen levels by regulating collagen mRNA. (A) Total proteome analysis of *gcn1-1(nc40)* reveals elevated collagen levels when compared to wild-type animals. (B) The higher abundance of collagens is driven by higher mRNA levels and not by increased translation, as both mRNA levels (x-axis) and translation (ribosome protected fragments (RPF); y-axis) follow the same trend.

Collagens are characterized by numerous structurally critical X-Pro-Pro (XPP) motifs (Krane, 2008), which tend to induce ribosomal stalling during translation (Manjunath et al., 2019; Peil et al., 2013; Schuller et al., 2017). We therefore investigated the effect of GCN-1 on ribosome pausing at various tri-peptide motifs by computing a pause score based on ribosome occupancy ((Li et al., 2020) and Methods). Notably, pausing at XPP motifs was enhanced in wild-type animals compared to the *gcn1-1(nc40)* mutant, an effect that was magnified during aging (Figure 65).

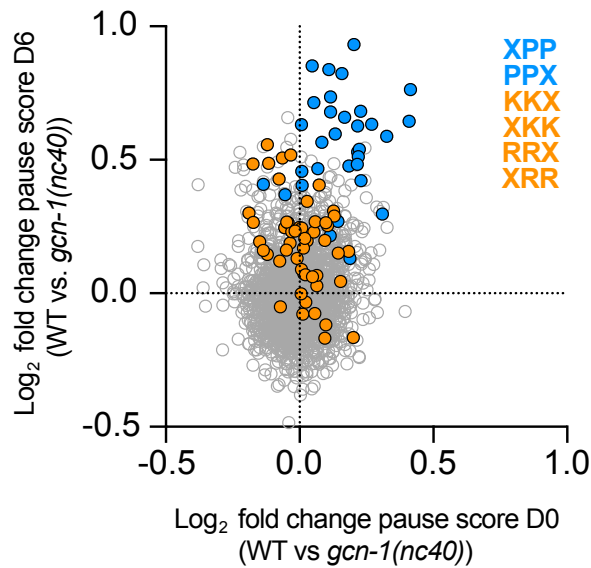


Figure 65: GCN-1 prolongs ribosomal pausing at stalling motifs. Loss of functional GCN-1 leads to a reduced translational pausing at motifs rich in proline, arginine, and lysine, known to induce translational slowdown.

Accordingly, we observed a lower ribosome density at polyproline stretches in young (D0) *gcn-1(nc40)* mutant nematodes, which was exacerbated in aged (D6) animals (Figure 66). Besides the lower pausing around polyproline, we observed that the ribosome densities trailing the polyproline stretch appear to be higher in the aged *gcn-1(nc40)* mutants. This would suggest that translation more readily commences after the polyproline in the mutant animals compared to wild-type (Figure 66; right panel).

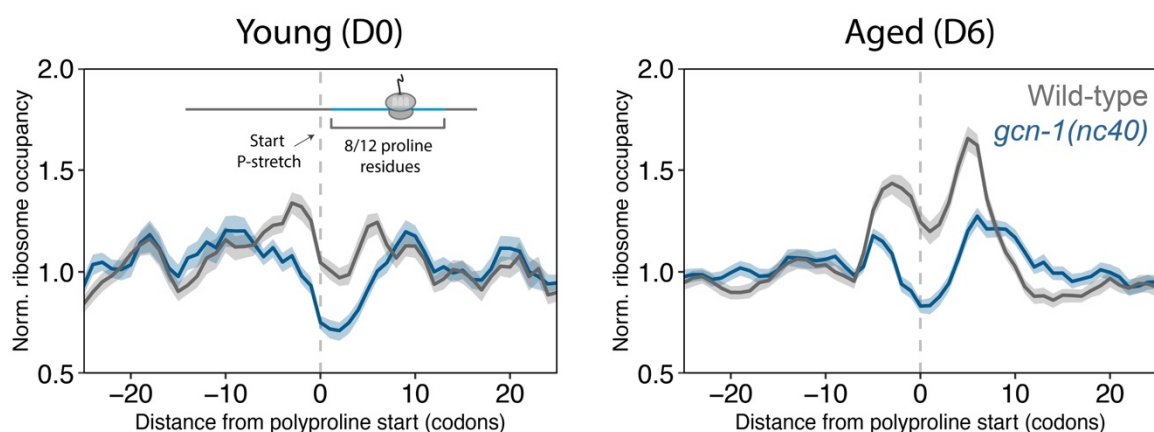


Figure 66: Ribosome dwell times at polyproline motifs are reduced in *gcn-1(nc40)* mutant animals compared to wild-type. The difference in ribosome occupancies in young animals between *gcn-1(nc40)* mutants and wild-type animals at polyproline motifs is small (left panel)

but increases as the organism ages (right panel). Mean-scaled ribosome occupancies are shown in gray (wild-type) and blue (*gcn-1(nc40)*). The shaded area indicates the bootstrapped 95% confidence interval.

Thus GCN-1 recruitment increases the residence time of ribosomes at proline-rich motifs. Importantly, this behavior applied generally to nonoptimal codons, as GCN-1 binding correlated with a low tAI score (Figure 67; left panel). Accordingly, aged wild-type animals displayed a higher ribosome A-site occupancy with nonoptimal codons than age-matched *gcn-1(nc40)* mutant nematodes (Figure 68; right panel). The preferential association of GCN-1 with ribosomes engaged at nonoptimal codons supports a model in which GCN-1 acts to further reduce elongation speed, presumably to ensure cotranslational folding.

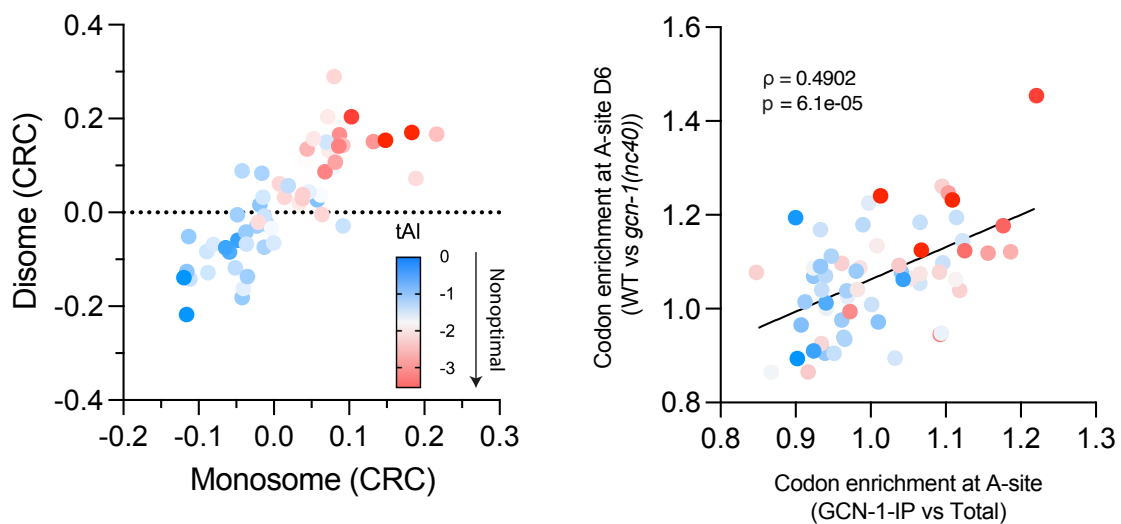


Figure 67: GCN-1 recruitment is influenced by codon optimality. Codon recruitment coefficients (CRC) were defined as the Pearson's correlation between codon frequency of transcripts and their (position independent) relative enrichment for GCN-1 binding (compared with wild-type) in both mono- and disome fractions (left panel). The CRCs correlate with codon optimality, with low codon optimality promoting GCN-1 recruitment. Ribosomes with non-optimal codons at the decoding center of ribosomes (A-site) are more likely to be engaged by GCN-1 compared to the input control (right panel). Ribosomes in wild-type animals are more likely to be engaged with non-optimal codons at the A-site compared to *gcn-1(nc40)* mutants (right panel).

To explore the consequences of reduced translational pausing caused by impairment of GCN-1 function during aging, we investigated the fate of collagen mRNA and proteins in young (D0)

and aged (D6) animals. We observed a substantial further stabilization of collagen mRNAs in aged *gcn-1(nc40)* mutant worms (Figure 69). This mRNA stabilization resulted in a strong increase in translation of collagen proteins, as demonstrated by mass spectrometry of polysome fractions (Figure 68). However, total collagen levels did not increase and rather declined (Figure 68). This mismatch between changes in protein and translation levels suggests that cells recognize excess collagen translation products as aberrant and degrade them.

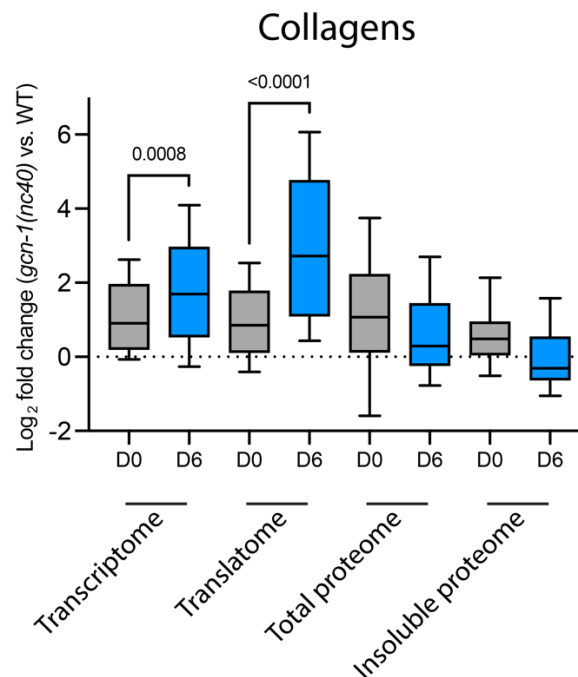


Figure 68: Efficient collagen biogenesis is dependent on functional GCN-1. Loss of functional GCN-1 in *gcn-1(nc40)* mutants leads to a strong stabilization of collagen mRNAs, especially in aged (D6) animals compared to wild-type nematodes (transcriptome). Translation of these transcripts is likewise strongly increased (translatome) but does not lead to a higher abundance in the total proteome or in the aggregate fraction (insoluble proteome).

Previous studies have implicated translational slowdown on nonoptimal codons in facilitating the cotranslational recruitment of protein folding chaperones, such as Hsp70 and the TRiC/CCT chaperonin (Stein et al., 2019). It seemed plausible that GCN-1 may modulate the recruitment of these factors. Indeed, mass spectrometric analysis of polysomes revealed reduced levels of the Hsp70 homolog HSP-1 and of TRiC/CCT on translating ribosomes in aged *gcn-1(nc40)* mutant animals (Figure 69). In addition to CCR4/NOT, the translation release factor ERFA-1 (eRF1 in mammals) was also reduced in mutant polysomes (Figure 69), which

would be consistent with a possible role of GCN-1 in recruiting ERFA-1 for premature translation termination on nonoptimal codons (Yang et al., 2019).

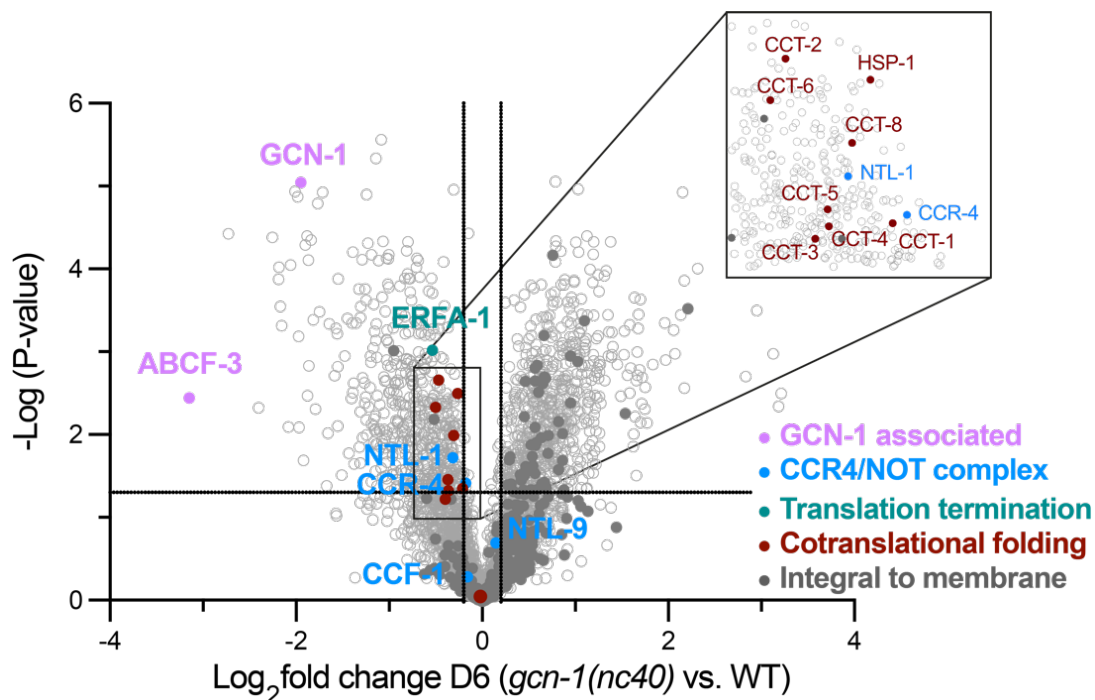


Figure 69: Loss of functional GCN-1 leads to a reduced recruitment of molecular chaperones to translating ribosomes. Polysome fractionation coupled to mass spectrometry of *gcn-1(nc40)* mutants compared to wild-type animals. GCN-1 associated proteins are highlighted in pink, translation termination factors in teal, CCR4/NOT associated proteins in blue, chaperones involved in cotranslational folding in red and integral to membrane proteins in dark gray.

Together these findings suggest that GCN-1 functions broadly in translational regulation. By prolonging ribosome pausing at nonoptimal codons (enriched in 3'UTRs, TMD proteins and collagens), GCN-1 facilitates the recruitment of quality control machinery to ensure efficient protein biogenesis and/or mediate mRNA decay. This function is increasingly important during aging.

### GCN-1 senses slow translating ribosomes

Codon optimality alone appears not to be the sole determining factor for GCN-1 recruitment to translating ribosomes. Pioneering work on GCN-1 identified it as a sensor for uncharged tRNAs and invoking the starvation response (Sattlegger and Hinnebusch, 2000). Later studies then elucidated additional roles, identifying the ability of GCN-1 to recognize collided

ribosomes. A prerequisite for ribosomal collisions is a prior slowdown of translation by the leading ribosome, allowing the trailing ribosome to catch up. The reasons for such a translational slowdown can be manifold, including reduced codon optimality. We therefore speculated that translational slowdown, not codon optimality per se, is the main driver for GCN-1 recruitment. The probability to find a ribosome at a given position is a function of the gene-specific flux (net translational rate of proteins) and position-specific dwelltime (DT) (Gobet et al., 2020). We reasoned that translational slowdown is more accurately portrayed computationally by flux calculations. While we observed a moderate positive correlation between ribosomal flux and codon optimality in *C. elegans* (Figure 70A), we found GCN-1 recruitment correlated negatively with ribosomal flux and codon optimality (Figures 70B and 70C). Interestingly, the negative correlation was stronger with ribosomal flux (-0.4493, Figure 70C) rather with codon optimality (-0.3843; Figure 70B).

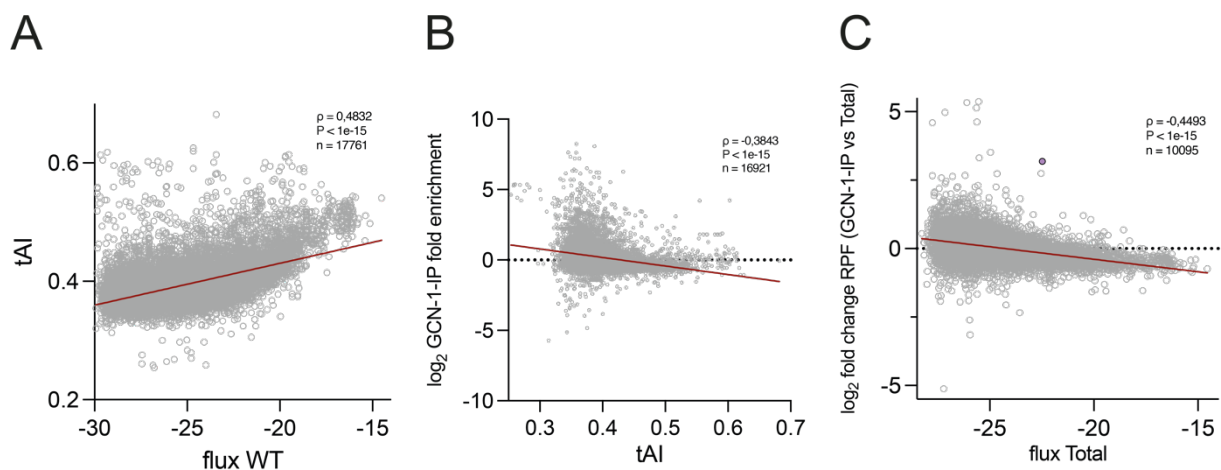


Figure 70: Recruitment of GCN-1 to translating ribosomes depends on low translational flux. (A) Translational flux positively correlates with codon optimality. (B) GCN-1 is recruited to transcripts with a low codon optimality. (C) A low translational flux of transcripts leads to increased GCN-1 recruitment.

Interestingly, a similar negative correlation can be observed for NOT4 and HEL2 recruitment in yeast when compared to ribosomal flux (Figures 71A and 71B).

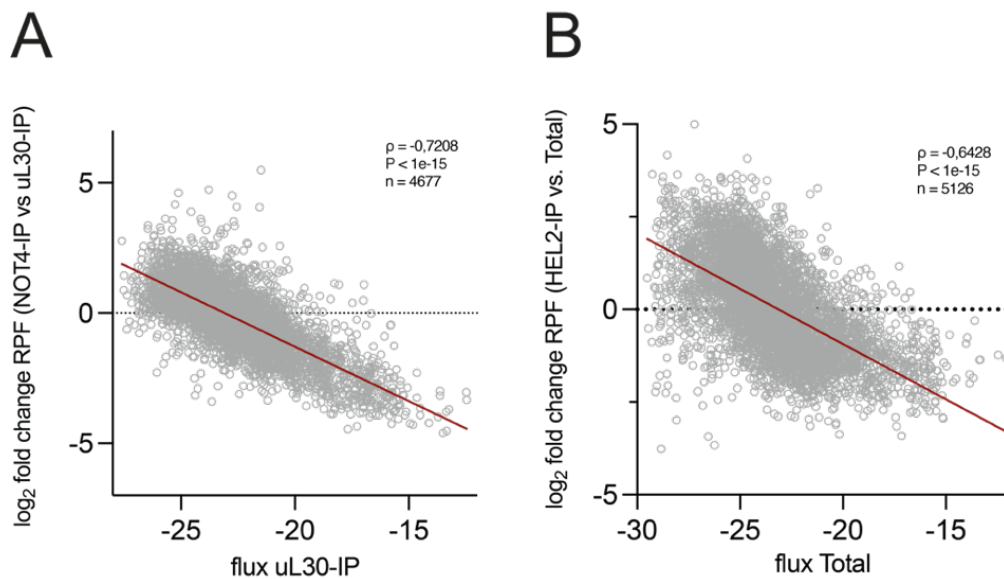


Figure 71: Low flux recruits quality control factors like NOT4 and HEL2 in yeast. (A) NOT4 and (B) HEL2 recruitment to transcripts is influenced by low flux

Importantly, a reduced flux appears to be the main driver of a functional GCN-1 recruitment resulting in mRNA decay of TMD containing transcripts. We noted that TMD transcripts which are upregulated in *gcn-1(nc40)* mutant worms have a significantly reduced flux (Figure 72).

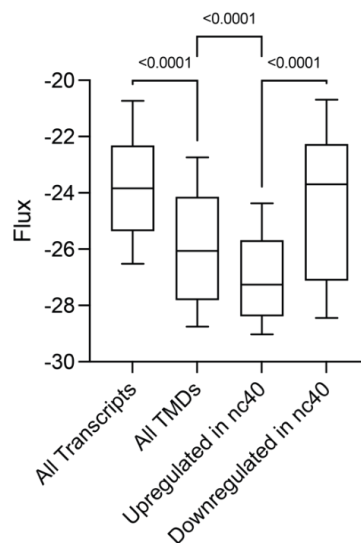


Figure 72: GCN-1 mediated mRNA decay of TMD containing transcripts depends on low ribosomal flux.

Taken together, these observations indicate that GCN-1 is recruited to ribosomes with a prolonged dwelltime on certain transcripts, initiating mRNA decay via CCR4/NOT.

## The function of GCN-1 is conserved in mammalian cells and is required for stress signaling

To analyze the function of GCN1 in translational surveillance in mammalian cells, we performed selective Ribo-seq in HEK293T cells. We induced stop codon readthrough with a low dose of the aminoglycoside antibiotic G418 in combination with CC-885, a small molecule that destabilizes the release factor eRF3 (Figure 73), thereby limiting translation termination capacity (Baradaran-Heravi et al., 2021; Matyskiela et al., 2016).

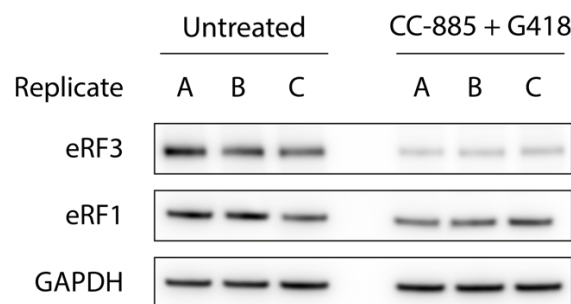


Figure 73: Immunoblot analysis of untreated and CC-885 + G418 treated cells confirms the high degradation efficiency of eRF3 mediated by CC-885.

Binding of GCN1 to ribosomes translating into 3'UTRs was modest in control cells but increased markedly upon treatment with G418 and CC-885 (Figure 74A). The protein classes targeted by GCN1 within coding sequences in untreated cells were essentially identical to those in *C. elegans*, with collagen transcripts again showing the highest enrichment of GCN1 binding (Figure 74B).

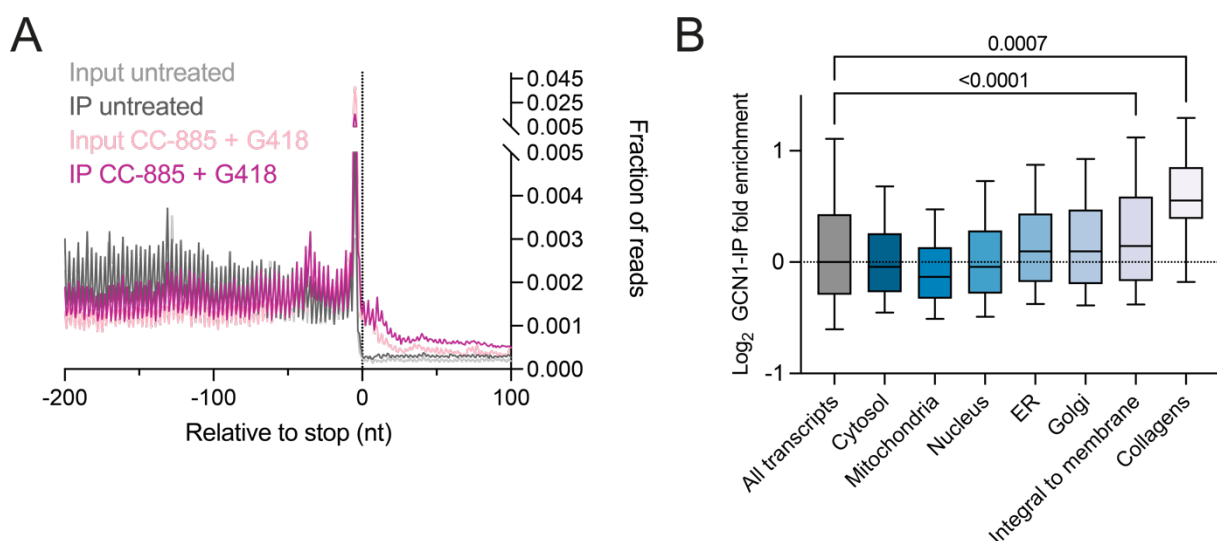


Figure 74: GCN1 recognizes ribosomes that translate into 3'UTRs of transcripts and is recruited to the same substrate classes as in *C. elegans*. A) Metagene profile of ribosome protected

fragments of input untreated (light gray), GCN1-IPed ribosomes untreated (dark gray), input of cells with increased readthrough treated with CC-885 + G418 (light purple) and GCN1-IPed ribosomes of cells with increased readthrough treated with CC-885 + G418 (dark purple) around the stop codon. B) Differential gene analysis (DEseq2) of GCN1-IPed ribosomes (compared to input) across different cellular components reveal preferential GCN1 recruitment to ribosomes translating transcripts of integral membrane proteins and collagens.

While in untreated cells around 1.2 % of all reads mapped in the 3'UTR regions of genes this value increased to 4.5 % in the treated samples treated to induce readthrough. Similar to the results obtained in *C. elegans*, we observed that GCN1 was efficiently recruited to ribosomes translating into 3'UTRs, reflected by 4.1 % of reads mapping in the 3'UTR regions of GCN1 bound ribosomes in untreated conditions and 10.5 % in the treated HEK293 cells (Figures 75A and 75B). Moreover, we observed that the ribosomes that fail to terminate at the canonical stop codon of transcripts, exhibit a +1-frameshift compared to ribosomes in the CDS region. In contrast, in treated cells, where translation termination cannot be efficiently executed, the reading frame 0 of the CDS was preserved in 3'UTRs (Figure 75C).

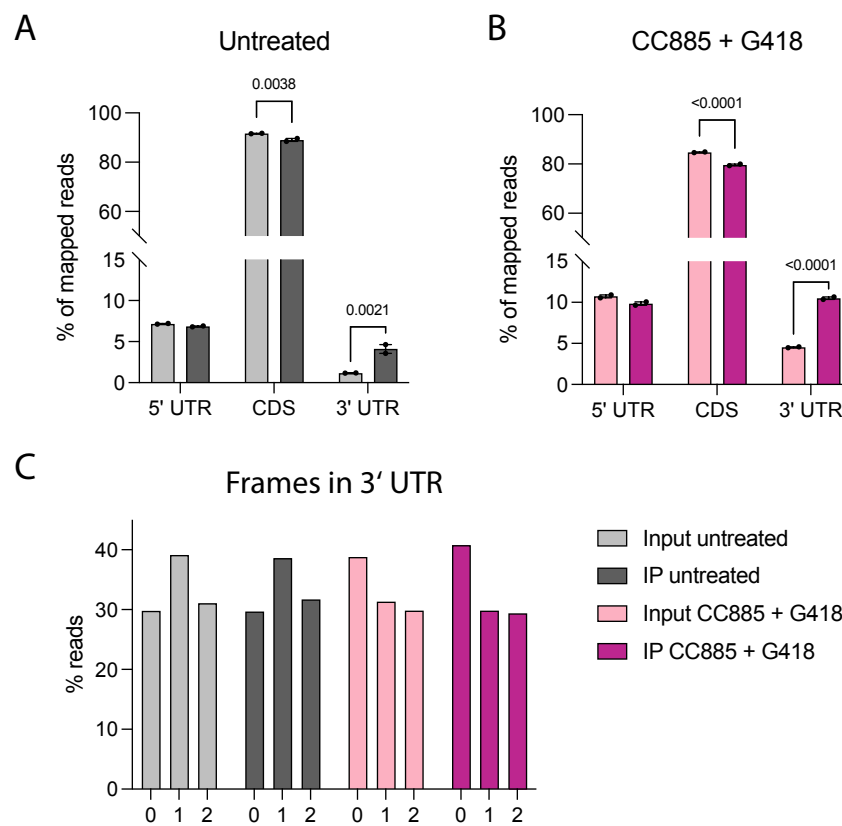


Figure 75: GCN1 is recruited to ribosomes translating into 3'UTR regions of transcripts. Read distribution across 5'UTR, CDS and 3'UTR regions of ribosomes across transcripts: A) of input untreated HEK293 (light gray) and GCN1-IPed ribosomes (dark gray), B) upon

pharmacologically induced stop codon readthrough treatment via CC-885 + G418 of input ribosomes (light purple) and GCN1-IPed ribosomes (dark purple). C) Frame distribution of ribosomes translating into the 3'UTR regions of transcripts in untreated conditions (light gray – input; dark gray – GCN1-IPed ribosomes) and pharmacologically induced readthrough (light purple – input; dark purple – GCN1-IPed ribosomes).

Mass spectrometry of polysome fractions in conditions of enhanced readthrough revealed recruitment of RQC-related factors, such as DRG1, promoting translation through stalling motifs (Zeng et al., 2021), the translational repressor GIGYF2 and SKI-exosome component SKIV2L. The recruitment of these factors is likely due to readthrough into polyA-tails occurring in a subset of mRNAs. However, we did not observe an enrichment for other RQC-related factors, including the collision sensor, ZNF598, and EIF4E2. Besides RQC-related factors, we confirmed the enrichment of GCN1 and the BAG6 machinery, as well as the depletion of eRF3 induced by CC-885. EDF1 and ZAK $\alpha$  (MAP3K), which cooperate with GCN1 in ribosome collision sensing (Juszkiewicz et al., 2020; Pochopien et al., 2021; Sinha et al., 2020; Wu et al., 2020), were also significantly enriched (Figure 76). ZAK $\alpha$  signals the ribotoxic stress response (RSR) upon ribosome stalling (Vind et al., 2020; Wu et al., 2020).

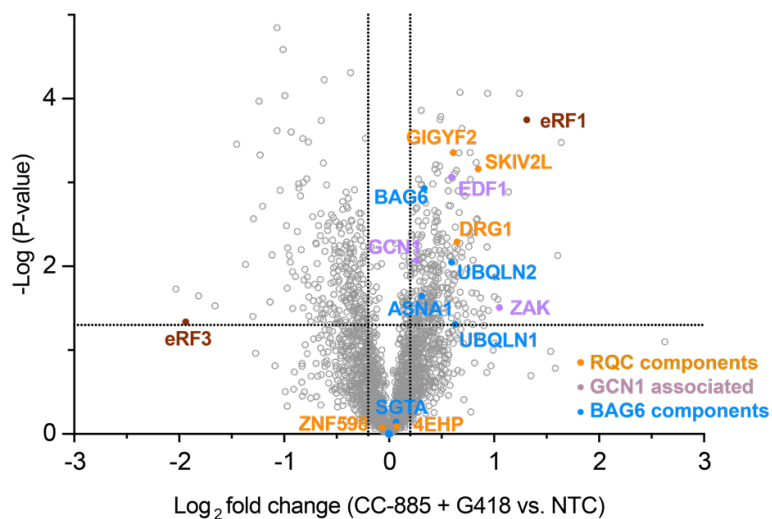


Figure 76: Increased stop codon readthrough leads to the recruitment of BAG6-components and GCN1 associated proteins to translating ribosomes. Volcano plot representation of sucrose-gradient isolated ribosomes of cells with induced stop codon readthrough (CC-885 + G418) and untreated HEK293T cells. RQC-related proteins are highlighted in yellow, GCN1 associated proteins in pink and BAG6-related proteins in blue.

Interestingly, increased stop codon readthrough induced by G418 was shown to activate the ISR to globally reduce translation (Wangen and Green, 2020). We therefore tested whether sensing of readthrough by GCN1 might be critical for this signaling effect, by mutating GCN1 using CRISPR/Cas9. Next, we sorted the cells by FACS to create a monoclonal cell line. Note that HEK293T cells remain viable after the deletion of GCN1 (Figure 77).

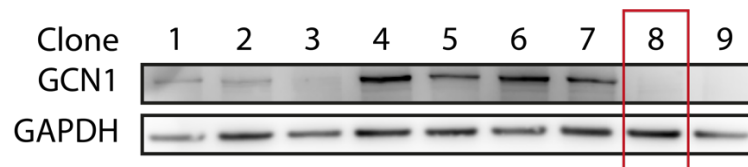


Figure 77: Immunoblot analysis of monoclonal CRISPR-Cas9-generated GCN1 knockout cell lines. The highlighted cell line (lane 8) was used for subsequent experiments.

Upon treatment with G418 and CC-885, wild-type cells showed a pronounced time-dependent accumulation of phosphorylated eIF2 $\alpha$  and p38 (Figures 78), indicative of ISR and RSR activation (Wu et al., 2020). Strikingly, GCN1 deletion completely suppressed the accumulation of phosphorylated eIF2 $\alpha$ , while phosphorylation of p38 was markedly reduced (Figures 78).

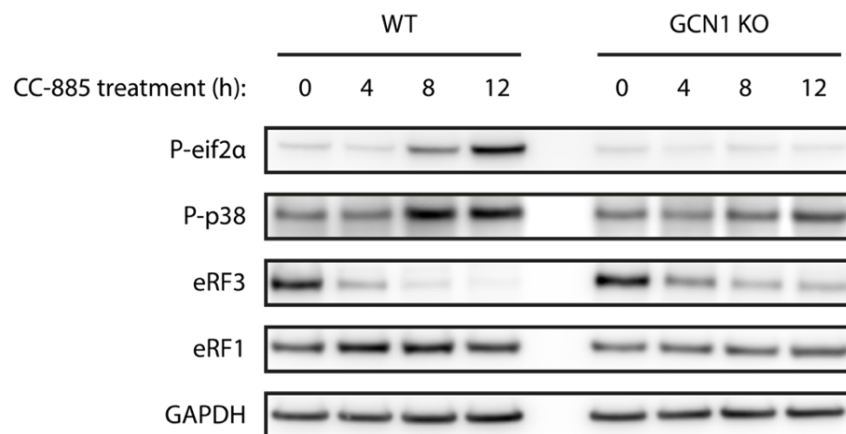
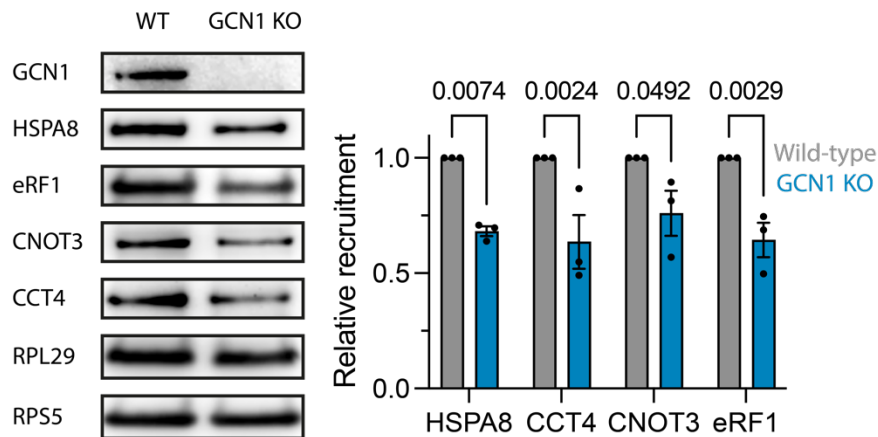


Figure 78: Integrated stress response activation upon induced readthrough. Wild-type and GCN1 deleted HEK293T cells were treated with CC-885/G418.

### GCN1 is a global modulator of mRNA stability

While we established in *C. elegans* that GCN1 is involved in the mRNA decay of collagens and certain TMD containing transcripts, how the turnover rates of specific mRNAs are affected in HEK293T cells remained unclear. Similar to our results in *C. elegans*, we observed that cotranslational recruitment of quality control factors is impaired in GCN1 deficient HEK293T

cells, including the molecular chaperone HSPA8, the TRiC chaperonin (subunit CCT4), the translation termination factor eRF1 and the CNOT3 subunit of the CCR4/NOT complex (Figure 79).



*Figure 79: Loss of GCN1 leads to the impaired recruitment of cotranslational quality control factors. Immunoblot analysis of sucrose-cushion purified ribosomes of wild-type and GCN1 KO HEK293T cells (left panel) and quantification by densitometry (right panel). p-Values were assessed by two-way ANOVA (n = 3).*

We predicted that this reduced recruitment of quality control factors has widespread effects on cotranslational folding and quality control, as well as global mRNA decay. To address effects on mRNA turnover in more detail, we performed RNA stability (SLAM-seq) measurements based on metabolic labelling of mRNA by using 4-thiouridine (4sU). This allowed us to label all preexisting mRNAs which can be distinguished from newly synthesized mRNAs by alkylation, leading to a T>C conversion at each position where 4sU was incorporated (Herzog et al., 2017). To gain insights on global mRNA turnover dynamics, we labelled all preexisting mRNA in wild-type and GCN1 KO cells for 24 hours. The media was exchanged with 100x Uridine, and the turnover dynamics were chased over the course of 8 hours (Figure 80).

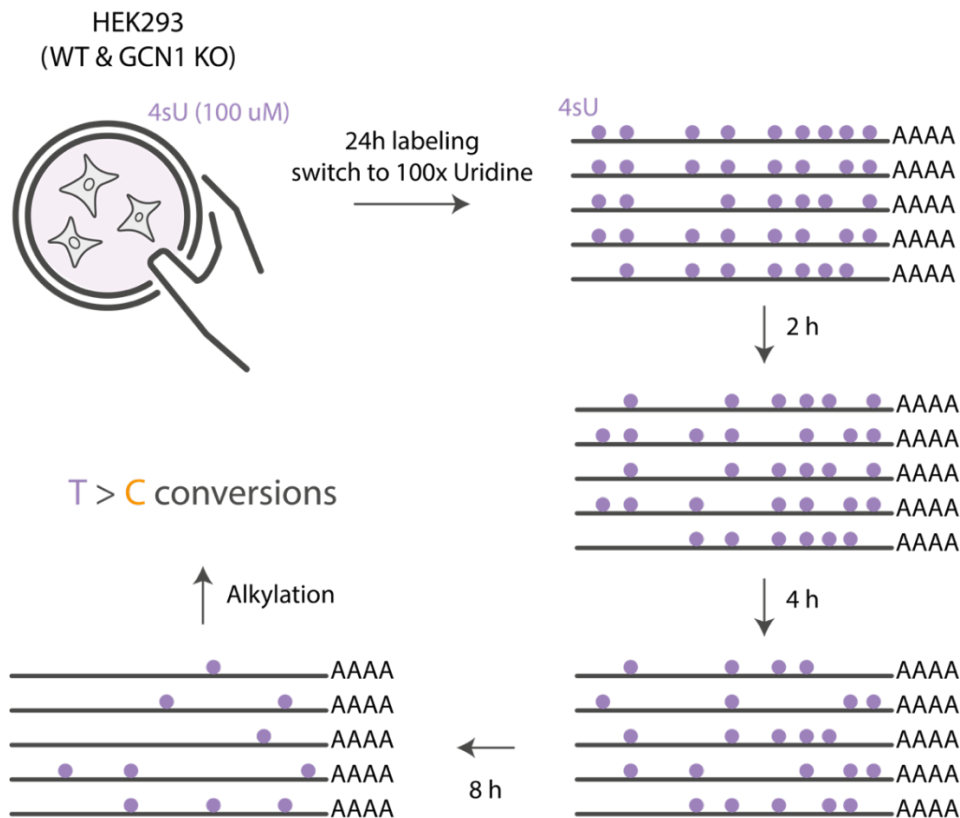


Figure 80: Schematic overview of the SLAM-seq approach to assess general mRNA turnover dynamics. HEK293T cells are cultured in 4sU containing media for 24 h, renewing the media every 3 h. After the pre-labeling, the chase is started by switching the media to 100x excess uridine (10 mM) containing media. At timepoints 0, 2, 4, and 8 h after the onset of the chase, the cells were collected, and mRNA was isolated. Over time, the labelled mRNA is lost due to mRNA decay. Based on T>C conversions by alkylating the incorporated 4sU, mRNA decay profiles can be analyzed, thus allowing a global view mRNA turnover dynamic.

We measured decay rates for ~5,500 transcripts (4 time points) that were detected with a high confidence ( $R^2 > 0.6$ ) for wild-type and GCN1 deleted cells. The mRNA half-lives measured in wild-type agree with previously published data, despite using a different method and cell line (Figure 81).

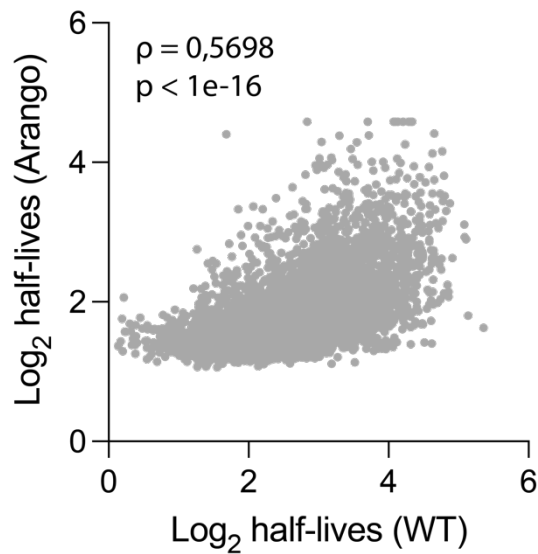


Figure 81: Comparison of mRNA half-lives determined by SLAM-seq (x-axis) in HEK293T and previously reported half-lives (y-axis) (n = 7151) (Arango et al., 2018).

GCN1 deletion had a severe impact on mRNA turnover, increasing the mean mRNA half-life from 5.1 h (wild-type) to 7.6 h upon GCN1 knockout (Figure 82). In line with the binding preference of GCN1 determined by ribosome profiling, TMD encoding transcripts showed a significant increase in mRNA stability, with a change in mean half-life from 5.4 h to 8.2 h for all mRNAs encoding TMD proteins analyzed (n = 698) and from 5.6 h to 8.6 h for proteins with multiple TMDs (n = 168) (Figure 82). Thus, the effect on TMD transcripts contributes significantly to the overall increase in mRNA half-lives in this data set.

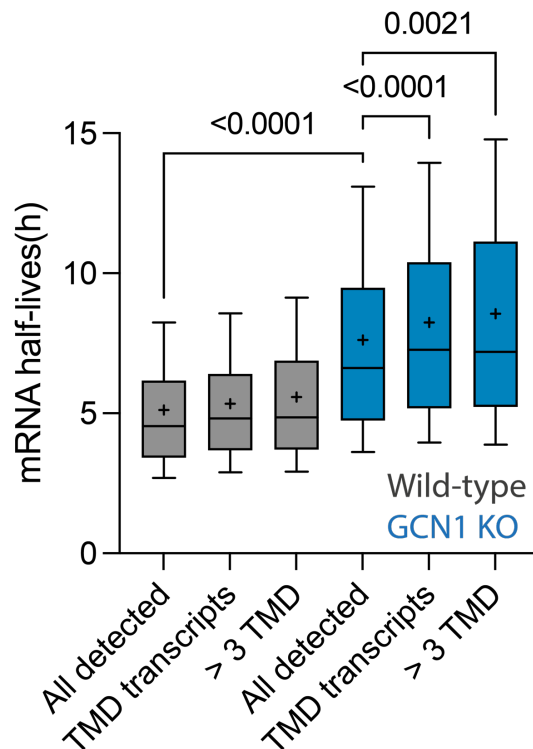


Figure 82: mRNA half-life analysis using SLAM-seq in wild-type and GCN1 deleted cells ( $n = 5455$ ), all TMD encoding transcripts ( $n = 698$ ) and TMD encoding transcripts with  $>3$  TMD segments ( $n = 168$ ). The horizontal line in the boxplots indicates the median; (+) the mean; boxes indicate upper and lower quartile and whisker caps 10th-90th percentile, respectively.  $p$ -Values were calculated by Holm-Sidak test.

Next, we wanted to investigate if short-lived mRNAs are the primary targets of GCN1. We therefore binned the mRNAs according to their half-life and inspected their tendency of GCN1 recruitment based on the selective Ribo-seq experiment. Interestingly, we observed that mRNAs with a half-life of less than 3 hours show the strongest GCN1 recruitment, whereas long-lived mRNAs with a half-life of greater than 8 hours are less likely targeted by GCN1 (Figure 83).

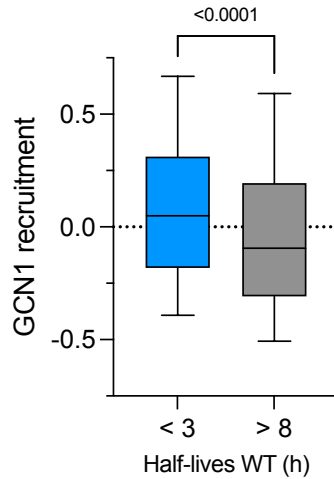


Figure 83: GCN1 is recruited to mRNAs with a shorter half-life. Box plot analysis shows the GCN1 recruitment to mRNAs with a half-life with less than 3 h (blue box) and greater than 8 h (gray box). The boxes indicate 25<sup>th</sup>-75<sup>th</sup> percentile, whiskers 10<sup>th</sup>-90<sup>th</sup> percentile and the line representing the median.

We then explored factors that define mRNA stability in mammalian cells. While codon optimality is a good predictor for mRNA stability in yeast, in higher eukaryotes the predictive power decreases. In HEK293T cells, we did not observe a significant correlation between the tAI score and mRNA half-lives (Figure 84).

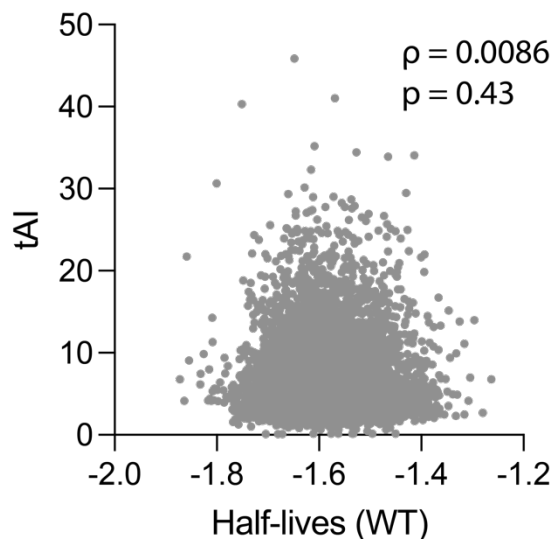
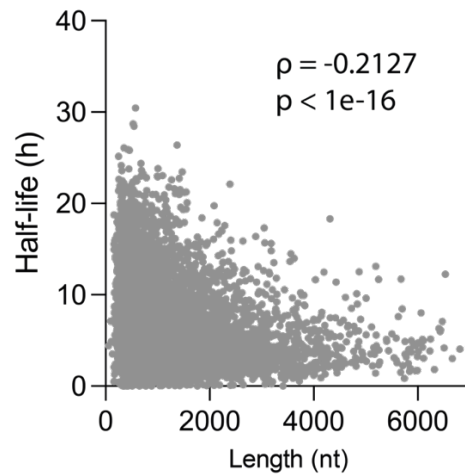


Figure 84: Scatter plot of mean codon-optimality (tAI scores, y-axis) and measured mRNA half-lives in wild-type HEK293T cells (x-axis) shows no correlation.

A negative correlation between transcript length and mRNA stability in yeast has been observed before (Santiago et al., 1986). While this trend can also be observed for HEK293T cells, the correlation is rather weak (Figure 85).



*Figure 85: Scatter plot of mRNA length (x-axis) and measure mRNA half-lives in wild-type cells (y-axis). With progressing length, the mRNA half-live decreases.*

In more recent years there have been efforts to establish better metrics describing regulatory effects of codons on mRNA stability, resulting in the introduction of the codon stability coefficient (CSC), which depends on tRNA availability and aminoacylation status. This coefficient is calculated as the Pearson's correlation coefficient between mRNA stability (half-life) and codon occurrence (frequency) (Forrest et al., 2020; Presnyak et al., 2015; Wu et al., 2019). While certain codons, such as CAT, have a destabilizing effect on mRNAs (Figure 86A), higher frequency of others act stabilizing, including CTG (Figure 86B).

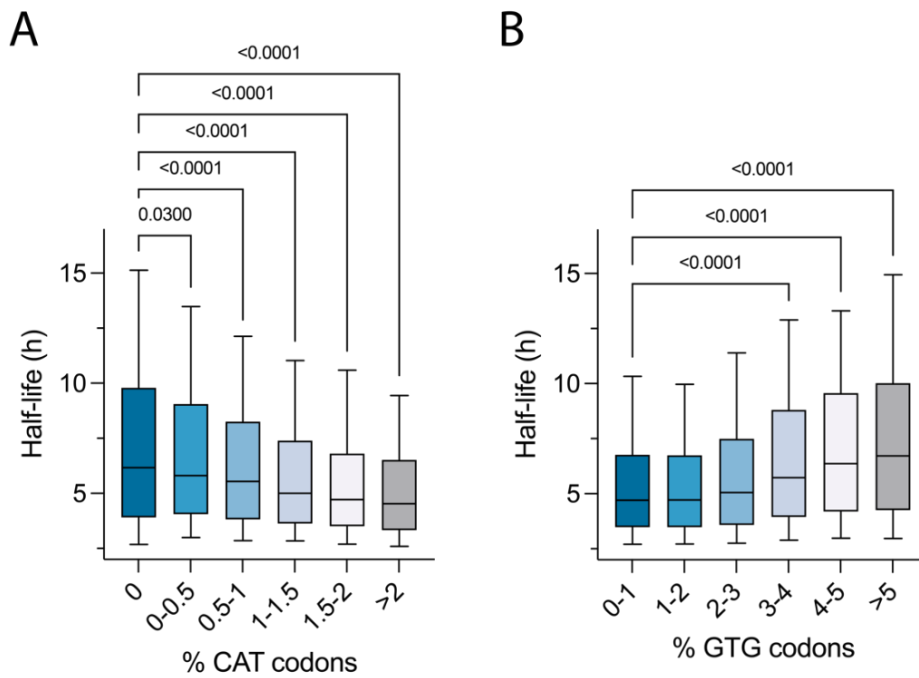


Figure 86: Correlation between codon frequency (bins are indicated at the x-axis) and mRNA half-lives, reveals (A) a negative correlation of CAT codons (coding for histidine) and (B) a positive correlation for GTG codons (coding for valine) in wild-type cells.

Based on our data, we calculated CSC scores for all 61 codons (excluding stop codons). Our determined values align almost perfectly with previously established scores for HEK293T cells (Wu et al., 2019) (Figure 87A). Next, we analyzed how the CSC scores change in the GCN1 KO cells. While overall the scores calculated in wild-type cells correlate well with the scores obtained from the knockout cells, we observed that codon effects are overall blunted in the mutant cells (Figure 87B).

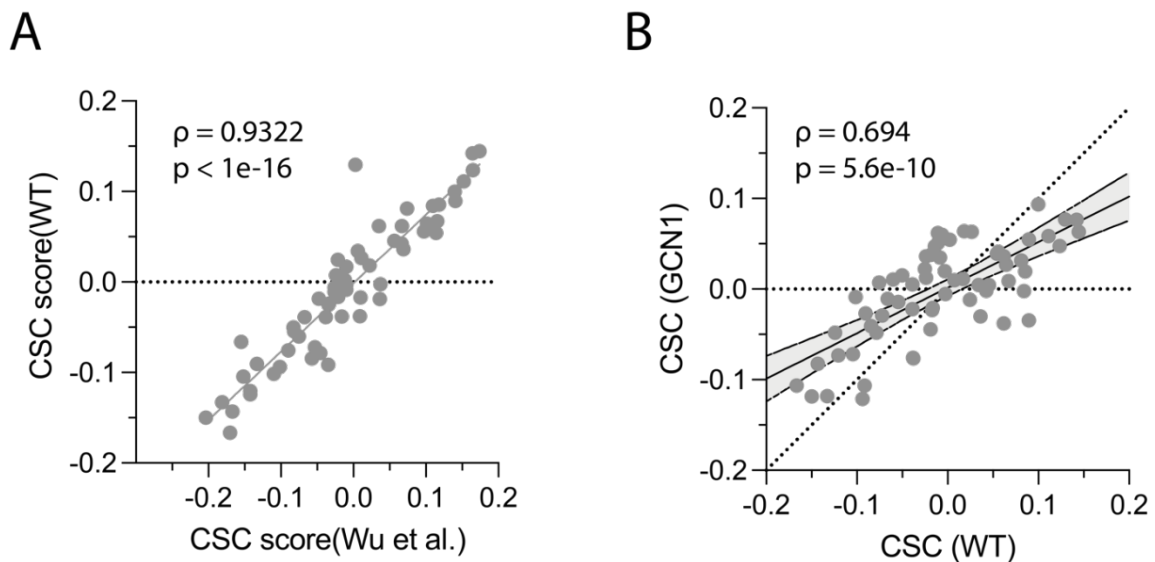


Figure 87: Codon-influence on mRNA-stability is partially decoupled in GCN1 KO cells compared to wild-type. (A) Codon stability coefficients (CSC), calculated as the Pearson's correlation coefficient between codon frequency and mRNA stability (half-life) for all 61 codons (excluding stop codons). The CSC scores obtained from our data agree very well with previously reported values (Wu et al.). (B) Scatter plot analysis of CSC scores calculated with half-lives from GCN1 KO cells compared to wild-type. While the CSC scores correlate well for GCN1 KO cells and wild-type HEK293T cells (Pearson's correlation coefficient of 0.694), the slope deviates significantly from 1, which would be expected if codon-influence would be preserved as indicated by the dotted line. The shaded area indicates the 95% confidence interval of the linear fit.

Calculating a global CSC score for each transcript served only as a poor proxy for mRNA stability (Figure 88A). When collapsing the scores for each codon (CSC) to amino acid level (AASC), the prediction accuracy improved slightly (Figure 88B).

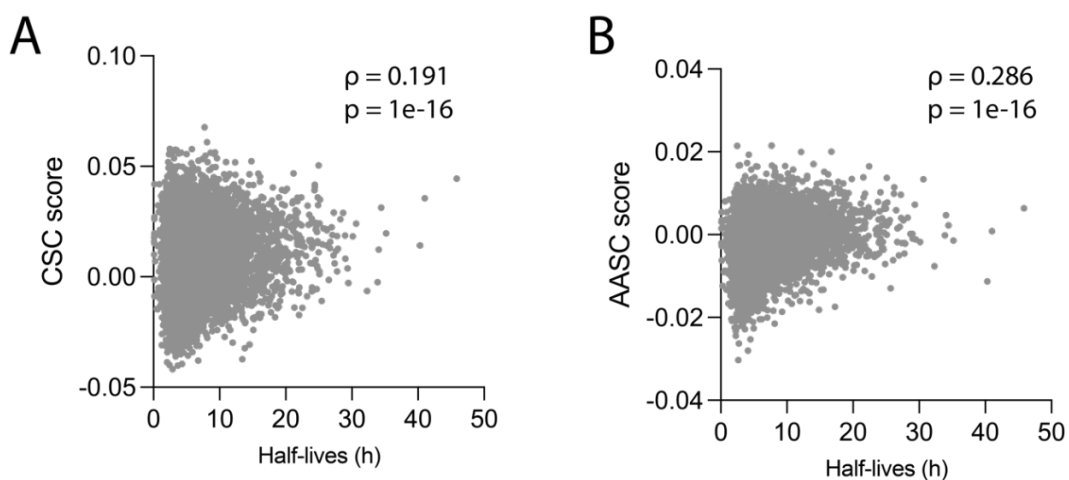


Figure 88: Codon stabilization coefficients (CSC) have only a weak predictive power on mRNA stability, whereas the amino acid stability coefficients (AASC) are better at predicting mRNA stability.

stability. (A) Scatter plot of mRNA half-lives of wild-type cells (x-axis) compared to global CSC scores of given transcripts. (B) As in (A) but plotted against AASC scores instead of CSC scores.

Next, we wanted to explore the underlying cause as to why certain codons are destabilizing. It is a commonly accepted that slow translation leads to reduced mRNA stability. Overall tRNA abundance and aminoacylation levels are two major determinants of translation speed. We therefore hypothesized that tRNA levels and their aminoacylation status influence the CSC scores. Indeed, utilizing previously published data that determined tRNA abundance and charging status (Evans et al., 2017), we observed that both tRNA availability (Figure 89A) and aminoacylation status (Figure 89B) positively correlate with CSC scores. Combining the two factors improved the prediction of CSC scores. (Figures 89C).

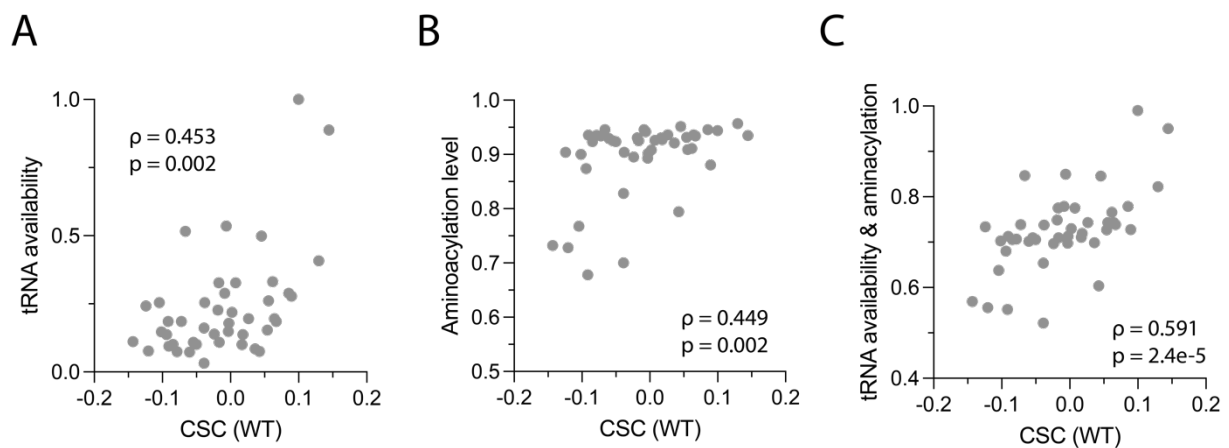


Figure 89: CSC scores are influenced by tRNA availability and charging status (aminoacylation). Scatter plots for CSC scores (x-axis) and (A) tRNA availability (tRNA abundance) (B) charging levels of tRNAs (aminoacylation) and (C) a combined score of tRNA availability and charging status. Significance was assessed by Spearman's correlation.

This suggests that GCN1 is recruited codons for destabilizing amino acids and modulates mRNA stability based on tRNA availability and charging status. Overall, our data suggests that GCN1 has a general in translational surveillance by acting as a recruitment platform for quality control factors. This function contributes to readthrough mitigation and more generally aids in the biogenesis of TMD proteins and collagens by slowing down translation at non-optimal codons. GCN1 dysfunction leads to a substantial increase in overall mRNA stability, partially decoupling mRNA turnover from codon-specific effects.

## Discussion

Translational readthrough of stop codons into 3'UTRs leads to the production of aberrant C-terminally extended proteins with potentially detrimental functional consequences. Previous studies discovered the existence of translational readthrough mitigation in metazoans. A key feature of readthrough mitigation was protein destabilization in a manner dependent on hydrophobicity of the 3'UTR regions (Arribere et al., 2016). However, the exact pathway and underlying mechanisms of how these aberrant readthrough protein products are detected and degraded remained unclear. Here, we provided evidence that hydrophobic readthrough products are recognized and efficiently cleared by the BAG6-RNF126 pathway. We also found indications that mRNA decay of the readthrough mRNA occurs via the CCR4/NOT complex and is orchestrated by GCN1 during readthrough mitigation. Further, we determined GCN1 targets at transcriptome scale to identify TMD encoding transcripts and collagens as key targets, with GCN1 preferentially recognizing ribosome slowdown and collisions resulting from nonoptimal codons enriched in these classes. We found that GCN1 balances translational kinetics on transcripts containing nonoptimal codon stretches and sequences encoding hydrophobic amino acids. This function of GCN1 is critical to maintain translational homeostasis and loss of GCN-1 aggravates the translational collapse associated with ageing.

### Interplay of BAG6/RNF-126 and sHSPs in quality control of readthrough proteins

Using mass spectrometry and fluorescence based ratiometric analysis, we discovered that readthrough protein mitigation in both nematodes and mammalian cells utilizes the BAG6 complex involved in quality control of TA-proteins (Farkas and Bohnsack, 2021), including SGTA, BAG6, ASNA1 (GET3), GET4, UBL4A and the E3 ligase RNF126 (Farkas and Bohnsack, 2021) (Figures 20, 30, 43 and 51). BAG6 acts downstream of the cytosolic chaperone SGTA as part of the TA pretargeting module. The pretargeting complex is recruited to ribosomes, poised to capture a hydrophobic TA sequence as soon as it has emerged from the ribosome exit tunnel (Leznicki and High, 2012, 2020; Mariappan et al., 2010). BAG6 is positioned to perform a critical triage decision: it either transfers the TA client to factors for membrane insertion (via GET3 and GET4) or, if unsuccessful, recruits RNF126 for ubiquitylation and subsequent degradation of TA-protein (Rodrigo-Brenni et al., 2014; Shao et al., 2017).

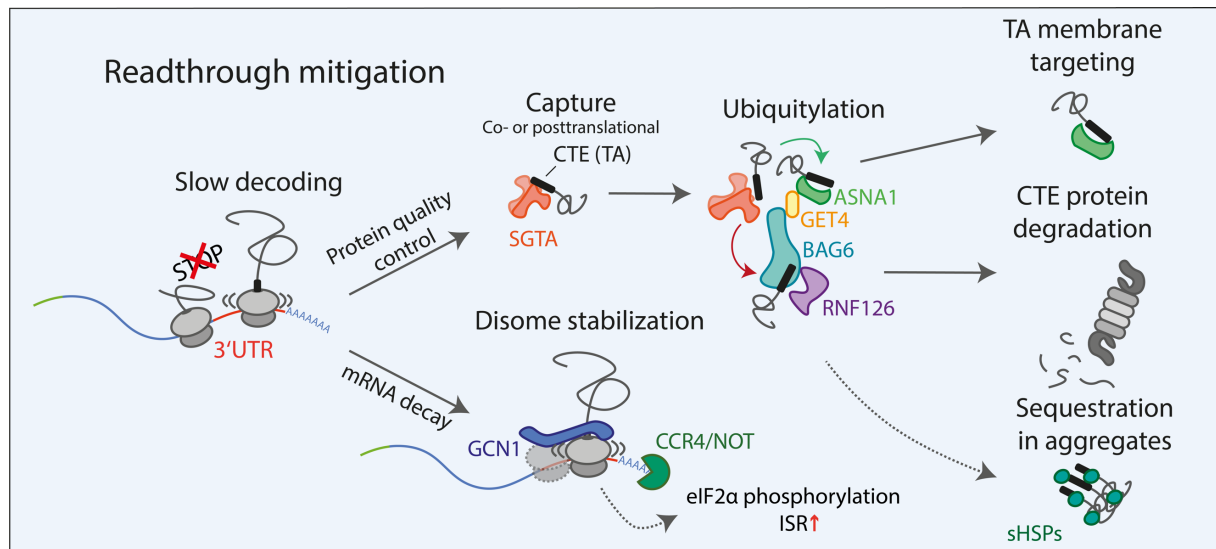


Figure 90. General model of translation readthrough mitigation. Proteins resulting from translational readthrough with hydrophobic CTEs resemble TA-proteins and are captured by SGTA, which may be recruited to ribosomes even before the hydrophobic CTE emerges. While bona fide TA-proteins are transferred to the membrane targeting unit consisting of GET4 and ASNA1 (GET3), aberrant CTE proteins resulting from translational readthrough are retained at the BAG6 complex for RNF126-mediated ubiquitylation and subsequent proteasomal degradation. CTE proteins that evade BAG6-mediated degradation are sequestered by sHSPs into foci, as observed in the nematode model. Ribosomes that translate into hydrophobic 3'UTRs are slowed down at nonoptimal codons, resulting in collided ribosomes that are recognized by GCN1, which in turn recruits CCR4/NOT to initiate mRNA decay.

We found that depletion of BAG6 or RNF126 stabilizes readthrough proteins with hydrophobic CTEs, suggesting that such sequences, similar to failed TA sequences, are captured by SGTA, followed by transfer to BAG6 and RNF126-dependent clearance (Figures 20 and 34). Indeed, bioinformatic analysis showed that the CTE sequences of readthrough proteins frequently contain regions similar in length and hydrophobicity to TA membrane spans (Figure 28), suggesting the possibility of mislocalization to membranes.

What are the consequences of CTEs inserted into membranes? Cells allocate tremendous resources for quality control pathways to ensure organelle function. For example, TA proteins that are missorted into the ER or mitochondrial membrane are recognized and shuttled back to the cytosol by retrotranslocases (McKenna et al., 2020; Wohlever et al., 2017). Having an additional source of mislocalized proteins arising from CTE translation may overwhelm this clearance mechanism and potentially alter protein composition at the ER and mitochondrial

membranes resulting in organelle dysfunction (Costa et al., 2018; Gamerdinger et al., 2015). Thus, clearance of CTEs by the BAG6 complex is crucial to relieve the burden on such retrotranslocases and ensure proteins are not improperly inserted into membranes.

Hydrophobic sequences further pose a risk to form aggregates that may interfere with myriad cellular pathways. Consistently, hydrophobic readthrough proteins formed aggregate inclusions upon impairing ubiquitylation or proteasome inhibition. Readthrough proteins escaping degradation strongly associated with members of the sHSP class of chaperones, which were dramatically upregulated upon overexpression of readthrough constructs (Figures 23 and 24). sHSPs, in addition to preventing protein aggregation, have been shown to function in spatial protein quality control by sequestering potentially harmful proteins into aggregates (Haslbeck et al., 2019; Mogk and Bukau, 2017). Their upregulation during aging (Walker and Lithgow, 2003; Walther et al., 2015) is associated with longevity in *C. elegans*. We suggest that sHSPs function in parallel to the BAG6 pathway in preventing readthrough proteins from engaging in aberrant protein-protein interactions. Indeed, we identified that spatial sequestration of readthrough proteins was dependent on sHSPs (Figure 22).

If degradation and spatial sequestration of readthrough proteins fail, backup mechanism may take over to prevent proteostatic collapse. Such a backup mechanism has been described for the ribosome associated quality control complex (RQC) (Sitron and Brandman, 2019). During this pathway, Rqc2 (NEMF in mammals) elongates nascent polypeptides with alanine and threonine chains (CAT-tails), which act as destabilizing sequences if stalled nascent chains escape ubiquitylation at the ribosome (Sitron and Brandman, 2019). Such degrons are small protein elements that facilitate the interaction with degradation machineries to promote their degradation. In recent years, different C-terminal degrons have been identified that shape general plasticity of the proteome (Koren et al., 2018; Sitron and Brandman, 2019). Given the potential unstructured nature of CTEs, a feature that is typical for degrons (Varshavsky, 2019), we suggest that hydrophobic CTEs can act as C-terminal degrons to facilitate their degradation if the BAG6 complex fails to detect them.

In conclusion, cells employ multiple pathways act in parallel at the protein level to ensure that aberrant protein species do not escape degradation or form promiscuous protein-protein interactions.

## GCN-1 mediated mRNA decay

RQC is equipped with an additional layer of quality control to reduce the burden on protein degradation pathways by reducing the mRNA level of faulty transcripts (Inada, 2020). Analyzing the readthrough mitigation mechanism revealed an additional level of quality control wherein translation into a 3'UTR coding for a hydrophobic CTE, and thus enriched in nonoptimal codons (Figures 29 and 56) results in mRNA destabilization (Figure 90). Using UV-induced mRNA crosslinking followed by mass spectrometry, we identified the ribosome collision sensor protein GCN1 and the CCR4/NOT deadenylase complex as critical factors in the readthrough mitigation pathway (Figure 37). While CCR4/NOT has a well-established role in mRNA decay (Buschauer et al., 2020; Webster et al., 2018), GCN1 is a cofactor of the ISR kinase GCN2 (Sattlegger and Hinnebusch, 2000, 2005; Wu et al., 2020; Yan and Zaher, 2021) with no known mRNA quality control function. GCN1 disruption stabilized mRNAs encoding hydrophobic readthrough proteins (Figure 39B). We found that GCN1 interacts with CCR4/NOT, mediating the cotranslational recruitment of the CCR4/NOT complex for mRNA degradation (Figure 42). This function synergizes with proteasomal degradation via the BAG6 pathway, strongly reduces the burden posed by potentially harmful readthrough proteins.

Considering that stop codon readthrough frequencies are as high as 15% (depending on stop codon sequence context) (Loughran et al., 2014) and most CTEs encoded by 3'UTRs are hydrophobic, the production of readthrough proteins may saturate the normal quality control capacity of the BAG6 complex within the biogenesis pathway of bona fide TA-proteins, potentially disturbing general proteostasis. A recent study reported that the BAG6 complex has a general role in clearing hydrophobic translation products originating from various sources of noncoding RNAs other than stop codon readthrough (Kesner, 2022). This would further increase the burden of aberrant translation products on the BAG6 complex, raising the question of how a single quality control module might deal with such a massive overload. While several protein quality control pathways may operate in parallel, our findings suggest that the mechanism of cotranslational mRNA decay by GCN1 and CCR4/NOT will likely be critical in mitigating noncoding RNA translation in addition to its role on readthrough mRNAs. By reducing the production of aberrant hydrophobic proteins at the level of translation, the GCN1-CCR4/NOT axis may relieve some of the burden on the BAG6 complex.

## GCN1 surveils translation

Our GCN1-selective Ribo-seq analysis in *C. elegans* and HEK293T cells uncovered a pervasive role of GCN1 in modulating translation dynamics and proteome balance by regulating mRNA turnover. In addition to 3'UTRs, we identified numerous coding sequences as GCN-1 targets, with a significant enrichment of TMD protein and collagen transcripts (Figures 58 and 74). GCN1 interacts preferentially with ribosomes engaged at nonoptimal codons, which are particularly frequent in these mRNAs. Nonoptimal codons result in slow decoding and have been proposed to induce transient ribosome collisions (Hanson and Coller, 2018). Slow-decoding ribosomes are targeted by the CCR4/NOT deadenylase (Buschauer et al., 2020), explaining the codon dependence of mRNA turnover, but whether codon-mediated mRNA decay depends on ribosome collisions has been questioned (Mishima et al., 2022). Our results indicate that disomes indeed form on nonoptimal codon stretches and are bound by GCN1. This function of GCN1 is consistent with recent evidence that disome formation is widespread across eukaryotic lineages (Han et al., 2020; Zhao et al., 2021) and may serve to recruit molecular chaperones to address folding problems of specific proteins (Zhao et al., 2021). Our analysis suggests that recognition by GCN1 stabilizes such disomes, slowing elongation further to facilitate chaperone recruitment to translating ribosomes. A similar mechanism was proposed for microRNAs that bind CDS regions of transcripts slowing translation to prevent misfolding of nascent polypeptides (Sako et al., 2023). Such a translational slowdown would likely cause ribosomal collisions that could in turn recruit GCN1. Therefore, GCN1 may play a role in the microRNA-mediated cotranslational folding by recruiting molecular chaperones. mRNA decay initiated by CCR4/NOT may be the consequence of folding problems that cannot be resolved. In such situations, translation might be terminated by recruitment of eRF1, as observed by polysome fractionation experiments (Figures 69 and 79), which can execute premature termination on rare codon stretches (Yang et al., 2019). In the context of translational readthrough, we identified the BAG6 complex to mediate the efficient clearance of CTEs. However, the fate of prematurely terminated proteins remains unclear. The AAA-ATPase valosin-containing protein (VCP) mediates the extraction of misfolded membrane proteins which are then degraded by BAG6-RNF126 (Hu et al., 2020). Translational problems arising during the biogenesis of TMD proteins would lead to the premature termination mediated by GCN1. Such faulty intermediate products, if inserted into the membrane, are

likely to be extracted by VCP, and subsequently captured by BAG6 to mediate their degradation.

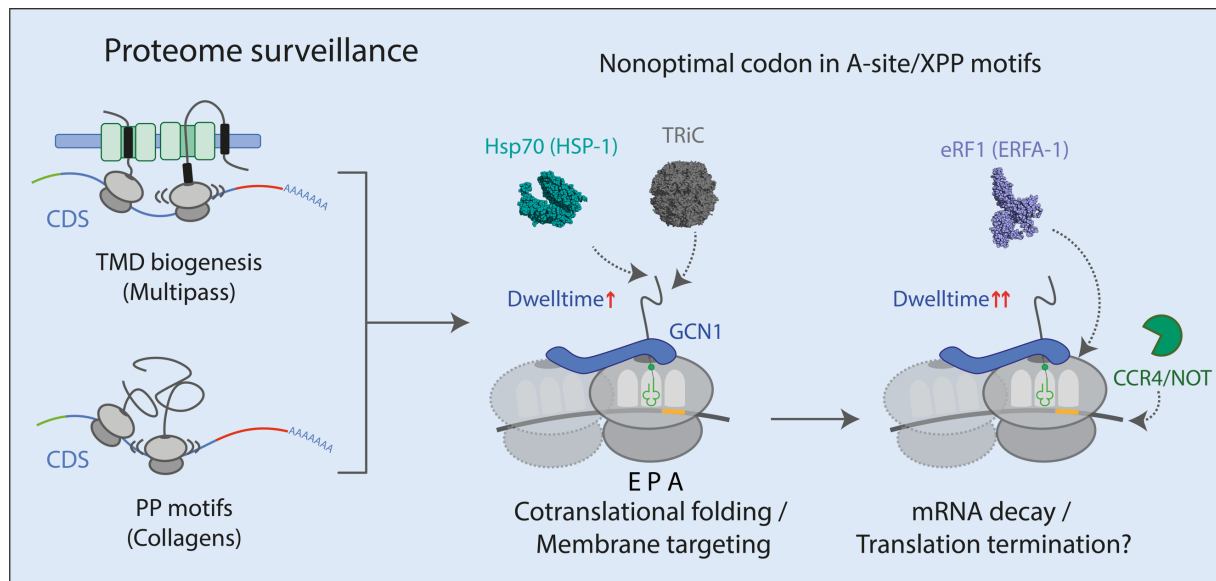


*Figure 91: Model of translational surveillance mediated by GCN1. Translation of nonoptimal codons (enriched in TMD containing transcripts and collagens) causes ribosome slowdown and (transient) collisions. GCN1 engages these ribosomes to stabilize disomes, thereby prolonging the time available for membrane protein assembly and/or association of chaperones for cotranslational folding. Extended ribosome (disome) dwelltimes, due to problems during biogenesis that cannot be resolved, result in CCR4/NOT recruitment to initiate mRNA degradation, which thereby limits aberrant protein accumulation. Recruitment of release factor eRF1 to stalled ribosomes may induce premature chain termination.*

In the case of TMD proteins, translational slowdown is thought to facilitate cotranslational targeting and membrane insertion of TMD proteins (Pechmann et al., 2014; Rodnina and Wintermeyer, 2016). We found that GCN1 is preferentially recruited to TMD proteins with multiple membrane spans. Assembly of such proteins is a complex and often inefficient process utilizing various membrane insertases, such as the Sec61 translocon and the EMC and PAT complexes (Miller-Vedam et al., 2020; O'Donnell et al., 2020; Phillips and Miller, 2020; Smalinskaite et al., 2022; Sundaram et al., 2022; Tector and Hartl, 1999; Trentini et al., 2020). Ribo-seq revealed that GCN1 tends to engage TMD proteins soon after a transmembrane sequence has emerged from the ribosome, possibly extending the time window available for successful insertion and assembly in the membrane. Interestingly, this binding preference is

opposite for what has been proposed for an RQC-associated ribosome collision sensor, HEL2 (ZNF598), which is preferentially recruited prior to translation of TMD segments (Matsuo and Inada, 2021). It remains unclear why two seemingly similar quality pathways act on the same mRNAs and what determines their binding preference. Structural differences observed for GCN1-bound disomes, and collided ribosomes engaged by RQC-related factors might contribute to this selectivity (Pochopien et al., 2021). However, how such structural differences would arise remains unknown and further research is required to understand the underlying mechanism mediating these binding preferences.

Slowing translation at nonoptimal codons by GCN1 aids in the folding of nascent chains and balancing mRNA levels via CCR4/NOT would limit the risk of overloading chaperone and assembly machinery. Slow decoding also underlies the preferential targeting of collagen transcripts by GCN1. Collagens, the most abundant proteins in mammals, are rich in XPP motifs, with prolines having a critical structural role in forming the characteristically tightly-wound collagen helix (Onursal et al., 2021; Shoulders and Raines, 2009). Prolines perform poorly in peptide bond formation and slow translation substantially by adopting an unfavorable topology for the peptidyl transferase reaction (Gutierrez et al., 2013; Pavlov et al., 2009; Peil et al., 2013; Schuller et al., 2017).

The role of GCN1 in mRNA decay extends beyond collagens and TMD proteins, affecting mRNA stability globally in a codon-dependent manner. Based on published mass spectrometry data (Kulak et al., 2014), we identified a ~17-fold higher abundance of GCN1 compared to CCR4/NOT. Therefore, it seems plausible that GCN1 acts upstream of CCR4/NOT. Recent findings that GCN1 engages E3 ligases for the ubiquitylation of stalled translation factors (Oltion et al., 2023) support the view that it functions in translational regulation as a more general recruitment platform. Yet, it remains unclear how GCN1 mediates the recruitment of CCR4/NOT on a molecular basis. The CCR4/NOT complex was shown to recognize empty ribosomal E-sites during translation via CNOT3 (Buschauer et al., 2020). However, structural evidence suggests that the E-site of the leading GCN1-bound collided ribosome is occupied by EIF5A, whereas the trailing ribosome is bound to tRNAs in the E/P and P/A confirmation (Pochopien et al., 2021). This would make both E-sites seemingly inaccessible for CNOT3 binding. However, CNOT3 is not always required for CCR4/NOT recruitment to ribosomes. In the translational surveillance pathway during tubulin autoregulation (Lin et al., 2020), S-phase

cyclin A associated protein residing in the ER (SCAPER) recruits CCR4/NOT to the ribosomes independently of CNOT3 (Hopfler et al., 2023). While this mode of CCR4/NOT tethering was described in the specific context of tubulin, it is possible that similar to SCAPER, GCN1 directly tethers CCR4/NOT to disomes and initiates mRNA decay.

### Implications of GCN-1 function in ageing

GCN1 is a positive regulator of the integrated stress response (ISR) induced by amino acid starvation (Sattlegger and Hinnebusch, 2000, 2005). In this signaling pathway, GCN1 activates the GCN2 kinase, which in turn phosphorylates eIF2a to downregulate global translation. Activation of the ISR also occurs upon increased production of readthrough proteins (Wangen and Green, 2020). Interestingly, we found this response to be fully dependent on GCN1 function, ruling out secondary effects on eIF2a phosphorylation, such as ER stress (Figure 78). GCN1-mediated EIF2a-phosphorylation blocks translation to reduce global translation and prevent further collision. When collisions persist, ZAKa-dependent apoptosis is triggered by p38-phosphorylation (Wu et al., 2020). Thus, GCN1 acts as a molecular gauge to determine the cell fate upon increased ribosome collisions during translational readthrough (Figure 92).

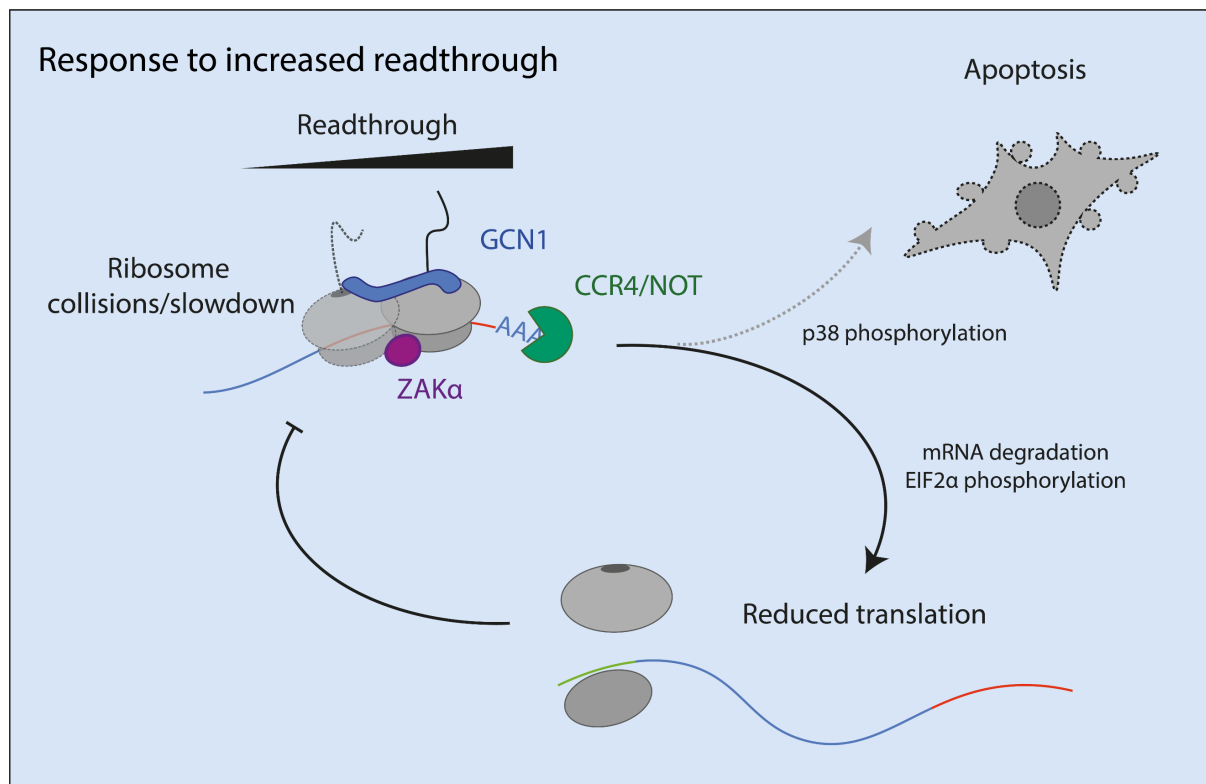


Figure 92. Model for cellular response to increased translational readthrough orchestrated by GCN1. Increased global readthrough into 3'UTRs of transcripts leads to elevated levels of ribosome collisions that are sensed by GCN1 to phosphorylate EIF2α. This in turn reduces translation initiation rates to prevent further ribosome collisions. If collisions exceed a threshold, apoptosis is initiated by ZAKα phosphorylating p38.

As translational errors have been associated with aging (Azpurua et al., 2013; Chen et al., 2020; Moore et al., 2021; Shcherbakov et al., 2022; Stein et al., 2022), it seemed likely that the wide-ranging role of GCN1 in translational surveillance described here is increasingly relevant during the aging process. Direct evidence for the importance of GCN1 in maintaining RNA and protein balance in aged nematodes was provided by our finding that GCN1 dysfunction resulted in the age-dependent accumulation of insoluble TMD proteins (Figure 61). Furthermore, *gcn-1(nc40)* mutant animals at day 6 of adulthood accumulated on average 3- to 4-fold higher mRNA levels for multiple collagens compared to young (D0) controls, resulting in higher levels of collagen translation. However, this increase in collagen translation was not reflected in total collagen abundance, but rather coincided with a decrease in collagen level (Figure 68). Surplus collagen molecules may be recognized as structurally aberrant, possibly resulting in a high burden on clearance pathways (Ito and Nagata, 2021). Indeed, declining collagen integrity is an important factor in aging, accompanied by a decrease in total

collagen mass and the accumulation of structurally damaged collagens (Shoulders and Raines, 2009). The profound impact of GCN-1 on collagen biogenesis in *C. elegans* illustrates the significance of GCN1-mediated translational surveillance in maintaining proteome balance.

Our study suggests that GCN-1 acts as master coordinator of the response to problematic translation aiding in the biogenesis of challenging proteins and possibly limiting their expression by mRNA decay (Figure 91). This process becomes increasingly important as organisms age and translational fidelity decreases. Reducing translation initiation by eIF2 $\alpha$  phosphorylation reduces the burden on the proteostasis system and ensures that protein quality control mechanisms are not overwhelmed. Addressing the question of the underlying reason why translational fidelity decreases, and problems arise as our cells age, remains a central task for future studies.

## Acknowledgements

I would like to express my deepest gratitude to my supervisor, Professor Ulrich Hartl, for his guidance and unwavering support throughout my doctoral journey. His insightful feedback, thought-provoking discussions, and meticulous attention to detail have consistently challenged me to push the boundaries of (my) knowledge and strive for excellence. I am grateful for his continuous encouragement, patience, and belief in my potential. His open-door policy, willingness to engage in meaningful academic conversations, and genuine interest in my progress have made this experience not only academically enriching but also personally fulfilling. I extend my heartfelt appreciation to Dr. Manajit Hayer-Hartl for her mentorship that goes beyond the realm of academia.

Also the administrative and technical staff helped me tremendously throughout the years. I thank Albert, Darija, Emmanuel, Massimo, Nadine, Romy, and Silvia for their support.

I would also like to acknowledge the invaluable contributions of my colleagues in the Hartl department, whose different perspectives have significantly enriched my research. The daily interactions with my colleagues both inside and outside the lab have helped me throughout the course of my PhD. In this context, I want to specifically mention a few people. First, I would like to acknowledge the coffee group involving David and Michael, who became close friends over the course of my PhD and were there with me from the first hour. I am truly grateful for your friendship and support throughout my time at the Hartl department. I would also point out Cole, who supported me tremendously throughout the last phase of my PhD, not only scientifically, but as a friend. I am truly sorry for all the paragraphs that you had to correct for me. Further, I would like to mention Gopal, Chandhuru and Lucas, who lifted my mood at Friday night dinners after a rough week. Also thank you Max for never being shy of a joke (not always good ones) throughout the day, which created a more pleasant working atmosphere.

Without the support of my friends, this work would have not possible. Having these friends in my corner offering unconditional support was of paramount importance to complete this work. I am truly thankful for your friendship (and I am going to name you alphabetically to avoid any favoritism) – Alkan, Cemal, Çihan, Dominik (both), Joscha, Klaus, Leo, Marc, Özgür, Sascha and Qiong. Furthermore, I would like to thank two friends who I have known basically my whole life – Jan and Simon. Thank you for your support and for always being at my side.

One of my biggest supporters throughout my PhD was my partner, Patricia, who always helped me to get through difficult times. Thank you for your love and support, lifting me up after a difficult day and being there for me whenever I needed someone to listen. You are one of the most selfless people I know, and I am thankful to have met you.

Finally, I extend my deepest gratitude to my parents and siblings for their unwavering love, support, and understanding throughout this long yet rewarding journey. Their belief in me has been a constant source of motivation and strength. Sorry that you had to wait so long for it.

## References

- Agashe, V.R., Guha, S., Chang, H.C., Genevoux, P., Hayer-Hartl, M., Stemp, M., Georgopoulos, C., Hartl, F.U., and Barral, J.M. (2004). Function of trigger factor and DnaK in multidomain protein folding: increase in yield at the expense of folding speed. *Cell* **117**, 199-209.
- Albanese, V., Reissmann, S., and Frydman, J. (2010). A ribosome-anchored chaperone network that facilitates eukaryotic ribosome biogenesis. *J Cell Biol* **189**, 69-81.
- Allen, S.P., Polazzi, J.O., Gierse, J.K., and Easton, A.M. (1992). Two novel heat shock genes encoding proteins produced in response to heterologous protein expression in *Escherichia coli*. *J Bacteriol* **174**, 6938-6947.
- Amm, I., Sommer, T., and Wolf, D.H. (2014). Protein quality control and elimination of protein waste: the role of the ubiquitin-proteasome system. *Biochim Biophys Acta* **1843**, 182-196.
- Anfinsen, C.B. (1973). Principles that govern the folding of protein chains. *Science* **181**, 223-230.
- Anisimova, A.S., Meerson, M.B., Gerashchenko, M.V., Kulakovskiy, I.V., Dmitriev, S.E., and Gladyshev, V.N. (2020). Multifaceted deregulation of gene expression and protein synthesis with age. *Proc Natl Acad Sci U S A* **117**, 15581-15590.
- Arpat, A.B., Liechti, A., De Matos, M., Dreos, R., Janich, P., and Gatfield, D. (2020). Transcriptome-wide sites of collided ribosomes reveal principles of translational pausing. *Genome Res* **30**, 985-999.
- Arribere, J.A., Cenik, E.S., Jain, N., Hess, G.T., Lee, C.H., Bassik, M.C., and Fire, A.Z. (2016). Translation readthrough mitigation. *Nature* **534**, 719-723.
- Arrigo, A.P., Suhan, J.P., and Welch, W.J. (1988). Dynamic changes in the structure and intracellular locale of the mammalian low-molecular-weight heat shock protein. *Mol Cell Biol* **8**, 5059-5071.
- Azpurua, J., Ke, Z., Chen, I.X., Zhang, Q., Ermolenko, D.N., Zhang, Z.D., Gorbunova, V., and Seluanov, A. (2013). Naked mole-rat has increased translational fidelity compared with the mouse, as well as a unique 28S ribosomal RNA cleavage. *Proc Natl Acad Sci U S A* **110**, 17350-17355.
- Balchin, D., Hayer-Hartl, M., and Hartl, F.U. (2020). Recent advances in understanding catalysis of protein folding by molecular chaperones. *FEBS Lett* **594**, 2770-2781.
- Baradaran-Heravi, A., Balgi, A.D., Hosseini-Farahabadi, S., Choi, K., Has, C., and Roberge, M. (2021). Effect of small molecule eRF3 degraders on premature termination codon readthrough. *Nucleic Acids Res* **49**, 3692-3708.
- Bard, J.A.M., Goodall, E.A., Greene, E.R., Jonsson, E., Dong, K.C., and Martin, A. (2018). Structure and Function of the 26S Proteasome. *Annu Rev Biochem* **87**, 697-724.
- Barreau, C., Paillard, L., and Osborne, H.B. (2005). AU-rich elements and associated factors: are there unifying principles? *Nucleic Acids Res* **33**, 7138-7150.
- Basha, E., Lee, G.J., Breci, L.A., Hausrath, A.C., Buan, N.R., Giese, K.C., and Vierling, E. (2004). The identity of proteins associated with a small heat shock protein during heat stress in vivo indicates that these chaperones protect a wide range of cellular functions. *J Biol Chem* **279**, 7566-7575.
- Baumketner, A., Jewett, A., and Shea, J.E. (2003). Effects of confinement in chaperonin assisted protein folding: rate enhancement by decreasing the roughness of the folding energy landscape. *J Mol Biol* **332**, 701-713.
- Becker, A.H., Oh, E., Weissman, J.S., Kramer, G., and Bukau, B. (2013). Selective ribosome profiling as a tool for studying the interaction of chaperones and targeting factors with nascent polypeptide chains and ribosomes. *Nat Protoc* **8**, 2212-2239.

Bellato, H.M., and Hajj, G.N. (2016). Translational control by eIF2 $\alpha$  in neurons: Beyond the stress response. *Cytoskeleton (Hoboken)* 73, 551-565.

Berkovits, B.D., and Mayr, C. (2015). Alternative 3' UTRs act as scaffolds to regulate membrane protein localization. *Nature* 522, 363-367.

Bloss, T.A., Witze, E.S., and Rothman, J.H. (2003). Suppression of CED-3-independent apoptosis by mitochondrial betaNAC in *Caenorhabditis elegans*. *Nature* 424, 1066-1071.

Brown, A., Shao, S., Murray, J., Hegde, R.S., and Ramakrishnan, V. (2015). Structural basis for stop codon recognition in eukaryotes. *Nature* 524, 493-496.

Bukau, B., Deuerling, E., Pfund, C., and Craig, E.A. (2000). Getting newly synthesized proteins into shape. *Cell* 101, 119-122.

Bukau, B., and Horwich, A.L. (1998). The Hsp70 and Hsp60 chaperone machines. *Cell* 92, 351-366.

Buschauer, R., Matsuo, Y., Sugiyama, T., Chen, Y.H., Alhusaini, N., Sweet, T., Ikeuchi, K., Cheng, J., Matsuki, Y., Nobuta, R., *et al.* (2020). The Ccr4-Not complex monitors the translating ribosome for codon optimality. *Science* 368.

Canovas, B., and Nebreda, A.R. (2021). Diversity and versatility of p38 kinase signalling in health and disease. *Nat Rev Mol Cell Biol* 22, 346-366.

Chadwick, S.R., Fazio, E.N., Etedali-Zadeh, P., Genereaux, J., Duennwald, M.L., and Lajoie, P. (2020). A functional unfolded protein response is required for chronological aging in *Saccharomyces cerevisiae*. *Curr Genet* 66, 263-277.

Chadwick, S.R., and Lajoie, P. (2019). Endoplasmic Reticulum Stress Coping Mechanisms and Lifespan Regulation in Health and Diseases. *Front Cell Dev Biol* 7, 84.

Chaney, J.L., and Clark, P.L. (2015). Roles for Synonymous Codon Usage in Protein Biogenesis. *Annu Rev Biophys* 44, 143-166.

Chang, L., Shav-Tal, Y., Trcek, T., Singer, R.H., and Goldman, R.D. (2006). Assembling an intermediate filament network by dynamic cotranslation. *J Cell Biol* 172, 747-758.

Chartron, J.W., Hunt, K.C., and Frydman, J. (2016). Cotranslational signal-independent SRP preloading during membrane targeting. *Nature* 536, 224-228.

Chen, C.Y., Chen, S.T., Juan, H.F., and Huang, H.C. (2012). Lengthening of 3'UTR increases with morphological complexity in animal evolution. *Bioinformatics* 28, 3178-3181.

Chen, C.Y., and Shyu, A.B. (1995). AU-rich elements: characterization and importance in mRNA degradation. *Trends Biochem Sci* 20, 465-470.

Chen, Y., Boland, A., Kuzuoglu-Ozturk, D., Bawankar, P., Loh, B., Chang, C.T., Weichenrieder, O., and Izaurralde, E. (2014). A DDX6-CNOT1 complex and W-binding pockets in CNOT9 reveal direct links between miRNA target recognition and silencing. *Mol Cell* 54, 737-750.

Chen, Y., Sun, T., Bi, Z., Ni, J.Q., Pastor-Pareja, J.C., and Javid, B. (2020). Premature termination codon readthrough in *Drosophila* varies in a developmental and tissue-specific manner. *Sci Rep* 10, 8485.

Chiocchetti, A., Zhou, J., Zhu, H., Karl, T., Haubenreisser, O., Rinnerthaler, M., Heeren, G., Oender, K., Bauer, J., Hintner, H., *et al.* (2007). Ribosomal proteins Rpl10 and Rps6 are potent regulators of yeast replicative life span. *Exp Gerontol* 42, 275-286.

Chiti, F., and Dobson, C.M. (2017). Protein Misfolding, Amyloid Formation, and Human Disease: A Summary of Progress Over the Last Decade. *Annu Rev Biochem* 86, 27-68.

Choe, Y.J., Park, S.H., Hassemer, T., Korner, R., Vincenz-Donnelly, L., Hayer-Hartl, M., and Hartl, F.U. (2016). Failure of RQC machinery causes protein aggregation and proteotoxic stress. *Nature* 531, 191-195.

Choi, J., Grosely, R., Prabhakar, A., Lapointe, C.P., Wang, J., and Puglisi, J.D. (2018). How Messenger RNA and Nascent Chain Sequences Regulate Translation Elongation. *Annu Rev Biochem* 87, 421-449.

Ciryam, P., Morimoto, R.I., Vendruscolo, M., Dobson, C.M., and O'Brien, E.P. (2013). In vivo translation rates can substantially delay the cotranslational folding of the Escherichia coli cytosolic proteome. *Proc Natl Acad Sci U S A* 110, E132-140.

Coffey, E.T. (2014). Nuclear and cytosolic JNK signalling in neurons. *Nat Rev Neurosci* 15, 285-299.

Cong, Y., Schroder, G.F., Meyer, A.S., Jakana, J., Ma, B., Dougherty, M.T., Schmid, M.F., Reissmann, S., Levitt, M., Ludtke, S.L., *et al.* (2012). Symmetry-free cryo-EM structures of the chaperonin TRiC along its ATPase-driven conformational cycle. *EMBO J* 31, 720-730.

Costa, E.A., Subramanian, K., Nunnari, J., and Weissman, J.S. (2018). Defining the physiological role of SRP in protein-targeting efficiency and specificity. *Science* 359, 689-692.

Costa-Mattioli, M., and Walter, P. (2020). The integrated stress response: From mechanism to disease. *Science* 368.

Curran, S.P., and Ruvkun, G. (2007). Lifespan regulation by evolutionarily conserved genes essential for viability. *PLoS Genet* 3, e56.

Delaidelli, A., Jan, A., Herms, J., and Sorensen, P.H. (2019). Translational control in brain pathologies: biological significance and therapeutic opportunities. *Acta Neuropathol* 137, 535-555.

Deng, J.M., and Behringer, R.R. (1995). An insertional mutation in the BTF3 transcription factor gene leads to an early postimplantation lethality in mice. *Transgenic Res* 4, 264-269.

Derisbourg, M.J., Wester, L.E., Baddi, R., and Denzel, M.S. (2021). Mutagenesis screen uncovers lifespan extension through integrated stress response inhibition without reduced mRNA translation. *Nat Commun* 12, 1678.

Derti, A., Garrett-Engle, P., Macisaac, K.D., Stevens, R.C., Sriram, S., Chen, R., Rohl, C.A., Johnson, J.M., and Babak, T. (2012). A quantitative atlas of polyadenylation in five mammals. *Genome Res* 22, 1173-1183.

Deuerling, E., Schulze-Specking, A., Tomoyasu, T., Mogk, A., and Bukau, B. (1999). Trigger factor and DnaK cooperate in folding of newly synthesized proteins. *Nature* 400, 693-696.

Dhamija, S., Yang, C.M., Seiler, J., Myacheva, K., Caudron-Herger, M., Wieland, A., Abdelkarim, M., Sharma, Y., Riester, M., Gross, M., *et al.* (2020). A pan-cancer analysis reveals nonstop extension mutations causing SMAD4 tumour suppressor degradation. *Nat Cell Biol* 22, 999-1010.

Dikic, I. (2017). Proteasomal and Autophagic Degradation Systems. *Annu Rev Biochem* 86, 193-224.

Dill, K.A., and MacCallum, J.L. (2012). The protein-folding problem, 50 years on. *Science* 338, 1042-1046.

Dinner, A.R., Sali, A., Smith, L.J., Dobson, C.M., and Karplus, M. (2000). Understanding protein folding via free-energy surfaces from theory and experiment. *Trends Biochem Sci* 25, 331-339.

Dong, J., Qiu, H., Garcia-Barrio, M., Anderson, J., and Hinnebusch, A.G. (2000). Uncharged tRNA activates GCN2 by displacing the protein kinase moiety from a bipartite tRNA-binding domain. *Mol Cell* 6, 269-279.

Dong, Y., Zhang, S., Wu, Z., Li, X., Wang, W.L., Zhu, Y., Stoilova-McPhie, S., Lu, Y., Finley, D., and Mao, Y. (2019). Cryo-EM structures and dynamics of substrate-engaged human 26S proteasome. *Nature* 565, 49-55.

Doring, K., Ahmed, N., Riemer, T., Suresh, H.G., Vainshtein, Y., Habich, M., Riemer, J., Mayer, M.P., O'Brien, E.P., Kramer, G., *et al.* (2017). Profiling Ssb-Nascent Chain Interactions Reveals Principles of Hsp70-Assisted Folding. *Cell* *170*, 298-311 e220.

Dunn, J.G., Foo, C.K., Belletier, N.G., Gavis, E.R., and Weissman, J.S. (2013). Ribosome profiling reveals pervasive and regulated stop codon readthrough in *Drosophila melanogaster*. *Elife* *2*, e01179.

Duttler, S., Pechmann, S., and Frydman, J. (2013). Principles of cotranslational ubiquitination and quality control at the ribosome. *Mol Cell* *50*, 379-393.

Ellis, R.J., and Minton, A.P. (2006). Protein aggregation in crowded environments. *Biol Chem* *387*, 485-497.

Escusa-Toret, S., Vonk, W.I., and Frydman, J. (2013). Spatial sequestration of misfolded proteins by a dynamic chaperone pathway enhances cellular fitness during stress. *Nat Cell Biol* *15*, 1231-1243.

Estebanez, B., de Paz, J.A., Cuevas, M.J., and Gonzalez-Gallego, J. (2018). Endoplasmic Reticulum Unfolded Protein Response, Aging and Exercise: An Update. *Front Physiol* *9*, 1744.

Evans, M.E., Clark, W.C., Zheng, G., and Pan, T. (2017). Determination of tRNA aminoacylation levels by high-throughput sequencing. *Nucleic Acids Res* *45*, e133.

Ewald, C.Y., Landis, J.N., Porter Abate, J., Murphy, C.T., and Blackwell, T.K. (2015). Dauer-independent insulin/IGF-1-signalling implicates collagen remodelling in longevity. *Nature* *519*, 97-101.

Farkas, A., and Bohnsack, K.E. (2021). Capture and delivery of tail-anchored proteins to the endoplasmic reticulum. *J Cell Biol* *220*.

Fedry, J., Silva, J., Vanevic, M., Fronik, S., Mechulam, Y., Schmitt, E., des Georges, A., Faller, W., and Forster, F. (2023). Visualization of translation reorganization upon persistent collision stress in mammalian cells. *bioRxiv*.

Ferbitz, L., Maier, T., Patzelt, H., Bukau, B., Deuerling, E., and Ban, N. (2004). Trigger factor in complex with the ribosome forms a molecular cradle for nascent proteins. *Nature* *431*, 590-596.

Ferraz, R.C., Camara, H., De-Souza, E.A., Pinto, S., Pinca, A.P., Silva, R.C., Sato, V.N., Castilho, B.A., and Mori, M.A. (2016). IMPACT is a GCN2 inhibitor that limits lifespan in *Caenorhabditis elegans*. *BMC Biol* *14*, 87.

Flach, J., Bakker, S.T., Mohrin, M., Conroy, P.C., Pietras, E.M., Reynaud, D., Alvarez, S., Diolaiti, M.E., Ugarte, F., Forsberg, E.C., *et al.* (2014). Replication stress is a potent driver of functional decline in ageing haematopoietic stem cells. *Nature* *512*, 198-202.

Forrest, M.E., Pinkard, O., Martin, S., Sweet, T.J., Hanson, G., and Collier, J. (2020). Codon and amino acid content are associated with mRNA stability in mammalian cells. *PLoS One* *15*, e0228730.

Fragkos, M., Ganier, O., Coulombe, P., and Mechali, M. (2015). DNA replication origin activation in space and time. *Nat Rev Mol Cell Biol* *16*, 360-374.

Friedman, R.C., Farh, K.K., Burge, C.B., and Bartel, D.P. (2009). Most mammalian mRNAs are conserved targets of microRNAs. *Genome Res* *19*, 92-105.

Friedrich, K.L., Giese, K.C., Buan, N.R., and Vierling, E. (2004). Interactions between small heat shock protein subunits and substrate in small heat shock protein-substrate complexes. *J Biol Chem* *279*, 1080-1089.

Frolova, L., Le Goff, X., Rasmussen, H.H., Cheperegin, S., Drugeon, G., Kress, M., Arman, I., Haenni, A.L., Celis, J.E., Philippe, M., *et al.* (1994). A highly conserved eukaryotic protein family possessing properties of polypeptide chain release factor. *Nature* *372*, 701-703.

Frolova, L.Y., Tsivkovskii, R.Y., Sivolobova, G.F., Oparina, N.Y., Serpinsky, O.I., Blinov, V.M., Tatkov, S.I., and Kisselev, L.L. (1999). Mutations in the highly conserved GGQ motif of class 1 polypeptide release factors abolish ability of human eRF1 to trigger peptidyl-tRNA hydrolysis. *RNA* 5, 1014-1020.

Gamerding, M., Hanebuth, M.A., Frickey, T., and Deuerling, E. (2015). The principle of antagonism ensures protein targeting specificity at the endoplasmic reticulum. *Science* 348, 201-207.

Garcia-Muse, T., and Aguilera, A. (2016). Transcription-replication conflicts: how they occur and how they are resolved. *Nat Rev Mol Cell Biol* 17, 553-563.

Gautschi, M., Mun, A., Ross, S., and Rospert, S. (2002). A functional chaperone triad on the yeast ribosome. *Proc Natl Acad Sci U S A* 99, 4209-4214.

Gerashchenko, M.V., Peterfi, Z., Yim, S.H., and Gladyshev, V.N. (2021). Translation elongation rate varies among organs and decreases with age. *Nucleic Acids Res* 49, e9.

Gobet, C., Weger, B.D., Marquis, J., Martin, E., Neelagandan, N., Gachon, F., and Naef, F. (2020). Robust landscapes of ribosome dwell times and aminoacyl-tRNAs in response to nutrient stress in liver. *Proc Natl Acad Sci U S A* 117, 9630-9641.

Gonskikh, Y., and Polacek, N. (2017). Alterations of the translation apparatus during aging and stress response. *Mech Ageing Dev* 168, 30-36.

Gu, Y., Mao, Y., Jia, L., Dong, L., and Qian, S.B. (2021). Bi-directional ribosome scanning controls the stringency of start codon selection. *Nat Commun* 12, 6604.

Guna, A., and Hegde, R.S. (2018). Transmembrane Domain Recognition during Membrane Protein Biogenesis and Quality Control. *Curr Biol* 28, R498-R511.

Gutierrez, E., Shin, B.S., Woolstenhulme, C.J., Kim, J.R., Saini, P., Buskirk, A.R., and Dever, T.E. (2013). eIF5A promotes translation of polyproline motifs. *Mol Cell* 51, 35-45.

Han, P., Shichino, Y., Schneider-Poetsch, T., Mito, M., Hashimoto, S., Udagawa, T., Kohno, K., Yoshida, M., Mishima, Y., Inada, T., *et al.* (2020). Genome-wide Survey of Ribosome Collision. *Cell Rep* 31, 107610.

Hansen, M., Taubert, S., Crawford, D., Libina, N., Lee, S.J., and Kenyon, C. (2007). Lifespan extension by conditions that inhibit translation in *Caenorhabditis elegans*. *Aging Cell* 6, 95-110.

Hanson, G., and Collier, J. (2018). Codon optimality, bias and usage in translation and mRNA decay. *Nat Rev Mol Cell Biol* 19, 20-30.

Harding, H.P., Ordonez, A., Allen, F., Parts, L., Inglis, A.J., Williams, R.L., and Ron, D. (2019). The ribosomal P-stalk couples amino acid starvation to GCN2 activation in mammalian cells. *Elife* 8.

Hartl, F.U. (1996). Molecular chaperones in cellular protein folding. *Nature* 381, 571-579.

Hartl, F.U., Bracher, A., and Hayer-Hartl, M. (2011). Molecular chaperones in protein folding and proteostasis. *Nature* 475, 324-332.

Hashimoto, S., Nobuta, R., Izawa, T., and Inada, T. (2019). Translation arrest as a protein quality control system for aberrant translation of the 3'-UTR in mammalian cells. *FEBS Lett* 593, 777-787.

Haslbeck, M., Walke, S., Stromer, T., Ehrnsperger, M., White, H.E., Chen, S., Saibil, H.R., and Buchner, J. (1999). Hsp26: a temperature-regulated chaperone. *EMBO J* 18, 6744-6751.

Haslbeck, M., Weinkauff, S., and Buchner, J. (2019). Small heat shock proteins: Simplicity meets complexity. *J Biol Chem* 294, 2121-2132.

Hayer-Hartl, M., and Minton, A.P. (2006). A simple semiempirical model for the effect of molecular confinement upon the rate of protein folding. *Biochemistry* 45, 13356-13360.

Hegde, R.S., and Keenan, R.J. (2022). The mechanisms of integral membrane protein biogenesis. *Nat Rev Mol Cell Biol* 23, 107-124.

Herzog, V.A., Reichholf, B., Neumann, T., Rescheneder, P., Bhat, P., Burkard, T.R., Wlotzka, W., von Haeseler, A., Zuber, J., and Ameres, S.L. (2017). Thiol-linked alkylation of RNA to assess expression dynamics. *Nat Methods* 14, 1198-1204.

Hessa, T., Sharma, A., Mariappan, M., Eshleman, H.D., Gutierrez, E., and Hegde, R.S. (2011). Protein targeting and degradation are coupled for elimination of mislocalized proteins. *Nature* 475, 394-397.

Hickey, K.L., Dickson, K., Cogan, J.Z., Replogle, J.M., Schoof, M., D'Orazio, K.N., Sinha, N.K., Hussmann, J.A., Jost, M., Frost, A., *et al.* (2020). GIGYF2 and 4EHP Inhibit Translation Initiation of Defective Messenger RNAs to Assist Ribosome-Associated Quality Control. *Mol Cell* 79, 950-962 e956.

Hipp, M.S., Kasturi, P., and Hartl, F.U. (2019). The proteostasis network and its decline in ageing. *Nat Rev Mol Cell Biol* 20, 421-435.

Hopfler, M., Absmeier, E., Peak-Chew, S.Y., Vartholomaiou, E., Passmore, L.A., Gasic, I., and Hegde, R.S. (2023). Mechanism of ribosome-associated mRNA degradation during tubulin autoregulation. *Mol Cell* 83, 2290-2302 e2213.

Horwich, A.L., Fenton, W.A., Chapman, E., and Farr, G.W. (2007). Two families of chaperonin: physiology and mechanism. *Annu Rev Cell Dev Biol* 23, 115-145.

Horwitz, J. (1992). Alpha-crystallin can function as a molecular chaperone. *Proc Natl Acad Sci U S A* 89, 10449-10453.

Horwitz, J., and Ricanati, S. (1992). Bradykinin and phorbol dibutyrate activate phospholipase D in PC12 cells by different mechanisms. *J Neurochem* 59, 1474-1480.

Hsieh, H.H., and Shan, S.O. (2021). Fidelity of Cotranslational Protein Targeting to the Endoplasmic Reticulum. *Int J Mol Sci* 23.

Hsu, A.L., Murphy, C.T., and Kenyon, C. (2003). Regulation of aging and age-related disease by DAF-16 and heat-shock factor. *Science* 300, 1142-1145.

Hu, X., Wang, L., Wang, Y., Ji, J., Li, J., Wang, Z., Li, C., Zhang, Y., and Zhang, Z.R. (2020). RNF126-Mediated Reubiquitination Is Required for Proteasomal Degradation of p97-Extracted Membrane Proteins. *Mol Cell* 79, 320-331 e329.

Hu, Z., Xia, B., Postnikoff, S.D., Shen, Z.J., Tomoiaga, A.S., Harkness, T.A., Seol, J.H., Li, W., Chen, K., and Tyler, J.K. (2018). Ssd1 and Gcn2 suppress global translation efficiency in replicatively aged yeast while their activation extends lifespan. *Elife* 7.

Inada, T. (2020). Quality controls induced by aberrant translation. *Nucleic Acids Res* 48, 1084-1096.

Inglis, A.J., Masson, G.R., Shao, S., Perisic, O., McLaughlin, S.H., Hegde, R.S., and Williams, R.L. (2019). Activation of GCN2 by the ribosomal P-stalk. *Proc Natl Acad Sci U S A* 116, 4946-4954.

Ingolia, N.T., Lareau, L.F., and Weissman, J.S. (2011). Ribosome profiling of mouse embryonic stem cells reveals the complexity and dynamics of mammalian proteomes. *Cell* 147, 789-802.

Isaacs, W.B., Cook, R.K., Van Atta, J.C., Redmond, C.M., and Fulton, A.B. (1989). Assembly of vimentin in cultured cells varies with cell type. *J Biol Chem* 264, 17953-17960.

Isaacs, W.B., and Fulton, A.B. (1987). Cotranslational assembly of myosin heavy chain in developing cultured skeletal muscle. *Proc Natl Acad Sci U S A* 84, 6174-6178.

Ito, S., and Nagata, K. (2021). Quality Control of Procollagen in Cells. *Annu Rev Biochem* 90, 631-658.

Jackson, R.J., Hellen, C.U., and Pestova, T.V. (2010). The mechanism of eukaryotic translation initiation and principles of its regulation. *Nat Rev Mol Cell Biol* 11, 113-127.

Jakob, U., Gaestel, M., Engel, K., and Buchner, J. (1993). Small heat shock proteins are molecular chaperones. *J Biol Chem* 268, 1517-1520.

Jan, A., Jansonius, B., Delaidelli, A., Bhanshali, F., An, Y.A., Ferreira, N., Smits, L.M., Negri, G.L., Schwamborn, J.C., Jensen, P.H., *et al.* (2018). Activity of translation regulator eukaryotic elongation factor-2 kinase is increased in Parkinson disease brain and its inhibition reduces alpha synuclein toxicity. *Acta Neuropathol Commun* 6, 54.

Jan, C.H., Friedman, R.C., Ruby, J.G., and Bartel, D.P. (2011). Formation, regulation and evolution of *Caenorhabditis elegans* 3'UTRs. *Nature* 469, 97-101.

Johnston, H.E., and Samant, R.S. (2021). Alternative systems for misfolded protein clearance: life beyond the proteasome. *FEBS J* 288, 4464-4487.

Jomaa, A., Gamedinger, M., Hsieh, H.H., Wallisch, A., Chandrasekaran, V., Ulusoy, Z., Scaiola, A., Hegde, R.S., Shan, S.O., Ban, N., *et al.* (2022). Mechanism of signal sequence handover from NAC to SRP on ribosomes during ER-protein targeting. *Science* 375, 839-844.

Juzskiewicz, S., Chandrasekaran, V., Lin, Z., Kraatz, S., Ramakrishnan, V., and Hegde, R.S. (2018). ZNF598 Is a Quality Control Sensor of Collided Ribosomes. *Mol Cell* 72, 469-481 e467.

Juzskiewicz, S., Slodkiewicz, G., Lin, Z., Freire-Pritchett, P., Peak-Chew, S.Y., and Hegde, R.S. (2020). Ribosome collisions trigger cis-acting feedback inhibition of translation initiation. *Elife* 9.

Kaeberlein, M., Powers, R.W., 3rd, Steffen, K.K., Westman, E.A., Hu, D., Dang, N., Kerr, E.O., Kirkland, K.T., Fields, S., and Kennedy, B.K. (2005). Regulation of yeast replicative life span by TOR and Sch9 in response to nutrients. *Science* 310, 1193-1196.

Kaiser, C.M., Chang, H.C., Agashe, V.R., Lakshminpathy, S.K., Etchells, S.A., Hayer-Hartl, M., Hartl, F.U., and Barral, J.M. (2006). Real-time observation of trigger factor function on translating ribosomes. *Nature* 444, 455-460.

Kampinga, H.H., Brunsting, J.F., Stege, G.J., Konings, A.W., and Landry, J. (1994). Cells overexpressing Hsp27 show accelerated recovery from heat-induced nuclear protein aggregation. *Biochem Biophys Res Commun* 204, 1170-1177.

Kesner, J.S.C., Z.; Aparicio, A. A.; Wu, X. (2022). A unified model for the surveillance of translation in diverse noncoding sequences. *bioRxiv*.

Khaminets, A., Behl, C., and Dikic, I. (2016). Ubiquitin-Dependent And Independent Signals In Selective Autophagy. *Trends Cell Biol* 26, 6-16.

Kim, Y.E., Hipp, M.S., Bracher, A., Hayer-Hartl, M., and Hartl, F.U. (2013). Molecular chaperone functions in protein folding and proteostasis. *Annu Rev Biochem* 82, 323-355.

Komar, A.A., Lesnik, T., and Reiss, C. (1999). Synonymous codon substitutions affect ribosome traffic and protein folding during in vitro translation. *FEBS Lett* 462, 387-391.

Koplin, A., Preissler, S., Ilina, Y., Koch, M., Scior, A., Erhardt, M., and Deuerling, E. (2010). A dual function for chaperones SSB-RAC and the NAC nascent polypeptide-associated complex on ribosomes. *J Cell Biol* 189, 57-68.

Koren, I., Timms, R.T., Kula, T., Xu, Q., Li, M.Z., and Elledge, S.J. (2018). The Eukaryotic Proteome Is Shaped by E3 Ubiquitin Ligases Targeting C-Terminal Degrons. *Cell* 173, 1622-1635 e1614.

Kramarski, L., and Arbely, E. (2020). Translational read-through promotes aggregation and shapes stop codon identity. *Nucleic Acids Res* 48, 3747-3760.

Kramer, G., Shiber, A., and Bukau, B. (2019). Mechanisms of Cotranslational Maturation of Newly Synthesized Proteins. *Annu Rev Biochem* 88, 337-364.

Krane, S.M. (2008). The importance of proline residues in the structure, stability and susceptibility to proteolytic degradation of collagens. *Amino Acids* 35, 703-710.

Krukowski, K., Nolan, A., Frias, E.S., Boone, M., Ureta, G., Grue, K., Paladini, M.S., Elizarraras, E., Delgado, L., Bernales, S., *et al.* (2020). Small molecule cognitive enhancer reverses age-related memory decline in mice. *Elife* 9.

Kulak, N.A., Pichler, G., Paron, I., Nagaraj, N., and Mann, M. (2014). Minimal, encapsulated proteomic-sample processing applied to copy-number estimation in eukaryotic cells. *Nat Methods* 11, 319-324.

Lareau, L.F., Hite, D.H., Hogan, G.J., and Brown, P.O. (2014). Distinct stages of the translation elongation cycle revealed by sequencing ribosome-protected mRNA fragments. *Elife* 3, e01257.

Lecroisey, C., Segalat, L., and Gieseler, K. (2007). The *C. elegans* dense body: anchoring and signaling structure of the muscle. *J Muscle Res Cell Motil* 28, 79-87.

Lee, G.J., Roseman, A.M., Saibil, H.R., and Vierling, E. (1997). A small heat shock protein stably binds heat-denatured model substrates and can maintain a substrate in a folding-competent state. *EMBO J* 16, 659-671.

Leznicki, P., and High, S. (2012). SGTA antagonizes BAG6-mediated protein triage. *Proc Natl Acad Sci U S A* 109, 19214-19219.

Leznicki, P., and High, S. (2020). SGTA associates with nascent membrane protein precursors. *EMBO Rep* 21, e48835.

Li, F., Xing, X., Xiao, Z., Xu, G., and Yang, X. (2020). RiboMiner: a toolset for mining multi-dimensional features of the translome with ribosome profiling data. *BMC Bioinformatics* 21, 340.

Li, W.J., Wang, C.W., Tao, L., Yan, Y.H., Zhang, M.J., Liu, Z.X., Li, Y.X., Zhao, H.Q., Li, X.M., He, X.D., *et al.* (2021). Insulin signaling regulates longevity through protein phosphorylation in *Caenorhabditis elegans*. *Nat Commun* 12, 4568.

Lin, Z., Gasic, I., Chandrasekaran, V., Peters, N., Shao, S., Mitchison, T.J., and Hegde, R.S. (2020). TTC5 mediates autoregulation of tubulin via mRNA degradation. *Science* 367, 100-104.

Liutkute, M., Samatova, E., and Rodnina, M.V. (2020). Cotranslational Folding of Proteins on the Ribosome. *Biomolecules* 10.

Longo, F., Mancini, M., Ibraheem, P.L., Aryal, S., Mesini, C., Patel, J.C., Penhos, E., Rahman, N., Mamcarz, M., Santini, E., *et al.* (2021). Cell-type-specific disruption of PERK-eIF2alpha signaling in dopaminergic neurons alters motor and cognitive function. *Mol Psychiatry* 26, 6427-6450.

Loughran, G., Chou, M.Y., Ivanov, I.P., Jungreis, I., Kellis, M., Kiran, A.M., Baranov, P.V., and Atkins, J.F. (2014). Evidence of efficient stop codon readthrough in four mammalian genes. *Nucleic Acids Res* 42, 8928-8938.

Malhotra, V., and Erlmann, P. (2015). The pathway of collagen secretion. *Annu Rev Cell Dev Biol* 31, 109-124.

Manjunath, H., Zhang, H., Rehfeld, F., Han, J., Chang, T.C., and Mendell, J.T. (2019). Suppression of Ribosomal Pausing by eIF5A Is Necessary to Maintain the Fidelity of Start Codon Selection. *Cell Rep* 29, 3134-3146 e3136.

Mariappan, M., Li, X., Stefanovic, S., Sharma, A., Mateja, A., Keenan, R.J., and Hegde, R.S. (2010). A ribosome-associating factor chaperones tail-anchored membrane proteins. *Nature* 466, 1120-1124.

Markesich, D.C., Gajewski, K.M., Nazimiec, M.E., and Beckingham, K. (2000). bicaudal encodes the *Drosophila* beta NAC homolog, a component of the ribosomal translational machinery\*. *Development* 127, 559-572.

Matheisl, S., Berninghausen, O., Becker, T., and Beckmann, R. (2015). Structure of a human translation termination complex. *Nucleic Acids Res* 43, 8615-8626.

Matsuo, Y., and Inada, T. (2021). The ribosome collision sensor Hel2 functions as preventive quality control in the secretory pathway. *Cell Rep* 34, 108877.

Matyskiela, M.E., Lu, G., Ito, T., Pagarigan, B., Lu, C.C., Miller, K., Fang, W., Wang, N.Y., Nguyen, D., Houston, J., *et al.* (2016). A novel cereblon modulator recruits GSPT1 to the CRL4(CRBN) ubiquitin ligase. *Nature* 535, 252-257.

Mayer, M.P. (2010). Gymnastics of molecular chaperones. *Mol Cell* 39, 321-331.

Mayr, C. (2017). Regulation by 3'-Untranslated Regions. *Annu Rev Genet* 51, 171-194.

McGlincy, N.J., and Ingolia, N.T. (2017). Transcriptome-wide measurement of translation by ribosome profiling. *Methods* 126, 112-129.

McHaourab, H.S., Dodson, E.K., and Koteiche, H.A. (2002). Mechanism of chaperone function in small heat shock proteins. Two-mode binding of the excited states of T4 lysozyme mutants by alphaA-crystallin. *J Biol Chem* 277, 40557-40566.

McKenna, M.J., Sim, S.I., Ordureau, A., Wei, L., Harper, J.W., Shao, S., and Park, E. (2020). The endoplasmic reticulum P5A-ATPase is a transmembrane helix dislocase. *Science* 369.

Merkhofer, E.C., Hu, P., and Johnson, T.L. (2014). Introduction to cotranscriptional RNA splicing. *Methods Mol Biol* 1126, 83-96.

Meydan, S., and Guydosh, N.R. (2020). Disome and Trisome Profiling Reveal Genome-wide Targets of Ribosome Quality Control. *Mol Cell* 79, 588-602 e586.

Miller-Vedam, L.E., Brauning, B., Popova, K.D., Schirle Oakdale, N.T., Bonnar, J.L., Prabu, J.R., Boydston, E.A., Sevillano, N., Shurtleff, M.J., Stroud, R.M., *et al.* (2020). Structural and mechanistic basis of the EMC-dependent biogenesis of distinct transmembrane clients. *Elife* 9.

Mishima, Y., Han, P., Ishibashi, K., Kimura, S., and Iwasaki, S. (2022). Ribosome slowdown triggers codon-mediated mRNA decay independently of ribosome quality control. *EMBO J* 41, e109256.

Mogk, A., and Bukau, B. (2017). Role of sHsps in organizing cytosolic protein aggregation and disaggregation. *Cell Stress Chaperones* 22, 493-502.

Moon, S.L., Sonenberg, N., and Parker, R. (2018). Neuronal Regulation of eIF2alpha Function in Health and Neurological Disorders. *Trends Mol Med* 24, 575-589.

Moore, J., Akbergenov, R., Nigri, M., Isnard-Petit, P., Grimm, A., Seebeck, P., Restelli, L., Frank, S., Eckert, A., Thiam, K., *et al.* (2021). Random errors in protein synthesis activate an age-dependent program of muscle atrophy in mice. *Commun Biol* 4, 703.

Moore, P.B., Hendrickson, W.A., Henderson, R., and Brunger, A.T. (2022). The protein-folding problem: Not yet solved. *Science* 375, 507.

Morley, J.F., and Morimoto, R.I. (2004). Regulation of longevity in *Caenorhabditis elegans* by heat shock factor and molecular chaperones. *Mol Biol Cell* 15, 657-664.

O'Donnell, J.P., Phillips, B.P., Yagita, Y., Juszkiwicz, S., Wagner, A., Malinverni, D., Keenan, R.J., Miller, E.A., and Hegde, R.S. (2020). The architecture of EMC reveals a path for membrane protein insertion. *Elife* 9.

Oltion, K., Carelli, J.D., Yang, T., See, S.K., Wang, H.Y., Kampmann, M., and Taunton, J. (2023). An E3 ligase network engages GCN1 to promote the degradation of translation factors on stalled ribosomes. *Cell* 186, 346-362 e317.

Oltion, K.C., J. D.; Yang, T.; See, S. K.; Wang, H.Y.; Kampmann, M.; Taunton, J. (2022). An E3 ligase network engages GCN1 to promote elongation factor-1 $\alpha$  degradation on stalled ribosomes. *bioRxiv*.

Onursal, C., Dick, E., Angelidis, I., Schiller, H.B., and Staab-Weijnitz, C.A. (2021). Collagen Biosynthesis, Processing, and Maturation in Lung Ageing. *Front Med (Lausanne)* 8, 593874.

Park, J., Park, J., Lee, J., and Lim, C. (2021). The trinity of ribosome-associated quality control and stress signaling for proteostasis and neuronal physiology. *BMB Rep* 54, 439-450.

Pavlov, M.Y., Watts, R.E., Tan, Z., Cornish, V.W., Ehrenberg, M., and Forster, A.C. (2009). Slow peptide bond formation by proline and other N-alkylamino acids in translation. *Proc Natl Acad Sci U S A* 106, 50-54.

Pechmann, S., Chartron, J.W., and Frydman, J. (2014). Local slowdown of translation by nonoptimal codons promotes nascent-chain recognition by SRP in vivo. *Nat Struct Mol Biol* 21, 1100-1105.

Pechmann, S., and Frydman, J. (2013). Evolutionary conservation of codon optimality reveals hidden signatures of cotranslational folding. *Nat Struct Mol Biol* 20, 237-243.

Pechmann, S., Willmund, F., and Frydman, J. (2013). The ribosome as a hub for protein quality control. *Mol Cell* 49, 411-421.

Peil, L., Starosta, A.L., Lassak, J., Atkinson, G.C., Virumae, K., Spitzer, M., Tenson, T., Jung, K., Remme, J., and Wilson, D.N. (2013). Distinct XPPX sequence motifs induce ribosome stalling, which is rescued by the translation elongation factor EF-P. *Proc Natl Acad Sci U S A* 110, 15265-15270.

Phillips, B.P., and Miller, E.A. (2020). Ribosome-associated quality control of membrane proteins at the endoplasmic reticulum. *J Cell Sci* 133.

Pochopien, A.A., Beckert, B., Kasvandik, S., Berninghausen, O., Beckmann, R., Tenson, T., and Wilson, D.N. (2021). Structure of Gcn1 bound to stalled and colliding 80S ribosomes. *Proc Natl Acad Sci U S A* 118.

Pohl, C., and Dikic, I. (2019). Cellular quality control by the ubiquitin-proteasome system and autophagy. *Science* 366, 818-822.

Preis, A., Heuer, A., Barrio-Garcia, C., Hauser, A., Eyler, D.E., Berninghausen, O., Green, R., Becker, T., and Beckmann, R. (2014). Cryoelectron microscopic structures of eukaryotic translation termination complexes containing eRF1-eRF3 or eRF1-ABCE1. *Cell Rep* 8, 59-65.

Preissler, S., and Deuerling, E. (2012). Ribosome-associated chaperones as key players in proteostasis. *Trends Biochem Sci* 37, 274-283.

Presnyak, V., Alhusaini, N., Chen, Y.H., Martin, S., Morris, N., Kline, N., Olson, S., Weinberg, D., Baker, K.E., Graveley, B.R., *et al.* (2015). Codon optimality is a major determinant of mRNA stability. *Cell* 160, 1111-1124.

Purvis, I.J., Bettany, A.J., Loughlin, L., and Brown, A.J. (1987). The effects of alterations within the 3' untranslated region of the pyruvate kinase messenger RNA upon its stability and translation in *Saccharomyces cerevisiae*. *Nucleic Acids Res* 15, 7951-7962.

Quintana-Gallardo, L., Martin-Benito, J., Marcilla, M., Espadas, G., Sabido, E., and Valpuesta, J.M. (2019). The cochaperone CHIP marks Hsp70- and Hsp90-bound substrates for degradation through a very flexible mechanism. *Sci Rep* 9, 5102.

Reissmann, S., Parnot, C., Booth, C.R., Chiu, W., and Frydman, J. (2007). Essential function of the built-in lid in the allosteric regulation of eukaryotic and archaeal chaperonins. *Nat Struct Mol Biol* 14, 432-440.

Rodnina, M.V. (2016). The ribosome in action: Tuning of translational efficiency and protein folding. *Protein Sci* 25, 1390-1406.

Rodnina, M.V., and Wintermeyer, W. (2016). Protein Elongation, Co-translational Folding and Targeting. *J Mol Biol* 428, 2165-2185.

Rodrigo-Brenni, M.C., Gutierrez, E., and Hegde, R.S. (2014). Cytosolic quality control of mislocalized proteins requires RNF126 recruitment to Bag6. *Mol Cell* 55, 227-237.

Rogov, V., Dotsch, V., Johansen, T., and Kirkin, V. (2014). Interactions between autophagy receptors and ubiquitin-like proteins form the molecular basis for selective autophagy. *Mol Cell* 53, 167-178.

Rudiger, S., Germeroth, L., Schneider-Mergener, J., and Bukau, B. (1997). Substrate specificity of the DnaK chaperone determined by screening cellulose-bound peptide libraries. *EMBO J* 16, 1501-1507.

Russmann, F., Stemp, M.J., Monkemeyer, L., Etchells, S.A., Bracher, A., and Hartl, F.U. (2012). Folding of large multidomain proteins by partial encapsulation in the chaperonin TRiC/CCT. *Proc Natl Acad Sci U S A* 109, 21208-21215.

Sako, H., Youssef, M., Elisseeva, O., Akimoto, T., Suzuki, K., Ushida, T., and Yamamoto, T. (2023). microRNAs slow translating ribosomes to prevent protein misfolding in eukaryotes. *EMBO J*, e112469.

Santiago, T.C., Purvis, I.J., Bettany, A.J., and Brown, A.J. (1986). The relationship between mRNA stability and length in *Saccharomyces cerevisiae*. *Nucleic Acids Res* 14, 8347-8360.

Saric, T., Graef, C.I., and Goldberg, A.L. (2004). Pathway for degradation of peptides generated by proteasomes: a key role for thimet oligopeptidase and other metallopeptidases. *J Biol Chem* 279, 46723-46732.

Sattlegger, E., and Hinnebusch, A.G. (2000). Separate domains in GCN1 for binding protein kinase GCN2 and ribosomes are required for GCN2 activation in amino acid-starved cells. *EMBO J* 19, 6622-6633.

Sattlegger, E., and Hinnebusch, A.G. (2005). Polyribosome binding by GCN1 is required for full activation of eukaryotic translation initiation factor 2{alpha} kinase GCN2 during amino acid starvation. *J Biol Chem* 280, 16514-16521.

Schuldiner, M., Metz, J., Schmid, V., Denic, V., Rakwalska, M., Schmitt, H.D., Schwappach, B., and Weissman, J.S. (2008). The GET complex mediates insertion of tail-anchored proteins into the ER membrane. *Cell* 134, 634-645.

Schuller, A.P., and Green, R. (2018). Roadblocks and resolutions in eukaryotic translation. *Nat Rev Mol Cell Biol* 19, 526-541.

Schuller, A.P., Wu, C.C., Dever, T.E., Buskirk, A.R., and Green, R. (2017). eIF5A Functions Globally in Translation Elongation and Termination. *Mol Cell* 66, 194-205 e195.

Seshadri, K., Garemyr, R., Wallin, E., von Heijne, G., and Elofsson, A. (1998). Architecture of beta-barrel membrane proteins: analysis of trimeric porins. *Protein Sci* 7, 2026-2032.

Shao, S., and Hegde, R.S. (2011). Membrane protein insertion at the endoplasmic reticulum. *Annu Rev Cell Dev Biol* 27, 25-56.

Shao, S., Rodrigo-Brenni, M.C., Kivlen, M.H., and Hegde, R.S. (2017). Mechanistic basis for a molecular triage reaction. *Science* 355, 298-302.

Shcherbakov, D., Nigri, M., Akbergenov, R., Brilkova, M., Mantovani, M., Petit, P.I., Grimm, A., Karol, A.A., Teo, Y., Sanchon, A.C., *et al.* (2022). Premature aging in mice with error-prone protein synthesis. *Sci Adv* 8, eabl9051.

Shen, P.S., Park, J., Qin, Y., Li, X., Parsawar, K., Larson, M.H., Cox, J., Cheng, Y., Lambowitz, A.M., Weissman, J.S., *et al.* (2015). Protein synthesis. Rqc2p and 60S ribosomal subunits mediate mRNA-independent elongation of nascent chains. *Science* 347, 75-78.

Shibata, N., Ohoka, N., Sugaki, Y., Onodera, C., Inoue, M., Sakuraba, Y., Takakura, D., Hashii, N., Kawasaki, N., Gondo, Y., *et al.* (2015). Degradation of Stop Codon Read-through Mutant Proteins via the Ubiquitin-Proteasome System Causes Hereditary Disorders. *J Biol Chem* 290, 28428-28437.

Shoulders, M.D., and Raines, R.T. (2009). Collagen structure and stability. *Annu Rev Biochem* 78, 929-958.

Simms, C.L., Yan, L.L., Qiu, J.K., and Zaher, H.S. (2019). Ribosome Collisions Result in +1 Frameshifting in the Absence of No-Go Decay. *Cell Rep* 28, 1679-1689 e1674.

Singhal, K., Vreede, J., Mashaghi, A., Tans, S.J., and Bolhuis, P.G. (2015). The Trigger Factor Chaperone Encapsulates and Stabilizes Partial Folds of Substrate Proteins. *PLoS Comput Biol* 11, e1004444.

Sinha, N.K., Ordureau, A., Best, K., Saba, J.A., Zinshteyn, B., Sundaramoorthy, E., Fulzele, A., Garshott, D.M., Denk, T., Thoms, M., *et al.* (2020). EDF1 coordinates cellular responses to ribosome collisions. *Elife* 9.

Sirur, A., and Best, R.B. (2013). Effects of interactions with the GroEL cavity on protein folding rates. *Biophys J* 104, 1098-1106.

Sitron, C.S., and Brandman, O. (2019). CAT tails drive degradation of stalled polypeptides on and off the ribosome. *Nat Struct Mol Biol* 26, 450-459.

Sitron, C.S., and Brandman, O. (2020). Detection and Degradation of Stalled Nascent Chains via Ribosome-Associated Quality Control. *Annu Rev Biochem* 89, 417-442.

Smalinskaite, L., Kim, M.K., Lewis, A.J.O., Keenan, R.J., and Hegde, R.S. (2022). Mechanism of an intramembrane chaperone for multipass membrane proteins. *Nature* 611, 161-166.

Song, H., Mugnier, P., Das, A.K., Webb, H.M., Evans, D.R., Tuite, M.F., Hemmings, B.A., and Barford, D. (2000). The crystal structure of human eukaryotic release factor eRF1--mechanism of stop codon recognition and peptidyl-tRNA hydrolysis. *Cell* 100, 311-321.

Sontag, E.M., Samant, R.S., and Frydman, J. (2017). Mechanisms and Functions of Spatial Protein Quality Control. *Annu Rev Biochem* 86, 97-122.

Specht, S., Miller, S.B., Mogk, A., and Bukau, B. (2011). Hsp42 is required for sequestration of protein aggregates into deposition sites in *Saccharomyces cerevisiae*. *J Cell Biol* 195, 617-629.

Stege, G.J., Li, G.C., Li, L., Kampinga, H.H., and Konings, A.W. (1994). On the role of hsp72 in heat-induced intranuclear protein aggregation. *Int J Hyperthermia* 10, 659-674.

Stein, K.C., Kriel, A., and Frydman, J. (2019). Nascent Polypeptide Domain Topology and Elongation Rate Direct the Cotranslational Hierarchy of Hsp70 and TRiC/CCT. *Mol Cell* 75, 1117-1130 e1115.

Stein, K.C., Morales-Polanco, F., van der Lienden, J., Rainbolt, T.K., and Frydman, J. (2022). Ageing exacerbates ribosome pausing to disrupt cotranslational proteostasis. *Nature* 601, 637-642.

Sundaram, A., Yamsek, M., Zhong, F., Hooda, Y., Hegde, R.S., and Keenan, R.J. (2022). Substrate-driven assembly of a translocon for multipass membrane proteins. *Nature* 611, 167-172.

Sweeney, P., Park, H., Baumann, M., Dunlop, J., Frydman, J., Kopito, R., McCampbell, A., Leblanc, G., Venkateswaran, A., Nurmi, A., *et al.* (2017). Protein misfolding in neurodegenerative diseases: implications and strategies. *Transl Neurodegener* 6, 6.

Szabo, A., Langer, T., Schroder, H., Flanagan, J., Bukau, B., and Hartl, F.U. (1994). The ATP hydrolysis-dependent reaction cycle of the *Escherichia coli* Hsp70 system DnaK, DnaJ, and GrpE. *Proc Natl Acad Sci U S A* 91, 10345-10349.

Tang, Y.C., Chang, H.C., Chakraborty, K., Hartl, F.U., and Hayer-Hartl, M. (2008). Essential role of the chaperonin folding compartment in vivo. *EMBO J* 27, 1458-1468.

Tector, M., and Hartl, F.U. (1999). An unstable transmembrane segment in the cystic fibrosis transmembrane conductance regulator. *EMBO J* 18, 6290-6298.

Teter, S.A., Houry, W.A., Ang, D., Tradler, T., Rockabrand, D., Fischer, G., Blum, P., Georgopoulos, C., and Hartl, F.U. (1999). Polypeptide flux through bacterial Hsp70: DnaK cooperates with trigger factor in chaperoning nascent chains. *Cell* 97, 755-765.

Thanaraj, T.A., and Argos, P. (1996). Protein secondary structural types are differentially coded on messenger RNA. *Protein Sci* 5, 1973-1983.

Trentini, D.B., Pecoraro, M., Tiwary, S., Cox, J., Mann, M., Hipp, M.S., and Hartl, F.U. (2020). Role for ribosome-associated quality control in sampling proteins for MHC class I-mediated antigen presentation. *Proc Natl Acad Sci U S A* 117, 4099-4108.

Udagawa, T., Seki, M., Okuyama, T., Adachi, S., Natsume, T., Noguchi, T., Matsuzawa, A., and Inada, T. (2021). Failure to Degrade CAT-Tailed Proteins Disrupts Neuronal Morphogenesis and Cell Survival. *Cell Rep* 34, 108599.

Ungelenk, S., Moayed, F., Ho, C.T., Grousl, T., Scharf, A., Mashaghi, A., Tans, S., Mayer, M.P., Mogk, A., and Bukau, B. (2016). Small heat shock proteins sequester misfolding proteins in near-native conformation for cellular protection and efficient refolding. *Nat Commun* 7, 13673.

Valastyan, J.S., and Lindquist, S. (2014). Mechanisms of protein-folding diseases at a glance. *Dis Model Mech* 7, 9-14.

van Heesch, S., Witte, F., Schneider-Lunitz, V., Schulz, J.F., Adami, E., Faber, A.B., Kirchner, M., Maatz, H., Blachut, S., Sandmann, C.L., *et al.* (2019). The Translational Landscape of the Human Heart. *Cell* 178, 242-260 e229.

Varshavsky, A. (2019). N-degron and C-degron pathways of protein degradation. *Proc Natl Acad Sci U S A* 116, 358-366.

Vind, A.C., Snieckute, G., Blasius, M., Tiedje, C., Krogh, N., Bekker-Jensen, D.B., Andersen, K.L., Nordgaard, C., Tollenaere, M.A.X., Lund, A.H., *et al.* (2020). ZAKalpha Recognizes Stalled Ribosomes through Partially Redundant Sensor Domains. *Mol Cell* 78, 700-713 e707.

Walker, G.A., and Lithgow, G.J. (2003). Lifespan extension in *C. elegans* by a molecular chaperone dependent upon insulin-like signals. *Aging Cell* 2, 131-139.

Walther, D.M., Kasturi, P., Zheng, M., Pinkert, S., Vecchi, G., Ciryam, P., Morimoto, R.I., Dobson, C.M., Vendruscolo, M., Mann, M., *et al.* (2015). Widespread Proteome Remodeling and Aggregation in Aging *C. elegans*. *Cell* 161, 919-932.

Walther, D.M., Kasturi, P., Zheng, M., Pinkert, S., Vecchi, G., Ciryam, P., Morimoto, R.I., Dobson, C.M., Vendruscolo, M., Mann, M., *et al.* (2017). Widespread Proteome Remodeling and Aggregation in Aging *C. elegans*. *Cell* 168, 944.

Wang, F., Durfee, L.A., and Huibregtse, J.M. (2013). A cotranslational ubiquitination pathway for quality control of misfolded proteins. *Mol Cell* 50, 368-378.

Wangen, J.R., and Green, R. (2020). Stop codon context influences genome-wide stimulation of termination codon readthrough by aminoglycosides. *Elife* 9.

Weber, R., Chung, M.Y., Keskeny, C., Zinnall, U., Landthaler, M., Valkov, E., Izaurralde, E., and Igreja, C. (2020). 4EHP and GIGYF1/2 Mediate Translation-Coupled Messenger RNA Decay. *Cell Rep* 33, 108262.

Webster, M.W., Chen, Y.H., Stowell, J.A.W., Alhusaini, N., Sweet, T., Graveley, B.R., Collier, J., and Passmore, L.A. (2018). mRNA Deadenylation Is Coupled to Translation Rates by the Differential Activities of Ccr4-Not Nucleases. *Mol Cell* 70, 1089-1100 e1088.

White, S.H., and von Heijne, G. (2005). Transmembrane helices before, during, and after insertion. *Curr Opin Struct Biol* 15, 378-386.

Wiedmann, B., Sakai, H., Davis, T.A., and Wiedmann, M. (1994). A protein complex required for signal-sequence-specific sorting and translocation. *Nature* 370, 434-440.

Willmund, F., del Alamo, M., Pechmann, S., Chen, T., Albanese, V., Dammer, E.B., Peng, J., and Frydman, J. (2013). The cotranslational function of ribosome-associated Hsp70 in eukaryotic protein homeostasis. *Cell* 152, 196-209.

Wohlever, M.L., Mateja, A., McGilvray, P.T., Day, K.J., and Keenan, R.J. (2017). Msp1 Is a Membrane Protein Dislocase for Tail-Anchored Proteins. *Mol Cell* 67, 194-202 e196.

Wohlgemuth, I., Brenner, S., Beringer, M., and Rodnina, M.V. (2008). Modulation of the rate of peptidyl transfer on the ribosome by the nature of substrates. *J Biol Chem* 283, 32229-32235.

Wolf, A.S., and Grayhack, E.J. (2015). Asc1, homolog of human RACK1, prevents frameshifting in yeast by ribosomes stalled at CGA codon repeats. *RNA* 21, 935-945.

Woodward, K., and Shirokikh, N.E. (2021). Translational control in cell ageing: an update. *Biochem Soc Trans* 49, 2853-2869.

Wruck, F., Avellaneda, M.J., Koers, E.J., Minde, D.P., Mayer, M.P., Kramer, G., Mashaghi, A., and Tans, S.J. (2018). Protein Folding Mediated by Trigger Factor and Hsp70: New Insights from Single-Molecule Approaches. *J Mol Biol* 430, 438-449.

Wu, C.C., Peterson, A., Zinshteyn, B., Regot, S., and Green, R. (2020). Ribosome Collisions Trigger General Stress Responses to Regulate Cell Fate. *Cell* 182, 404-416 e414.

Wu, Q., Medina, S.G., Kushawah, G., DeVore, M.L., Castellano, L.A., Hand, J.M., Wright, M., and Bazzini, A.A. (2019). Translation affects mRNA stability in a codon-dependent manner in human cells. *Elife* 8.

Xie, X., Lu, J., Kulbokas, E.J., Golub, T.R., Mootha, V., Lindblad-Toh, K., Lander, E.S., and Kellis, M. (2005). Systematic discovery of regulatory motifs in human promoters and 3' UTRs by comparison of several mammals. *Nature* 434, 338-345.

Yamamoto, Y., and Sakisaka, T. (2012). Molecular machinery for insertion of tail-anchored membrane proteins into the endoplasmic reticulum membrane in mammalian cells. *Mol Cell* 48, 387-397.

Yan, L.L., and Zaher, H.S. (2021). Ribosome quality control antagonizes the activation of the integrated stress response on colliding ribosomes. *Mol Cell* 81, 614-628 e614.

Yang, Q., Yu, C.H., Zhao, F., Dang, Y., Wu, C., Xie, P., Sachs, M.S., and Liu, Y. (2019). eRF1 mediates codon usage effects on mRNA translation efficiency through premature termination at rare codons. *Nucleic Acids Res* 47, 9243-9258.

Yordanova, M.M., Loughran, G., Zhdanov, A.V., Mariotti, M., Kiniry, S.J., O'Connor, P.B.F., Andreev, D.E., Tzani, I., Saffert, P., Michel, A.M., *et al.* (2018). AMD1 mRNA employs ribosome stalling as a mechanism for molecular memory formation. *Nature* 553, 356-360.

Yu, C.H., Dang, Y., Zhou, Z., Wu, C., Zhao, F., Sachs, M.S., and Liu, Y. (2015). Codon Usage Influences the Local Rate of Translation Elongation to Regulate Co-translational Protein Folding. *Mol Cell* 59, 744-754.

Zaessinger, S., Busseau, I., and Simonelig, M. (2006). Oskar allows nanos mRNA translation in *Drosophila* embryos by preventing its deadenylation by Smaug/CCR4. *Development* 133, 4573-4583.

Zeng, F., Li, X., Pires-Alves, M., Chen, X., Hawk, C.W., and Jin, H. (2021). Conserved heterodimeric GTPase Rbg1/Tma46 promotes efficient translation in eukaryotic cells. *Cell Rep* 37, 109877.

Zhang, W., Dunkle, J.A., and Cate, J.H. (2009). Structures of the ribosome in intermediate states of ratcheting. *Science* 325, 1014-1017.

Zhang, Y., De Laurentiis, E., Bohnsack, K.E., Wahlig, M., Ranjan, N., Gruseck, S., Hackert, P., Wolfle, T., Rodnina, M.V., Schwappach, B., *et al.* (2021). Ribosome-bound Get4/5 facilitates the capture of tail-anchored proteins by Sgt2 in yeast. *Nat Commun* 12, 782.

Zhang, Y., Sinning, I., and Rospert, S. (2017). Two chaperones locked in an embrace: structure and function of the ribosome-associated complex RAC. *Nat Struct Mol Biol* 24, 611-619.

Zhao, T., Chen, Y.M., Li, Y., Wang, J., Chen, S., Gao, N., and Qian, W. (2021). Disome-seq reveals widespread ribosome collisions that promote cotranslational protein folding. *Genome Biol* 22, 16.